

**Development of the Annual Spectral Matrix  
Simulation Method and Assessment of the Effect of  
Spectral Discretization on Annual Lighting Energy  
Demand**

**Dissertation**

approved by

the Department of Civil Engineering of Rheinland-Pfälzische  
Technische Universität Kaiserslautern-Landau

for the award of the academic degree of

**Doctor of Engineering (Dr.-Ing.)**

to

**Margarita Alwalidi**

Date of the defense: 25.07.2024

Dean: Prof. Dr.-Ing. Karsten Körkemeyer

Supervisor and first advisor: Prof. Dr.-Ing. Sabine Hoffmann

Second advisor: Prof. Dr. Caroline Karmann

DE-386



## Acknowledgement

This work would be incomplete without extending my deepest gratitude to the people who have supported me in this undertaking. First and foremost, I would like to express my sincere appreciation to my supervisor, Prof. Dr.-Ing. Sabine Hoffmann, for granting me the opportunity to write my thesis at the Chair of Built Environment in RPTU Kaiserslautern-Landau. Her immense expertise and guidance have contributed to all stages of my dissertation. Besides her invaluable scholarly advice, I am extremely grateful for the funding opportunity that Prof. Dr.-Ing. Sabine Hoffmann has secured for me, which allowed me to focus on my PhD endeavor.

I am also sincerely grateful to Prof. Dr. Caroline Karman for reviewing my work and for her constructive comments that have improved the value of my thesis. I would also like to extend my appreciation to Dr. Priji Balakrishnan for sharing her profound knowledge of spectral sky simulation that cannot be underestimated.

I am deeply indebted to my teammates and former colleagues who have kindly helped me in my scientific ventures. Special thanks to Dr. Abolfazl Ganji for his help in writing the first version of the point-in-time spectral simulation code. I would also like to thank Dr. Sarith Subramaniam for supporting me when I had questions related to Radiance. Many thanks to Aaron Pfaff for teaching me various tricks to write more elegant and maintainable Python code. I am also grateful to Christoph Degel for donating and helping repurpose the model used for the validation of point-in-time spectral simulation. I would like to emphasize my deepest appreciation to all my colleagues for the cheerful work atmosphere!

I would like to gratefully acknowledge our secretary, Christiane Köhler, for her friendly character and unwavering support with the organizational side of things that oftentimes greatly alleviated the load and allowed me to concentrate on my thesis.

The success of my PhD journey is not an individual accomplishment. I would like to thank my brother, Michel, for helping me proofread my thesis and for his words of encouragement. I cannot begin to express my gratitude to Daniel for his love and the tremendous support that made these years very special and memorable. Last but not least, the completion of my dissertation would not have been possible without the support of my parents, Galina and Farhan, who never compromised on my education. Their love and belief in me have kept my spirits and motivation high during this process.





# Abstract

As suggested by recent findings, light affects humans non-visually by impacting alertness, cognitive performance and various physiological responses. While the research about non-visual photoreception is still ongoing, architects and designers have begun to conceive ways of integrating provisional recommendations into lighting design practices to enable healthy lighting in living and working spaces. Consequently, there has been a growing demand for annual lighting simulation tools that consider spectral properties of light for prediction and decision-making purposes.

This thesis presents the annual spectral matrix simulation (ASMS) method. ASMS is based on integrating a precomputed annual spectral sky profile into the daylight coefficient approach to predict the spectral distribution of daylight. ASMS serves as the basis for evaluating annual lighting energy demand using spectral simulation of electric light. ASMS and point-in-time simulation with three-, nine-, 27- and 81-channel discretization are presented and discussed. The main aim is to examine the extent of increased accuracy of illuminance and annual lighting energy demand predictions that finer spectral discretization provides in comparison to the simulations with low spectral resolution. This investigation considers photopic as well as melanopic daylight equivalent illuminance.

Finer discretization was found to be particularly beneficial for light sources with discontinuous spectral power distribution. When simulating a prototypical office room with fluorescent luminaires, annual lighting energy demand was underpredicted by 32.2 % or 16.9 kWh/m<sup>2</sup>a in a three-channel simulation in comparison to finer discretization with 81 channels. For LED luminaires with relatively continuous spectra, the difference ranged between 2.1 % and 7.8 % or 0.2 kWh/m<sup>2</sup>a and 0.7 kWh/m<sup>2</sup>a.

As of today, the provision of an adequate level of melanopic equivalent daylight illuminance indoors is not required. The assessment showed that annual lighting energy demand was significantly lower when only photopic illuminance was regarded, but the minimum threshold of melanopic equivalent daylight illuminance was not met for most of the occupied hours. This finding highlights that additional consideration of melanopic equivalent daylight illuminance will lead to higher lighting energy demand. For the implementation of spectrum-based metrics in building and lighting design, high-resolution spectral simulation is therefore highly recommended.

# Contents

<b>Acknowledgement</b> .....	<b>i</b>
<b>Abstract</b> .....	<b>iii</b>
<b>1. Introduction</b> .....	<b>1</b>
1.1 Problem statement.....	1
1.2 Research objectives.....	2
1.3 Research question .....	3
1.4 Research outline.....	3
<b>2. State of the art of non-visual effects of light in simulation tools</b> .....	<b>6</b>
2.1 Background and significance of non-visual effects of light on humans.....	6
2.1.1 Effect of the illuminance on alertness during daytime .....	8
2.1.2 Effect of the CCT on alertness during daytime .....	9
2.1.3 Effect of the monochromatic light on alertness during daytime.....	10
2.2 Non-photopically weighted quantities .....	11
2.3 Background of generation of non-photometric quantities in post-processing ...	14
2.4 State-of-the-art spectral simulation tools .....	17
2.4.1 Adaptive Lighting for Alertness (ALFA) .....	18
2.4.2 LARK Spectral Lighting.....	19
2.4.3 Occupant Wellbeing through Lighting (OWL).....	20
2.4.4 Point-in-time spectral simulation.....	21
<b>3. Annual spectral matrix simulation (ASMS) method</b> .....	<b>24</b>
3.1 Tools for ASMS .....	24
3.2 ASMS framework .....	25
3.3 Precomputation of the spectral sky patch matrix .....	28
3.3.1 Generation of absolute radiance patch values.....	29
3.3.2 Generation of relative spectral radiance profile for the sky.....	29
3.3.3 Discretization of the sky SPD into $N$ -bins .....	31
3.4 ASMS and post-processing steps.....	34

<b>4. ASMS for daylighting.....</b>	<b>37</b>
4.1 Reference room .....	37
4.2 Weather data for the ASMS .....	38
4.3 Variability in the simulation of daylight.....	41
4.4 Results of ASMS for daylighting.....	45
4.4.1 Results of photopic illuminance.....	46
4.4.2 Results of melanopic equivalent daylight illuminance .....	47
4.5 Discussion of the ASMS results .....	48
<b>5. ASMS and point-in-time spectral simulation with electric light.....</b>	<b>52</b>
5.1 Photopic and spectral properties of the luminaires .....	52
5.2 Maintenance factors of the luminaires.....	53
5.3 Luminaire groups in the office room .....	54
5.4 Simulation framework of electric lighting in Radiance .....	55
5.5 Variability in the simulation of electric light.....	56
5.6 Illuminance in the prototypical room provided by luminaires.....	57
5.7 Group-dependent dimming of the luminaires .....	60
5.8 Discussion of the spectral simulation with electric light .....	62
<b>6. Lighting energy demand and dimming factor .....</b>	<b>64</b>
6.1 Lighting energy demand with photopic- and melanopic-based dimming .....	64
6.1.1 Impact of the number of channels in daylight simulation.....	68
6.1.2 Impact of the number of channels in electric light simulation.....	69
6.1.3 Impact of the number of channels in electric and daylight simulation .....	70
6.2 Lighting energy demand with photopic-based dimming .....	72
6.3 Analysis of the dimming factor.....	76
6.3.1 Photopic- and melanopic-based dimming.....	76
6.3.2 Photopic-based dimming .....	82
6.4 Discussion of the electric lighting energy.....	88
<b>7. Discussion .....</b>	<b>90</b>
7.1 Summary .....	90
7.2 Recommendations.....	92

<b>8. Conclusion .....</b>	<b>96</b>
8.1 Conclusion .....	96
8.2 Limitations .....	98
8.3 Outlook .....	99
<b>Abbreviations .....</b>	<b>101</b>
<b>Nomenclature .....</b>	<b>102</b>
<b>References .....</b>	<b>103</b>
<b>Appendix A .....</b>	<b>112</b>
<b>Appendix B .....</b>	<b>115</b>
<b>Appendix C .....</b>	<b>121</b>
<b>Appendix D .....</b>	<b>125</b>
<b>Appendix E .....</b>	<b>127</b>
<b>List of Figures.....</b>	<b>130</b>
<b>List of Tables .....</b>	<b>138</b>
<b>Declaration.....</b>	<b>142</b>
<b>Curriculum Vitae .....</b>	<b>143</b>

# Section 1

## Introduction

### 1.1 Problem statement

Light affects humans in visual and non-visual ways. In recent years, a growing body of research has continuously presented new information about the non-visual effect of light on well-being of humans. The new discoveries suggest a strong need to incorporate non-visual aspects of light in the evaluation of illumination in spaces to be able to maintain healthy lighting in living and working environments that align with physiological processes of humans.

Currently, lighting simulations primarily focus on the visual aspects of light to maintain thresholds prescribed by standards and guidelines. Since the discoveries regarding the non-visual effect of light are relatively new and ongoing, only a few recommendations regarding the appropriate levels of light that account for the latest findings exist [1, 2]. Nevertheless, there is a growing demand for lighting tools that consider the spectral properties of light, which is essential for calculating non-visual metrics. Several tools that produce non-visual metrics based on the spectral properties of light have been previously proposed. However, a few ambiguities are associated with their use. The appropriate number of channels in a spectral simulation and whether it significantly impacts the outcome remains to be determined. Furthermore, a framework that produces matrix-based annual simulations has not been previously proposed.

Spectral simulations may also potentially influence the evaluation of lighting energy demand. Lighting makes up a significant part of the end-use energy in non-residential buildings in Germany, approximately 17 % or 55 TWh [3], although higher percentages have also been reported in the literature, presumably before the universal shift to LED lighting. Provided a reasonable framework for annual simulations is proposed, the effect of spectral simulations on the annual lighting energy demand must be investigated. Since multichannel spectral simulations depict the spectrum of light with higher accuracy than what is commonly granted by the non-spectral simulation tools, the findings may be relevant for more accurate predictions of lighting energy demand, especially for light

sources with discontinuous spectra, such as fluorescent luminaires. However, finer spectral discretization of the commonly used LED lights that do not have a perfectly even spectral power distribution in the visible spectrum between 380 nm and 780 nm can potentially influence the annual lighting energy demand evaluation.

## 1.2 Research objectives

The objective of this dissertation is twofold. The main goal is to develop a matrix-based method for annual multichannel daylight simulations that includes the possibility of spectral modeling of the sky for each timestep. A point-in-time multichannel simulation of electric light should complete the framework for determining the annual lighting energy demand for the luminaires needed to maintain acceptable illuminance levels in the reference office room.

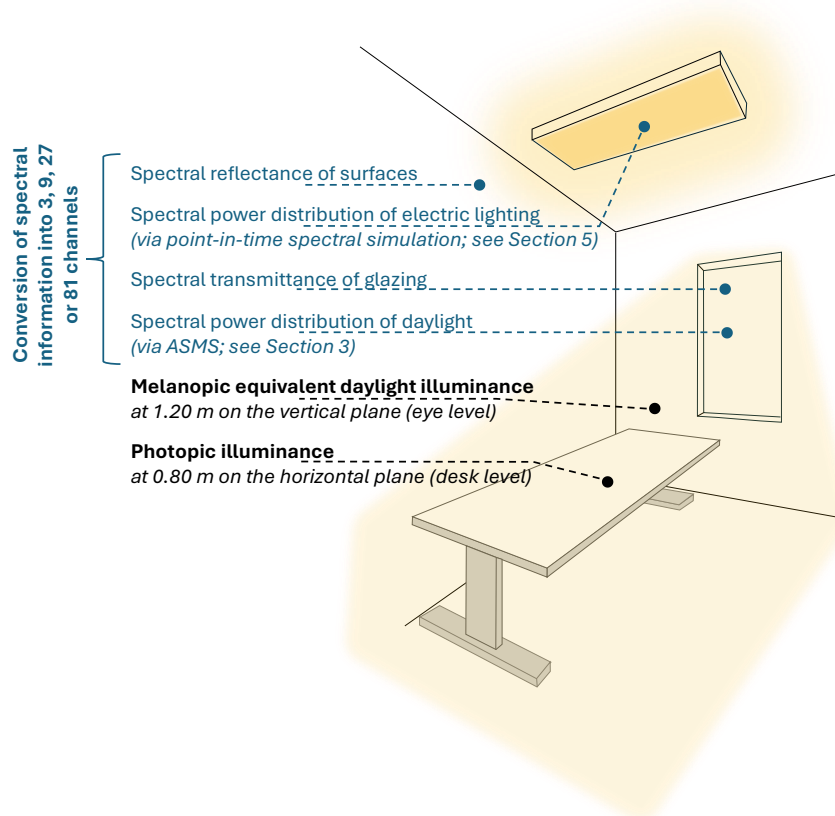


**Figure 1.** Aspects that need to be considered in the development of the annual multichannel lighting simulation.

The second objective is to compare the influence of discretization on the accuracy of the results. This work considered discretization of the visible spectrum into three, nine, 27 and 81 channels. Here, metrics that describe visual and non-visual effects of light, namely photopic illuminance and melanopic equivalent daylight illuminance, are evaluated.

Additionally, the annual lighting energy demand of the supplementary electric light needed to maintain an appropriate light level is compared between the simulations with fine and coarse discretization for luminaires with continuous and discontinuous spectra.

### **1.3 Research question**

Provided that a matrix-based annual spectral simulation of daylight is feasible, the research questions are as follows:

1. How does the spectral discretization of daylight and electric light influence photopic and melanopic equivalent daylight illuminance?
2. How does spectral discretization of daylight and electric light influence electric lighting demand?

### **1.4 Research outline**

This section provides an overview of the dissertation:

#### Section 2: State of the art of non-visual effects of light in simulation tools

This section provides a background about the non-visual effects of light to inform the reader about the state-of-the-art discoveries in the field. Here, a review of studies investigating the effect of illuminance, correlated color temperature (CCT) and monochromatic light on alertness is summarized. Additionally, this section presents various quantities previously proposed in the literature that consider the spectrum of light. In terms of simulation-based evaluations, simplified methods that generate non-photopic metrics via various post-processing workarounds in conventional lighting simulations are reported here. Lastly, this section discusses state-of-the-art spectral simulation tools, including the previously developed and validated point-in-time multichannel simulation tool by the author of this thesis.

#### Section 3: Annual spectral matrix simulation (ASMS) method

This section presents the ASMS method, starting with a description of the tools necessary for its generation. The framework of ASMS, based on the daylight coefficient approach, is broken down into two main parts. The first part is the precomputation of the spectral sky patch matrix, where each of the 145 sky patches is assigned an individual spectral power distribution based on luminance-to-CCT correlation. Discretization of the spectral power distribution into three, nine, 27 and 81 channels is also introduced here. The second part describes the setup of the ASMS and post-processing steps needed to convert the output

into the metrics considered in this thesis, namely the photopic illuminance and the melanopic equivalent daylight illuminance.

#### Section 4: ASMS for daylighting

This section presents the results of the ASMS for daylighting. Firstly, the properties of the office room and the climate are elaborated here. Then, the variability associated with hemispherical sampling was investigated by running ten ASMS with  $N$ -channels and analyzing the standard deviation of the hourly integral irradiance in the visible spectrum. Further, this section presents the annual hourly results of photopic and melanopic equivalent daylight illuminance obtained via ASMS with three, nine, 27 and 81 channels. The results of the ASMS serve as a basis for spectral simulations for electric lighting in Section 5. Finally, this section ends with a short discussion about the reason behind the difference between photopic and melanopic equivalent daylight illuminance results.

#### Section 5: ASMS and point-in-time spectral simulation with electric light

Here, the framework for generating spectrally resolved electric light via point-in-time simulation needed to supplement daylighting is described. Two LED and one fluorescent luminaires are selected for the comparative analysis. The section presents the spectral power distribution, luminous intensity distribution and the respective maintenance factors of the luminaires, along with their positions in the office room. The simulation framework needed to set up a multichannel spectral simulation in Radiance is elaborated here. The variability and illuminance of the simulations with electric light with three, nine, 27 and 81 channels are examined. Additionally, this section explains the group-dependent dimming of the luminaires needed to supplement daylight and maintain an appropriate level of illuminance indoors. Lastly, the section ends with a short discussion of the spectral simulation with electric light

#### Section 6: Lighting energy demand and dimming factor

This section discusses the annual lighting energy demand of the three types of luminaires in a multichannel spectral simulation. First, the results generated based on photopic- and melanopic-based dimming in the simulation with three, nine, 27 and 81 channels were investigated. Then, conventional photopic-only dimming was discussed. This section also examines the triggering of the dimming factor in different zones of the office room based on photopic-melanopic dimming and the photopic-only dimming strategy. The section ends



with a discussion of the lighting energy demand regarding different channels and dimming possibilities.

#### Section 7: Discussion

This section contains the summary of the thesis and the recommendations that resulted from this work for architects and lighting designers.

#### Section 8: Conclusion

The last section contains the conclusion of the thesis, limitations and outlook for future work.

## Section 2

# State of the art of non-visual effects of light in simulation tools

### 2.1 Background and significance of non-visual effects of light on humans

Recent discoveries suggest that light impacts humans in a non-visual manner by affecting alertness, cognitive performance, and physiological responses such as circadian clock, hormone production, and temperature regulation in humans [4–10]. These findings are attributed to the newly discovered type of photoreceptor, intrinsically photosensitive retinal ganglion cells (ipRGCs) that contain the melanopsin photopigment with a peak spectral sensitivity in the short-wavelength range (~ 490 nm) [11–14]. Light is, therefore, converted by photoreceptors into signals that stimulate various biological processes in humans.

The ipRGCs transmit light information to the mammalian internal clock, the suprachiasmatic nuclei in the hypothalamus. Light information allows the suprachiasmatic nuclei to synchronize physiological processes that influence the mechanisms responsible for sleepiness, alertness, vigilant attention, psychomotor and perceptual-cognitive speed and working memory to fit a near-24-hour circadian cycle [15–17]. It was found that even some blind individuals with preserved ipRGCs can experience melatonin suppression [16], reset of the circadian pacemaker, and improvement in alertness when exposed to cool-white or short-wavelength light despite non-functioning cones and rods [18].

The link between light and circadian rhythm is complex, with several factors such as timing, intensity, duration, pattern, wavelength and previous history of light exposure having a resetting effect, thereby playing an essential role in mediating alertness [19]. However, ipRGCs are not the sole photoreceptors that non-visually affect humans. Rods and cones, with their respective photopigments rhodopsin, cyanopsin, chloropsin and erythropsin, also contribute to non-image-forming (NIF) responses [20, 21]. In well-sighted mammals, NIF responses to light are partially sustained by signals from cones in addition to the dominant inputs from melanopsin-expressing photoreceptors [22, 23]. Figure 2

shows the relative spectral sensitivity curves of the five photoreceptors with their respective photopigments.

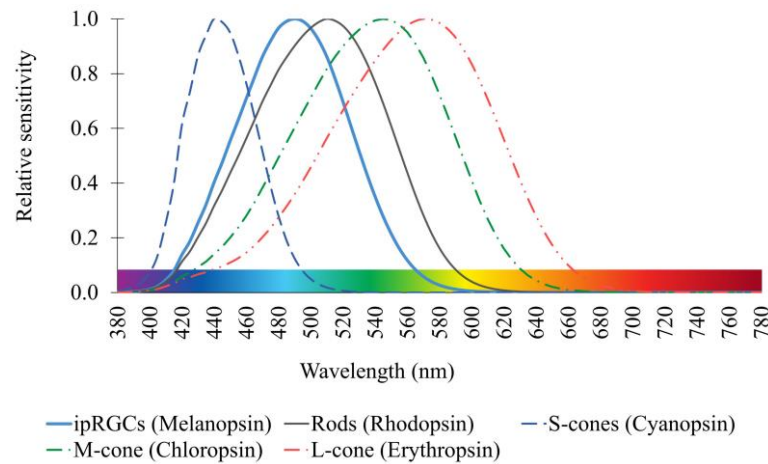


**Figure 2.** Relative spectral sensitivity in the visible spectrum (from 380 nm to 780 nm) of the five photoreceptors and their photopigments: ipRGCs (melanopsin), rods (rhodopsin), S-cone (cyanopsin), M-cone (chloropsin) and L-cone (erythropsin).

Previous studies have indicated that light can increase morning vitality and counter daytime mental fatigue [24, 25]. Understanding the properties of light that enhance alertness through sustained attention and increased productivity during daytime can improve the illumination of workspaces as well as living spaces. The following sections present studies that investigated alerting effects of light induced by illuminance, CCT and monochromatic light during daytime.

A total of 142 studies were retrieved from Science Direct (n = 40), PubMed (n = 62) and Scopus (n = 40) based on the keywords “alertness” and “light”. Only original research papers were considered (n = 109). The duplicates that occurred across different databases were removed (n = 65). Only papers that looked at the effect of light during daytime were retained (n = 26). After screening the papers, 20 papers were left for review. The studies investigated the effect of the illuminance (n = 10), CCT (n = 6) of polychromatic light and monochromatic light (n = 4) on alertness during daytime. Figure 3 shows the summary of the selection process of the studies that were retrieved for the review. The full review has been previously presented in [26].

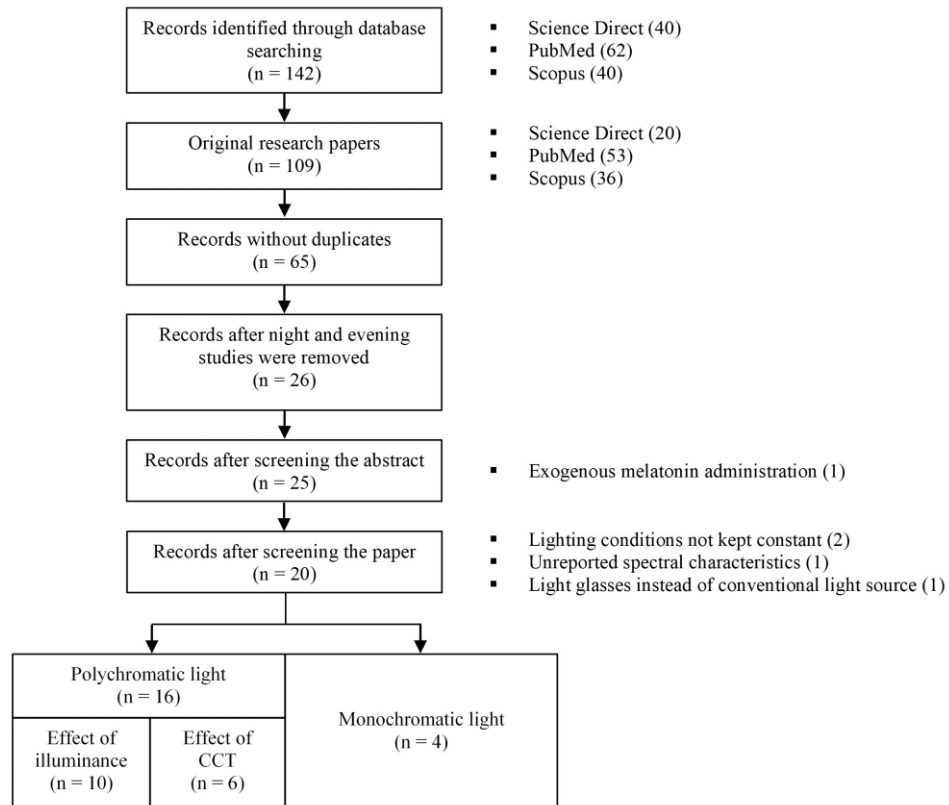


**Figure 3.** Summary of the selection process of the studies for the review that investigated the alerting effect of light during daytime.

### 2.1.1 Effect of the illuminance on alertness during daytime

Three of the studies recorded no increase in alertness when illuminance was increased compared to the control conditions in the respective studies [8, 27, 28]. One study reported a very modest linear relationship between the log-transformed illuminance and subjective correlates of alertness [29]. Another study reported a modest reduction in subjective sleepiness after exposure to bright light [30]. Another work found that the immediate alerting effect, which increased subjective vitality and decreased subjective sleepiness, was attributed to the abrupt increase of illuminance [31].

Elsewhere, it was found that the increase in illuminance increased vitality and reduced subjective sleepiness [25]. One of the investigated studies recorded that an increase in illuminance affected the electric activity of the human brain more than subjective and objective markers of alertness [32]. Two further studies found an altering effect of bright light [33, 34]. However, the effects were analyzed in comparison to dim lighting conditions. Figure 4 shows the main outcomes of the studies that isolated the effect of illuminance on alertness during daytime in the review.

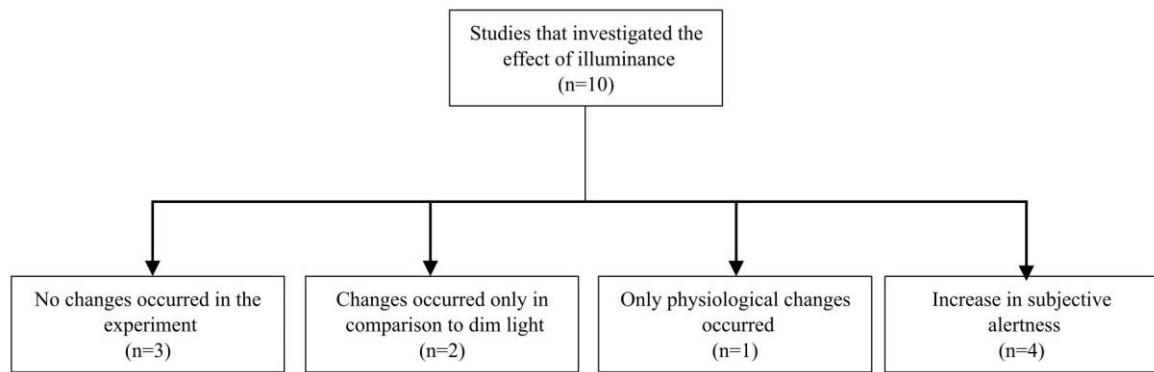


**Figure 4.** *The main conclusions of the studies that investigated the alerting effect of illuminance during daytime.*

### 2.1.2 Effect of the CCT on alertness during daytime

All studies in this category showed at least a minor effect of CCT on alertness. One study found that exposure to light with 12000 K and 2700 K at 500 lx improved the physiological indicators in comparison to neutral white and dim light but did not affect subjective alertness or performance [35]. Another study reported an improvement in physiological indicators due to exposure to blue and green LED pulses combined with dim background illumination [36]. The study did not investigate the effects of LED pulses on performative and subjective markers of alertness

In another work that examined the impact of light transitions on measures of alertness, it was found that study participants felt significantly more vital and alert after switching from warm white light to cool white light [37]. A different study looked at seasonal aspects of light by investigating the effect of CCT on alertness in autumn and spring [38]. The authors found that exposure to daylight with CCT of 12370 K fostered higher levels of alertness in students in the afternoon in autumn when compared to daylight with CCT of 3870 K.

Further investigation found that red monochromatic light reduced reaction time in the performance tests compared to the polychromatic white light of the same irradiance and dim light [39]. Another study found that the light with 7717 K slightly improved the response speed on a performance test in sleep-restricted individuals [40]. The summary of the studies that isolated the effect of CCT on indicators of alertness during daytime is shown in Figure 5.

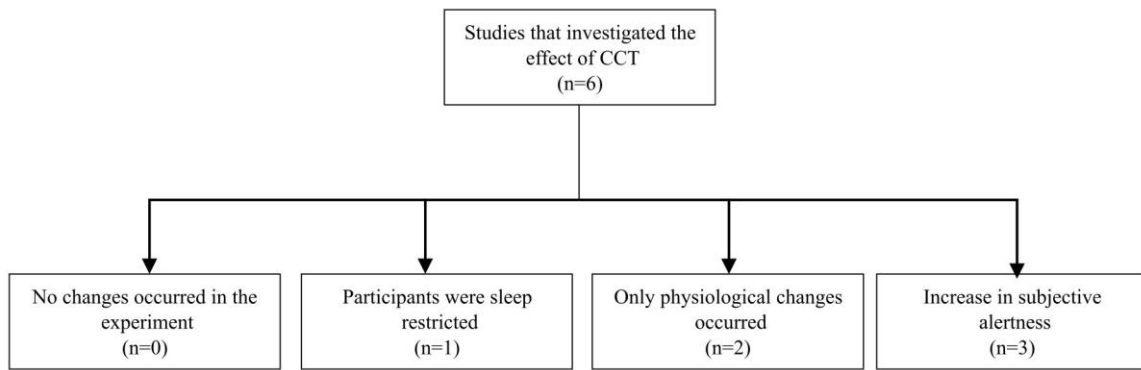


**Figure 5.** The main conclusions of the studies investigated the alerting effect of CCT during daytime.

### 2.1.3 Effect of the monochromatic light on alertness during daytime

Out of the four articles in this category, only one study has not recorded any alerting effect in relation to the exposure to blue, green or red monochromatic light [41]. One study concluded that the alerting effect to red (625 nm) or blue monochromatic light (465 nm) was minimal and did not translate into performative or subjective improvements in alertness [42].

Another study compared the alerting effects of monochromatic light at identical levels of irradiance against dim light. The authors concluded that the subjects of their study felt less sleepy under monochromatic light with 455 nm than under 508 nm, 629 nm or dim light [43]. Another work found physiological changes using electroencephalographic registration that signified increased alertness after exposure to blue light (465 nm). The impact of red light (630 nm) was not apparent, but the tendency of increased alertness was evident. Figure 6 shows the primary outcomes of the studies that isolated the effect of different monochromatic light sources on alertness during daytime in the review.

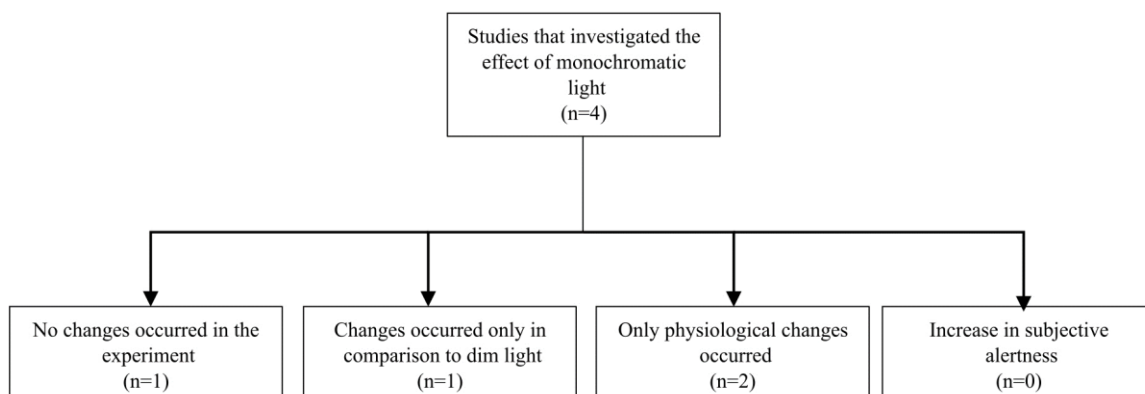


**Figure 6.** The main conclusions of the studies that investigated the alerting effect of monochromatic light during daytime.

## 2.2 Non-photopically weighted quantities

Current regulations primarily focus on controlling the visual effect of light in the built environment due to a lack of consensus about the exact relationship between light and NIF responses. The following section presents non-photometric quantities that weigh spectral power distribution of light by different spectral functions, as this is an essential step toward addressing the non-visual effects of light.

The circadian action factor,  $a_{cv}$ , describes the circadian efficiency of a light source through a relative ratio between spectral irradiance weighted by the circadian and the photopic spectral sensitivity functions [44, 45]. Circadian spectral sensitivity function was established based on the trial in which the suppression of nocturnal melatonin production as a response to light at different wavelengths was investigated [46, 47]. No optimal threshold for  $a_{cv}$  ratio has been previously proposed in the literature. The  $a_{cv}$  metric is expressed through Equation 1:

$$a_{cv} = \frac{\int E_{e,\lambda}(\lambda) C(\lambda) d\lambda}{\int E_{e,\lambda}(\lambda) V(\lambda) d\lambda} \quad (1)$$

where:

- $a_{cv}$ : circadian action factor  
 $E_{e,\lambda}(\lambda)$ : spectral irradiance (W/m<sup>2</sup>/nm)  
 $C(\lambda)$ : circadian spectral sensitivity function  
 $V(\lambda)$ : photopic spectral sensitivity function

Another quantity entitled circadian ratio,  $\eta_c$ , was previously introduced in [48]. Here, the ratio is between the integral of the spectrally circadian-weighted irradiance and integrated spectral irradiance. The calculation takes place according to Equation 2:

$$\eta_c = \frac{\int E_{e,\lambda}(\lambda) C(\lambda) d\lambda}{\int E_{e,\lambda}(\lambda) d\lambda} \quad (2)$$

where:

- $\eta_c$ : circadian ratio  
 $E_{e,\lambda}(\lambda)$ : spectral irradiance (W/m<sup>2</sup>/nm)  
 $C(\lambda)$ : circadian spectral sensitivity function

Previously, melanopic illuminance, a metric that weights the spectral power distribution of light with the spectral sensitivity function of ipRGCs, was proposed in [49]. The calculations are done according to Equation 3, where constant 4,557 ensures one melanopic lux to one photopic lux scaling at 555 nm:

$$E_{mel} = 4,557 \int E_{e,\lambda}(\lambda) s_{mel}(\lambda) d\lambda \quad (3)$$

where:

$E_{mel}$ : melanopic illuminance (melanopic-lx)

$E_{e,\lambda}(\lambda)$ : spectral irradiance (W/cm<sup>2</sup>/nm)

$s_{mel}(\lambda)$ : melanopic spectral sensitivity function

The emergence of equivalent melanopic lux (EML) replaced melanopic illuminance, in which the scaling of the melanopic sensitivity function was adjusted [50]. In doing so, the melanopic illuminance became equivalent to photopic illuminance for the equal-energy radiator. Equation 4 presents the calculation for equivalent melanopic lux:

$$EML = 72,983.25 \int E_{e,\lambda}(\lambda) s_{mel}(\lambda) d\lambda \quad (4)$$

where:

$EML$ : equivalent melanopic lux (EML)

$E_{e,\lambda}(\lambda)$ : spectral irradiance ( $\mu$ W/cm<sup>2</sup>/nm)

$s_{mel}(\lambda)$ : melanopic spectral sensitivity function

WELL Building Standard provides recommendations for the equivalent melanopic lux levels that should be maintained in various spaces [2]. For example, it recommends at least 150 EML at the vertical eye level for all workstations, where at least 75 % of workstations maintain 200 EML. In breakrooms, the standard suggests maintaining 250 EML at the vertical eye level. In living spaces, WELL prescribes 200 EML at the vertical eye level during daytime and not more than 50 EML at the horizontal level during nighttime. Equivalent melanopic lux of 125 at the vertical eye level for at least 4 hours per day is suggested for learning areas for students under 25 years of age. However, the particular sources of the selected thresholds are not referenced in the WELL Building Standard.



The most recent version of melanopically weighted illuminance was proposed by the International Commission on Illumination (CIE). CIE has previously published standard CIE S 026:2018 entitled “CIE System for Metrology of Optical Radiation for ipRGC-Influenced Responses to Light.” The standard presented the spectral sensitivity functions and metrics of five ( $\alpha$ -opic) photoreceptors (refer to Figure 1) that contribute to evoking non-visual effects in humans [51]. The standard does not provide recommendations or predictions regarding ipRGC-influenced responses but presents the steps to calculate  $\alpha$ -opically weighted metrics from spectral radiance or irradiance. A derivative metric of melanopic irradiance is the melanopic equivalent daylight (D65) illuminance (mEDI), which represents the illuminance of the D65 illuminant needed to achieve the same melanopic irradiance. MEDI can be calculated according to Equation 5:

$$E_{v,mel}^{D65} = \frac{\int E_{e,\lambda}(\lambda) s_{mel}(\lambda) d\lambda}{K_{mel,v}^{D65}} \quad (5)$$

where:

$E_{v,mel}^{D65}$ : melanopic equivalent daylight (D65) illuminance (lx)

$E_{e,\lambda}(\lambda)$ : spectral irradiance (mW/m<sup>2</sup>/nm)

$s_{mel}(\lambda)$ : melanopic spectral weighting function

$K_{mel,v}^{D65}$ : melanopic daylight (D65) efficacy ratio (1.3263 mW/lm)

Recently, a publication entitled “Recommendations for daytime, evening, and nighttime indoor light exposure to best support physiology, sleep, and wakefulness in healthy adults” was published by a group of researchers in the respective field [1]. The publication provides recommendations for healthy daytime, evening and nighttime light exposure for humans. The authors of the publication reached a consensus that melanopic equivalent daylight illuminance of at least 250 lux at the eye level should be reached during daytime through daylight but also deemed polychromatic white light an acceptable option. The publication suggests a maximum melanopic equivalent daylight illuminance of 10 lux at eye level in the evening. For unavoidable nighttime activities, maximum melanopic equivalent daylight illuminance of 1 lx at the eye level was deemed an acceptable degree of exposure in the publication. A newer version of the WELL Standard (WELL v2) adopted the suggestion for daytime exposure [52].

The Circadian Stimulus (CS) metric was previously introduced to quantify how circadian-effective light ( $CL_A$  2.0, referring to the updated definition in [53, 54]) stimulates the neural signal that reaches the biological clock in suprachiasmatic nuclei in terms of melatonin suppression. CS model is based on the concept that circadian phototransduction is evoked by the receptor signals determined by the opponent process theory. This means that if the blue channel (S-cone response) has a weaker signal than the yellow channel (sum of M-cone and L-cone responses), which typically occurs with “warm” light sources, the circadian phototransduction is evoked solely by the ipRGC signals. Otherwise, the model considers that the signal is evoked by the combination of ipRGC, cones and rods, which occurs with “cool” light sources [53].

The above-described model has been previously introduced in the form of the CS Calculator [55]. The CS calculator quantifies light in terms of  $CL_A$  2.0. based on the power distribution and photopic illuminance. Based on  $CL_A$  2.0., the CS is then calculated alongside other metrics such as correlated color temperature, color rendering index and gamut area index. For example, a CS of 0.7 indicates 70 % of melatonin suppression. A recommended circadian-effective light dose ( $CS_d$ ) of 0.43 was previously proposed in [56]. The CS calculator proposes the exposure duration based on the provided spectral power distribution and photopic illuminance needed to reach the functionally recommended  $CS_d$ . However, it is unclear whether exceeding this threshold at a later time in the workday may affect the circadian rhythm in a counterproductive way.

While many quantities have been previously proposed for evaluation of the non-visual spectral effectiveness of light, usually, the suggestion for the appropriate threshold is not provided. Such quantities are usually helpful in comparative assessments rather than in actual lighting design, for which references are necessary to consider an appropriate level of illumination with respect to non-visual aspects in spaces. This is the case with most of the quantities described in this section except for CS and melanopic equivalent daylight illuminance, for which appropriate levels were indicated by the respective research groups.

### **2.3 Background of generation of non-photometric quantities in post-processing**

Prior to the invention of spectral simulation tools, many studies proposed simplified frameworks to generate non-photometric quantities via various post-processing steps in

conventional lighting simulations. The following section presents studies that have employed such an approach.

One study assessed circadian efficacy in a hospital room [57]. The unit was defined as circadian-weighted irradiance with certain assumptions. The relative spectral power distribution of known illuminants was weighted by the circadian sensitivity function with respect to photopic illuminance that was obtained through DAYSIM and RELUX simulations. Another study extended the approach to examining the effects of architectural decisions in row housing on available daylight necessary for synchronizing the circadian system [58].

A more complex human-light response model that is based on a non-linear function of light intensity and non-visual relative response and is also dependent on light spectrum, timing of exposure, prior light history and age was implemented in post-processing of DAYSIM daylight simulation [59, 60]. The same model was used to evaluate light exposure holistically in a Radiance-based lighting simulation tool [61, 62]. Another study proposed a framework that uses Radiance calculation engine to generate an illuminance profile to investigate how lighting conditions affect health and delight by additionally considering the spectral component as well as other relevant factors in post-processing steps [63].

A climate-based simulation framework that investigates potential non-visual effects of daylight in buildings was previously proposed in [64]. The framework relies on the Radiance-based simulation tool for the annual prediction of illuminance at the eye level. The post-processing steps included integrating a photobiology-based model that considers the effect of spectrum, intensity and timing of the daylight exposure to evaluate the cumulative annual non-visual effect. Another climate-based study used melanopic ratio conversion to obtain equivalent melanopic lux for each hour of the year and compare it to the requirements prescribed by the WELL Building Standard [65].

One study proposed a framework to expand the traditional lighting simulation approach to obtain equivalent melanopic lux and  $CL_A$  via post-processing steps based on theoretical conversions [66]. In another work, CS was post-processed based on the illuminance obtained from Honeybee simulation and the assumption that the spectral power distribution of daylight corresponds to the D65 CIE illuminant [67]. Elsewhere simplified approach to obtain equivalent melanopic lux, melanopic equivalent daylight illuminance,  $CL_A$  and CS

was presented in [68], where the quantities were obtained by applying various conversions to vertical illuminance simulated via DIALux lighting simulation software.

The following two studies utilize a similar idea of applying additional post-processing steps to the photometric quantities to obtain non-visual ones. However, the spectral reflectance and spectral properties of the materials in the room are regarded in addition to the spectral power distribution of the illuminants in the below-mentioned studies. Both studies present steps to derive CS and the Circadian Stimulus Autonomy (CSA) from photopic illuminance obtained via DAYSIM simulation and manually calculated resultant spectral reflectance of the considered surfaces and illuminants [69, 70].

Some studies have proposed workflows to obtain non-photopic metrics using Radiance lighting simulation tool by intervening in the conventional post-processing steps of the Red, Green and Blue (RGB) triplets [71, 72]. One study converted the Radiance RGB triplets to obtain circadian-weighted irradiance [73]. Another study applied post-processing steps to convert the RGB triplets to melanopic illuminance [74]. However, neither study specified whether surfaces and illuminants were considered spectrally in three channels in their workflows. Another work proposed rough approximations to obtain the circadian action factor,  $a_{cv}$ , from RGB-rendered images [75].

The studies in this section have presented multiple frameworks to obtain non-photometric quantities by proposing various post-processing steps to conventional lighting simulation tools. However, these methods should be regarded as limited workarounds to obtain approximate non-photometric quantities since actual values must be derived based on the spectral information of the entire environment to ensure complete accuracy. For example, most of the methods in the studies presented in this section considered only the spectral power distribution of illuminants without considering the spectral properties of the other materials, which significantly undermines the actual spectrum perceived by the observer, as previously reported in [69, 76]. Two studies included information about the spectral reflectance of the surfaces. However, this was done in a simplified manner by multiplication of spectral power distribution and spectral reflectance of selected surfaces without considering the spectral properties of the reflected and inter-reflected light. [69, 70].

## 2.4 State-of-the-art spectral simulation tools

Since the spectrum of light is one of the main components that affect various biological processes, spectral simulation at a detailed resolution that accounts for the full spectral characteristics of illuminants and materials must be utilized to quantify the non-photometric effect. Eventually, spectral simulation tools will be used to predict precise non-visual effects of light in spaces once the exact link between photoreceptor contribution and NIF responses is established in the respective field of research.

Previously a tool entitled Color Quality Assessment Tool (CQAT), otherwise known as Spectral Color Property Assessment Tool (SCPAT), which incorporates spectral input for surfaces and illuminants, has been developed and compared against real-life measurements to ensure accurate evaluation [76, 77]. The tool generates total luminous flux and spectral power distribution of light from the viewpoint of the observer based on the calculation of direct and indirect reflection of light across finite meshes that are determined by the room grid. The spectral output enables the generation of metrics such as CCT, color coordinates and  $a_{cv}$ . Unfortunately, the tool is not available for public access and the methodology that processes spectral information has not been published elsewhere.

A commonly used framework to achieve physical accuracy for spectral modeling in Radiance lighting simulation tool, the  $N$ -step algorithm, was previously introduced in the field of psychophysics [78–80]. The  $N$ -step algorithm discretizes the visible spectrum from 380 nm to 780 nm into  $N$  channels. If the visible spectrum is to be discretized into nine channels ( $N = 9$ ), three separate Radiance simulations for a discrete spectral band must be performed. This approach is unlike a single simulation in the conventional RGB method, where three channels can be used to represent the visible spectrum. The number of channels in the  $N$ -step algorithm is not restricted to nine. It is an arbitrary number that can be defined based on the needed fineness of discretization.

A similar stepwise approach has been previously used in color computation, in which the spectral curve is reduced to several spectral values [81]. The  $N$ -step algorithm was previously used in spectral rendering with nine channels and validated for luminance and color accuracy in a room with electric lighting [78]. Many studies in the field of built environment have adopted the  $N$ -step algorithm to predict metrics weighted by the circadian and melanopic spectral sensitivity functions [71, 82].

Currently, a few relatively new Radiance-based tools implement the  $N$ -step algorithm for the same purpose. The following sections present studies that either utilized or invented  $N$ -step algorithm tools. Sections 2.4.1, 2.4.2 and 2.4.3 present spectral simulation tools that are based on  $N$ -step approach: ALFA, LARK and OWL. Finally, Section 2.4.4 summarizes the point-in-time  $N$ -channel spectral simulation framework that was previously proposed by the author of this thesis in [83].

#### **2.4.1 Adaptive Lighting for Alertness (ALFA)**

ALFA is a licensed plug-in for Rhinoceros 3D software that uses Radiance as a lighting engine renderer to perform 81-channel spectral simulations for daylight and electric light [84, 85]. The sun and sky are both regarded spectrally and are generated with the help of a radiative transfer library (libRadtran) for every location that provides atmospheric inputs such as oxygen, water vapor, pressure and other information necessary for the calculation [86, 87]. There is a possibility of selecting sky conditions, spectral properties of ground and materials in ALFA [86].

Several studies have explored the spectral simulation tool. One study investigated the effect of daylighting, various luminaires and several glazing types in a theoretical office room [88]. The spectral functionality of the tool enabled the evaluation of equivalent melanopic lux in a room. A threshold of 200 EML was adopted in the analysis. The investigation was done for a total of eleven hours on March 21<sup>st</sup>. Since ALFA does not support annual simulations, analysis is only possible for a limited number of hours at a time.

Another study investigated the increase in lighting energy when equivalent melanopic lux was considered according to recommendations of the WELL standard in a classroom and an office room [89]. ALFA tool was used to calculate equivalent melanopic lux for the relevant positions in the room. The study compared the energy demand for different luminaires, assuming that the luminaires operated a total of 4000 hours in an office room and 1500 hours in a classroom annually. While this study uses a very simplified approach without involving findings of daylighting simulation as the basis for the calculation of electric lighting demand, it is one of the very few studies that considered the aspect of lighting energy in combination with non-photopic metrics.

ALFA was used in another study to simulate equivalent melanopic lux during the summer solstice, winter solstice and fall equinox at 11 am in a simplified office room [90]. The study evaluated the impact of various architectural parameters via Useful Daylight

Illuminance and melanopic equivalent daylight illuminance according to the recommendations of the WELL Building Standard in point-in-time simulation.

Enhancement of the environment to promote well-being and cognitive health in individuals with vulnerabilities via simulation of non-visual effects of daylighting was investigated in [91]. Using ALFA, the study analyzed how many hours between 7 am and 6 pm on June 21<sup>st</sup>, September 21<sup>st</sup>, and December 21<sup>st</sup> reached 450 -500 EML in a north-facing bedroom in a nursing home. This threshold of equivalent melanopic lux was regarded as adequate to entrain the circadian system of elders or individuals with cognitive health vulnerabilities.

Another work examined the influence of various preferred wall colors on CS between 7:00 and 17:00 on December 21<sup>st</sup> and March 21<sup>st</sup> in a simulated work environment for four view directions (north, south, west and east) [92]. Since ALFA does not report CS, the tool was used to obtain the resultant spectral power distribution at the eye level, which was later used for manual calculations of CS. In a later study, the authors investigated the impact of seven glazing systems and six wall color hues (at three reflectance levels) on CS and equivalent melanopic lux in a simulated office room [93].

Only a few studies have investigated the accuracy of ALFA in comparison to actual measurements to understand the possible accuracy. One study has compared ALFA and another spectral simulation tool against real-life spectral measurements of three luminaires. The study found that ALFA had the most accurate prediction of spectral irradiance between the two tools. However, the discrepancy between the ALFA simulation and the measurements ranged from -28.6 % to 33.4 % [94].

Another study compared the accuracy of spectral simulation tools, including ALFA, in a scenario with daylighting conditions. The authors found that the average fluctuation from the measured spectra was rather significant, where the difference between measurements and the ALFA tool reached up to 37 % [95]. In a later study, the authors investigated the accuracy of ALFA and another spectral tool in relation to ipRGC-influenced light responses. They found that at least 26 % of the daylight exposures simulated for six hours using ALFA tool led to a significant error [96].

#### **2.4.2 LARK Spectral Lighting**

LARK is an open-source plug-in for Grasshopper that predicts photopic illuminance, circadian-weighted illuminance and equivalent melanopic lux [97, 98]. The tool is operated through Rhinoceros 3D software and relies on Radiance simulation engine. The tool allows

users to assign custom spectral compositions for the sky, spectral transmittance of glazing and spectral reflectance of surfaces. LARK implements the  $N$ -step algorithm, thereby representing the visible spectrum with nine channels, where each channel accounts for a discrete wavelength band. Nevertheless, spectral simulations with three channels are possible too. Recently, two improved versions of the tool were released: LARK 2.0 and 3.0. LARK 2.0 includes the possibility of simulating electric lighting [99]. LARK 3.0 improves on the 2.0 version by considering the spectrum of the sun [100].

The learning curve to use the tool is relatively steep since LARK requires the knowledge of Grasshopper. Thereby, fewer studies have investigated the functionalities of this tool in literature. However, a relatively recent study has integrated a component from LARK tool into a Climate Based Daylight Modelling (CBDM) tool entitled Design Assist Tool in order to predict annual circadian lighting requirements. However, the study has not specified how the dynamic spectral nature of daylight was considered for each timestep in annual calculations [101].

A study used LARK simulation tool to evaluate equivalent melanopic lux in the office room and analyze whether it complies with the WELL building standard [102]. LARK was used as part of a broader framework in the study to ensure that a daily minimum threshold of 200 EML is achieved in the early part of the day in order to entrain circadian rhythm of the office room occupants.

Other studies have compared LARK and other spectral simulation tools with actual measurements in order to evaluate the accuracy of the programs. One study found that LARK had the most accurate prediction when investigating indoor daylight. The accuracy of LARK tool is comparable to the typical Radiance daylight simulation (i.e., errors in  $\pm 20\%$  range) despite being more time-consuming than the other tools [95]. Another study found that only 9% of the daylight exposures simulated for a six-hour period using LARK led to a significant error, which significantly outperformed ALFA [96].

### **2.4.3 Occupant Wellbeing through Lighting (OWL)**

OWL is a Grasshopper plug-in tool originally scripted to generate spatially and spectrally resolved sky models using luminance-to-CCT correlation (see Section 3.3 for elaboration of the correlation) [103, 104]. This development overcomes the limitation of LARK tool, where spectral power distribution or CCT of the sky must be assigned by the user. The luminance-to-CCT conversion is based on the generation of false color images, from which



luminance information for each respective sky patch is obtained and converted to CCT and, consequently, spectral power distribution according to the CIE reconstruction procedure [105]. The tool uses Radiance as its simulation engine and  $N$ -step algorithm. However, only three-channel simulations are possible in OWL.

The other output of the OWL tool is the resultant spectral power distribution at any point of view inside a room. The spectral power distribution at the viewpoint is then post-processed in the tool to derive photopic, circadian and melanopically weighted metrics. As of today, the tool has not been compared to other spectral simulation tools nor validated by measurements. Therefore, the accuracy of the results that are yielded by OWL is still to be determined.

#### **2.4.4 Point-in-time spectral simulation**

In another publication, the author of this thesis developed a multichannel spectral simulation tool and experimentally validated it for different lighting scenarios [83]. The tool adapted and extended the  $N$ -step algorithm by implementing several changes to the source code of LARK 1.0. The main changes included extending the spectral channels beyond three and nine to 27 and 81 and adding the possibility to perform spectral simulations with electric light and combined light (electric + daylight). The paper aimed to investigate the effect of low and high spectral resolution of different lighting scenarios on the prediction accuracy.

The  $N$ -step algorithm was validated for the calculation of integral irradiance (between 380 nm and 780 nm) in a physical model with three lighting scenarios: diffuse daylight, LED electric light and a combination of diffuse daylight and LED electric light. The “shoebox” model, which was elevated from the ground by 0.09 m, had the following dimensions: 1.00 m  $\times$  1.01 m  $\times$  0.91 m. The interior surfaces were painted with pure white paint (RAL 9010) with an average reflectance of 85 %. The model had a removable wall, which was used in the scenario with LED electric light and replaced by electrochromic glazing for the scenario with daylight or combined light. Irradiance measurements were conducted on 14 (daylight or combined light scenario) or 17 points (electric light scenario) in the physical and theoretical models for validation purposes. Figure 7 shows the model and grid of points used in validation.

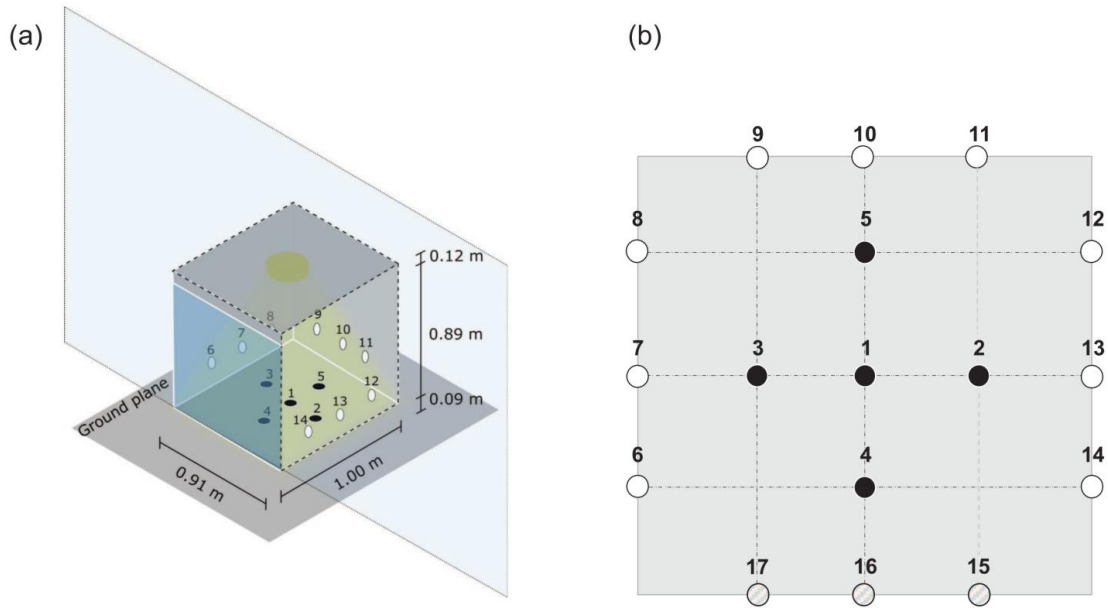


**Figure 7.** (a) Dimensions of the model with a removed wall positioned against a glazed façade. (b) Grid of the sensors points. Points 1-5 recorded horizontal illuminance on the floor of the model. Points 6-14 recorded vertical illuminance; the sensors were placed flat against the wall 0.20 m above the floor level. Points 15-17 were included additionally to measure vertical illuminance in the scenario with electric light.

All three lighting scenarios were simulated with three, nine, 27 and 81 channels. For scenarios with LED electric light and a combination of daylight and LED electric light, the nine-channel simulation improved the mean absolute percentage error (MAPE) between 13.9 % and 33.9 % compared to the three-channel simulation. For continuous diffuse daylight, there was only a small improvement of 0.4 % when increasing from three to 27 channels. Compared to nine channels, 27 channels slightly improved MAPE in all the scenarios but substantially increased the simulation time. It is noteworthy that the simulation time was affected by the fact that the  $N$ -intervals were not simulated in parallel. Additionally, all simulations considered continuous sky.

Increasing the number of channels to 81 is more likely to contribute to more complex scenarios, for example, in spaces where surfaces and luminaires in the room display discontinuous spectral properties. Nevertheless, the study shows that increasing the number of channels from three to nine significantly reduced integral irradiance even for sources with relatively continuous spectrum, such as LED electric light. This finding implies that an increase in the number of channels can potentially influence the photopic and non-photopic output of the luminaires, thereby affecting the lighting energy, too. Since the

developed tool was originally designed for point-in-time simulations, annual multichannel spectral evaluations, which would be necessary to investigate annual lighting energy demand, are not feasible here. Section 3 describes the annual spectral matrix simulation (ASMS) method developed to make such evaluations possible.

## Section 3

# Annual spectral matrix simulation (ASMS) method

### 3.1 Tools for ASMS

The following section describes the tools needed to set up the ASMS. The simulation relies on the use of Radiance, a validated suite of command-line programs for lighting simulation [62, 106]. Radiance uses backward ray tracing, meaning that light rays are traced from a measurement point (a viewpoint) back to the sources (emitters). Input files that specify the space geometry, surface materials, time, date and sky conditions (for daylight calculations) and luminaires (for calculations featuring electric lighting) are required in order to set up Radiance simulation. The simulation output can be presented as rendered images, diagrams or values representing different metrics.

Radiance employs a hybrid method that combines deterministic ray tracing with Monte Carlo sampling to provide a relatively accurate result rather quickly. Deterministic sampling is intended for sources with a direct contribution of light, such as the sun or luminaires. This type of sampling assumes that the emitter of light is known and sends the rays towards it. Deterministic sampling applies to the material type “light” that emits light in Radiance.

Monte Carlo ray tracing is a type of stochastic simulation method that relies on random sampling to generate outcomes. It is influenced by simulation parameters such as ambient bounces and ambient divisions. Ambient bounces describe how many diffuse inter-reflections will occur before discarding a ray path. To ensure that the ray is reflected enough times, this parameter needs to be chosen while taking the complexity of the geometry into account. The number of sample rays that are sent from a point during an ambient calculation is determined by ambient divisions. This parameter must be assigned considering the brightness gradient in the geometry. More sample rays need to be sent out from the points with low brightness.

The stochastic simulation method assumes that light can be traced in many directions. This is the case with skylight, where many directions must be “sampled” to determine where light comes from. This is known as hemispherical sampling, which applies to self-luminous surfaces described by material type “glow” in Radiance.

Many building simulation tools have integrated Radiance as the underlying lighting simulation engine. For example, Evalglare [107], OpenStudio [108], Groundhog [109] and Honeybee[+] [110] are Radiance-based tools. Furthermore, other tools rely on Radiance-based implementation of daylight coefficient [111] through Daysim such as DIVA4Rhino [112] and Ladybug-Honeybee [113] for the generation of various climate-based daylight metrics.

However, using Radiance programs via the command line grants users a lot more flexibility for the development of new and customized workflows. For this reason, the command-line use of Radiance in combination with Python is adopted in this thesis. Python is a programming language used for a multitude of purposes. In this work, Python (version 3.8.5) is used as an interface for calling various Radiance command-line tools [114]. This approach is common among users of Microsoft Windows, as Radiance was originally developed for Unix operating system.

### **3.2 ASMS framework**

This section presents the basic workflow of the ASMS method, which consists of the two main steps:

- 1) precomputation of the spectral sky patch matrix (refer to Section 3.3); and
- 2) the main ASMS followed by the post-processing steps to obtain required metrics (refer to Section 3.4).

ASMS aims to facilitate the spectral component in the commonly used two-phase method. The fundamental idea behind the two-phase method is the establishment of relationship coefficients (also known as the daylight coefficient) between sky luminance and geometry. The daylight coefficient is affected by the room geometry, geometry of the surroundings, transmittance and reflectance of the materials. The sky is divided into 145 (or more) patches using Reinhart discretization with the purpose of multiplying the luminance of each sky patch by the daylight coefficient. The resultant 145 (or more) values are summed up to derive the illuminance at a point in the geometry. Figure 8 shows the graphical

representation of daylight coefficient approach. The illuminance is calculated according to Equation 6:

$$\Delta E_v = D_{\theta\phi} L_{v\theta\phi} \Delta S_{\theta\phi} \quad (6)$$

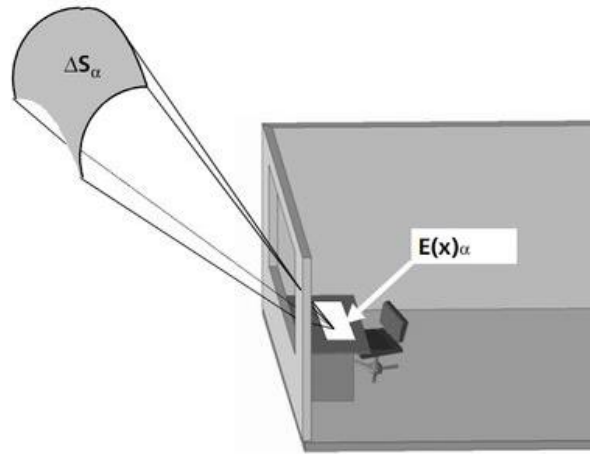


**Figure 8.** Graphical representation of daylight coefficient shows luminance contribution from a discrete sky patch on arbitrary point in the room. Contributions from all patches make up the total photopic illuminance at any point in the room. Picture source: Christoph Reinhart, 2001 [115].

where:

$\Delta E_v$  : Illuminance at a point in the room produced by a sky patch ( $lx$ )

$D_{\theta\phi}$  : Daylight coefficient

$L_{v\theta\phi}$  : Luminance of the sky patch ( $cd/m^2$ )

$S_{\theta\phi}$  : Projected solid angle of the sky patch at an altitude of  $\theta$  and azimuth of  $\Phi$  ( $sr$ )

As a first step to set up an annual simulation using the two-phase method, a matrix of 145 sky patches (or more) with radiance values is created according to the Perez All-Weather Sky Model using the annual irradiance values from the weather files [116, 117]. An additional patch is created for the ground plane in the model. In Radiance simulation software, this step is accomplished using *gendaymtx* program. Figure 9 shows a matrix of RGB triplet radiance values that is produced as the output of this step. In total, the matrix produces 1,278,960 RGB triplets (8760 x 146). The matrix presents radiance triplet values for 8760 hours and 146 patches (i.e., 145 sky patches and one ground patch).

In the *gendaymtx* program, the *-c* option can be used to assign color to the sky in the annual matrix simulation. Selection of RGB weightings must maintain the energy balance in the Radiance simulation, which is satisfied by the Equation 7 [118]. The specific coefficients (0.265, 0.670 and 0.065) in the equation are derived from the photopic sensitivity function.

$$0.265R + 0.670G + 0.065B = 1 \quad (7)$$

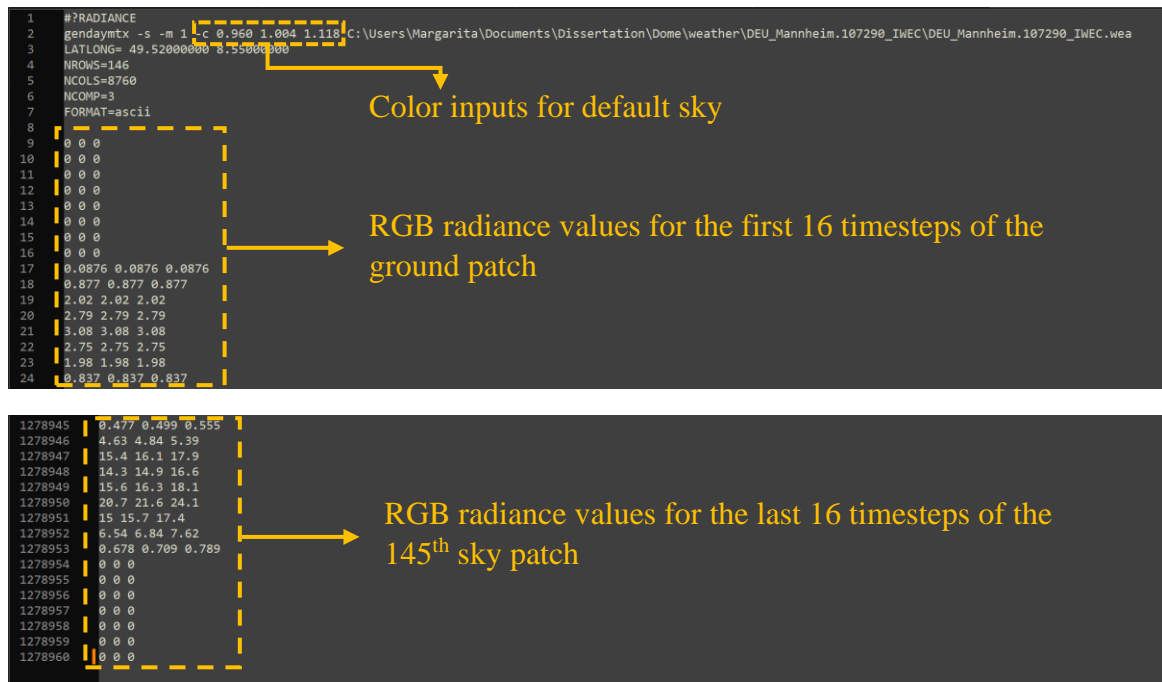


**Figure 9.** The output file of the *gendaymtx* program. The second line shows the sky color inputs (*-c* option) that are used to represent the default sky in Radiance. The triplets represent the RGB radiance values. The first 8760 RGB values show that the ground patch is not affected by the color option, as seen in the top screenshot for the first sixteen timesteps (i.e.,  $R = G = B$ ). The *-c* option affects the rest of the sky patches differently, as seen in the lower image, where  $R \neq G \neq B$ .

Considering the example with the default sky color in Radiance from Figure 9, the energy balance is maintained through the following calculation:

$$(0.265 \times 0.960) + (0.670 \times 1.004) + (0.065 \times 1.118) = 1$$

However, it is noteworthy that the steps described above assign the same RGB triplets to the entire sky dome for all hours assessed in the simulation. This assumption is incorrect when the goal is to perform annual spectral simulation because:

1. in real life, spectral properties of the sky are not constant throughout the entire dome; and

- the spectral properties of the sky fluctuate constantly and cannot be constant throughout the year.

For this reason, this thesis proposes a framework for generating **the spectral sky patch matrix**. It also proposes discretizing spectral information into  $N$ -channels. Figure 10 schematically presents the workflow discussed in the next sections.

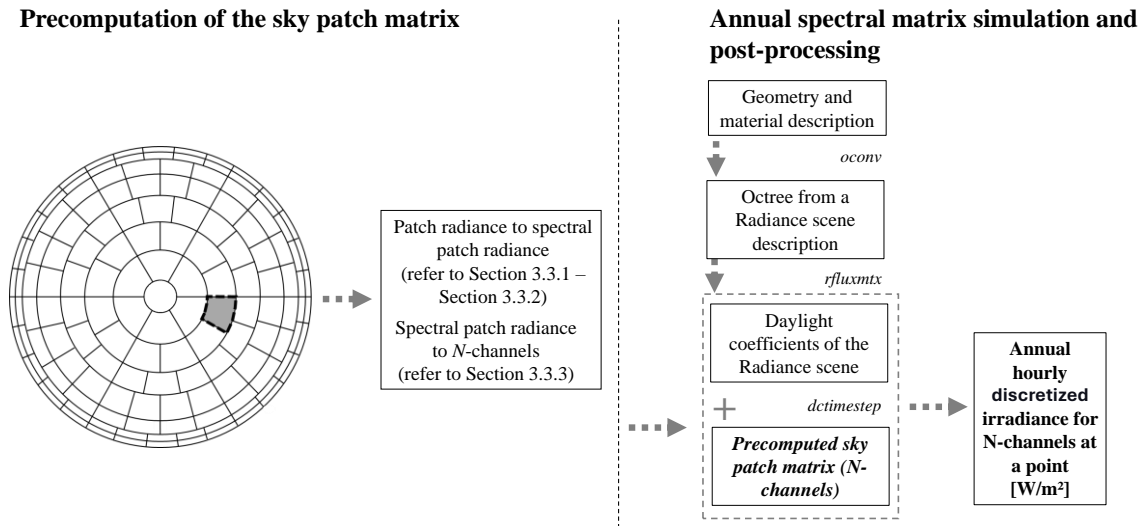


**Figure 10** Schematic framework of precomputation of the sky patch matrix and steps for the ASMS based on the daylight coefficient.

### 3.3 Precomputation of the spectral sky patch matrix

The following subsections present the steps necessary to create a spectral sky patch matrix that is “feedable” to the main ASMS. Broadly, the main principle consists of generating a **relative spectral radiance matrix** and multiplying it by the **matrix of absolute radiance patch values**. To be able to “feed” the spectral data into ASMS, the **resultant absolute spectral radiance** of each patch at each timestep must be arranged into  $N$  channels. In this work, three, nine, 27 and 81 channels are regarded. Thereby, the following subsections describe the below-mentioned points that must be accomplished in greater detail:

- the matrix of absolute radiance patch values;
- the matrix of relative spectral radiance from 380 nm to 780 nm; and
- the discretization of resultant absolute spectral radiance into  $N$ -channels



### 3.3.1 Generation of absolute radiance patch values

A matrix of absolute radiance patch values is generated by running the *gendaymtx* program in Radiance with equal coefficients in the color option (*-c 1 1 1* i.e. grey sky) that produces a matrix of absolute RGB radiance patch values. Figure 11 shows the output of running the program with the above-described settings. In comparison to Figure 9, RGB triplets are equal beyond the ground patch.

The image shows two screenshots of the *gendaymtx* program output. The top screenshot shows the first 24 lines of output, with a dashed box highlighting the first 16 lines (lines 9-24) and an arrow pointing to the text 'Color inputs for gray sky'. The bottom screenshot shows lines 1278945-1278960, with a dashed box highlighting the last 16 lines (lines 1278945-1278960) and an arrow pointing to the text 'RGB radiance values for the last 16 timesteps of the 145<sup>th</sup> sky patch'.

```

1  #?RADIANCE
2  gendaymtx -s -m 1 -c 1 1 1 C:\Users\Margarita\Documents\Dissertation\Dome\weather\DEU_Mannheim.107290_IWEC\DEU_Mannheim.107290_IWEC.wea
3  LATLONG= 49.52000000 8.55000000
4  NROWS=146
5  NCOLS=8760
6  NCOMP=3
7  FORMAT=ascii
8
9  0 0 0
10 0 0 0
11 0 0 0
12 0 0 0
13 0 0 0
14 0 0 0
15 0 0 0
16 0 0 0
17 0.0876 0.0876 0.0876
18 0.877 0.877 0.877
19 2.02 2.02 2.02
20 2.79 2.79 2.79
21 3.08 3.08 3.08
22 2.75 2.75 2.75
23 1.98 1.98 1.98
24 0.837 0.837 0.837

1278945 0.497 0.497 0.497
1278946 4.82 4.82 4.82
1278947 16 16 16
1278948 14.9 14.9 14.9
1278949 16.2 16.2 16.2
1278950 21.5 21.5 21.5
1278951 15.6 15.6 15.6
1278952 6.81 6.81 6.81
1278953 0.706 0.706 0.706
1278954 0 0 0
1278955 0 0 0
1278956 0 0 0
1278957 0 0 0
1278958 0 0 0
1278959 0 0 0
1278960 0 0 0

```

**Figure 11.** The output file of the *gendaymtx* program when the color option is set to grey (*-c 1 1 1*). The triplets represent the RGB radiance values. Each patch shows that the radiance at any time of the year equals to  $(R + G + B) / 3$ .

Through the above-mentioned steps, it is possible to determine the hourly radiance of each sky patch, which is necessary for the following:

1. scaling of relative spectral radiance from 380 nm to 780 nm for each sky patch and hour; and
2. generation of the relative spectral radiance for each sky patch (see Section 3.3.2).

### 3.3.2 Generation of relative spectral radiance profile for the sky

According to validated findings, there is a correlation between sky luminance and sky CCT [103, 119]. Therefore, this section describes the needed steps to apply the correlation to the sky-patch-radiance from Section 3.3.1 in order to convert it into sky-patch-spectral-radiance. Firstly, the radiance-based matrix must be converted to a luminance-based matrix.

Equation 8 presents the conversion, where 179 lm/W is the luminous efficacy of equal-energy light [118]:

$$L_v = 179 \cdot (0.265R + 0.670G + 0.065B) \quad (8)$$

where:

$L_v$ : Luminance of the sky patch ( $cd/m^2$ )

The conversions in Table 1 are applied to the luminance-based matrix in order to convert it to the CCT-based matrix. The conversion depends on the sky type and the luminance range.

**Table 1.** Validated luminance-to-CCT correlations for clear and overcast sky types. Correlations for clear sky are based on the luminance range of each patch. CCT of the overcast sky is constant.  $L_v$  = Luminance ( $cd/m^2$ ); LCF = Luminance Color Factor.

First author	Luminance range	Luminance and CCT correlation
Clear sky		
Chain (1999) [120]	$L_v < 3172 \text{ cd/m}^2$	$CCT = \frac{10^6}{-132.1 + 59.77 \cdot \log_{10} L_v}$
Rusnak (2012) [121]	$L_v < 5200 \text{ cd/m}^2$ & $L_v > 3172 \text{ cd/m}^2$	$CCT = \frac{10^6}{p \cdot L_v^q}$ where: $p$ and $q$ are the mean values of the empirical measurements per sky type in Rusnak (p. 81).
Chain (2004) [122]	$L_v > 5200 \text{ cd/m}^2$	$CCT = \frac{10^6}{181.35233 + LCF (-4.22630 + \log_{10} L_v)}$ where: $LCF = 21.56308 + (82.33165 - 0.77050 \cdot \gamma_s) \cdot (1.10439 + \log_{10}(\varepsilon - 0.9))$ $\gamma_s$ is solar altitude and $\varepsilon$ is the sky clearness
Overcast		
Chain (1999) [120]	All	$CCT = 6415 (\pm 133) \text{ K}$

Whether the sky type is clear or overcast is determined according to the epsilon value, which represents the clearness of the sky and is identified for each hour of the year from direct and global irradiance as specified in [116]. The following gradation for sky type were considered [123]:

- Overcast sky if  $\epsilon < 1.065$
- Intermediate sky if  $\epsilon \geq 1.065$  and  $\leq 4.5$
- Clear sky if  $\epsilon > 4.5$

Since luminance-to-CCT correlation does not exist for the intermediate sky condition, this type of sky is preliminarily treated as an overcast sky with a constant CCT of 6415 K. However, this can easily be adjusted in the simulation once new, validated correlations for intermediate sky emerge. The luminance-to-CCT correlation for clear sky condition is determined individually based on the luminance range of each patch. Notably, the correlations are only valid for the diffuse component of radiation, so the direct component is removed from the sky matrix by applying the *-s* option in *gendaymtx* program (see Figure 9 and Figure 11).

The above-described conversions achieve 1,270,200 CCT values for each of the patches of the sky dome for each hour of the year. In the post-processing steps, only working hours between 8:30 and 18:30 when the solar altitude exceeded  $10^\circ$  were regarded. The solar altitude is relevant because the correlations have not been validated for extremely low altitudes. Solar altitude is deduced (by running *gendaylit* program) for each hour of interest. As a result, 3,265 hours were left for analysis after post-processing.

The CCT of each sky patch is converted to relative spectral radiance from 380 nm to 780 nm. In this method, the CCT is converted to *xy* coordinates on the CIE 1931 color space chromaticity diagram. Once the *xy* coordinates are known, spectral power distribution of illuminant D can be characterized mathematically [124]. The conversion is valid when the CCT is between 4000 K and 25000 K.

### **3.3.3 Discretization of the sky SPD into *N*-bins**

Several steps are necessary to convert the relative spectral radiance of each sky patch into a readable format for ASMS. Firstly, the relative spectral radiance of each patch must be interpolated at 0.1 nm interval to allow precise division between RGB bands. These bands are determined according to RGB coefficients in Equation 7 (0.265, 0.670 and 0.065) that represent the area under the curve of the area-normalized photopic  $V(\lambda)$  function:

$$\int_{380}^{780} V(\lambda) d\lambda = 1 \quad (9)$$

According to this, the coefficients R, G and B correspond to the area under the photopic curve between 586.5 - 780.0 nm, 499.0 - 586.5 nm and 380 - 499.0 nm. These boundaries were determined by applying trapezoidal integration to the area-normalized  $V(\lambda)$  curve in Equation 9. Therefore, to discretize the spectral radiance of any sky patch into three channels, it is averaged in the red, green and blue wavelength boundaries following the Equations 10 to 12:

$$Relative \bar{L}_{e,Red} = \left( \sum_{i=586.5}^{780} L_{e,\lambda i} \right) / 780.0 - 586.5 \quad (10)$$

$$Relative \bar{L}_{e,Green} = \left( \sum_{i=499.0}^{586.5} L_{e,\lambda i} \right) / 586.5 - 499.0 \quad (11)$$

$$Relative \bar{L}_{e,Blue} = \left( \sum_{i=380}^{499.0} L_{e,\lambda i} \right) / 499.0 - 380.0 \quad (12)$$

where:

$\bar{L}_{e,wavelength\ band}$  : relative average radiance in the respective wavelength band  
( $W/m^2/sr$  per wavelength band)

$L_{e,\lambda i}$  : relative spectral radiance at wavelength  $i$  ( $W/m^2/sr/nm$ )

However, it is noteworthy that the relative average radiance values from Equations 10 to 12 do not satisfy the energy balance in Equation 7. The relative average radiance ( $\bar{L}_{e,wavelength\ band}$ ) in each channel must be divided by the following scaling factor to preserve the energy balance in Radiance simulation:

$$\begin{aligned} & \text{Scaling factor} \\ & = (Rel. \bar{L}_{e,Red} \times 0.265) + (Rel. \bar{L}_{e,Green} \times 0.670) \\ & + (Rel. \bar{L}_{e,Blue} \times 0.065) \end{aligned} \quad (13)$$

Finally, assuming that the spectral radiance in the discretized wavelength bands is constant (i.e., flat), the *scaled* relative average radiance of R, G and B bins is multiplied by the absolute radiance value of the sky patch (see Section 3.3.1) to obtain the *absolute average spectral radiance* for each channel (i.e., wavelength band). Therefore, if a three-channel spectral simulation is performed, one sky matrix with 1,278,960 triplets will be produced, similar to that presented in Figure 9 and Figure 11. However, each line will contain the

following three values: absolute average spectral radiance for wavelength intervals 586.5 - 780.0 nm (R), 499.0 - 586.5 nm (G) and 380 - 499.0 nm (B). This information is then “fed” to the ASMS (Section 3.4).

If nine channels are considered, then relative spectral radiance must be derived for three blue, three green and three red bins. The bands for the finer bins are obtained by dividing the main wavelength boundaries equidistantly, which results in the following intervals: 380.0 - 419.6 nm, 419.6 - 459.3 nm, 459.3 - 499.0 nm, 499.0 - 528.1 nm, 528.1 - 557.3 nm, 557.3 - 586.5 nm, 586.5 - 651.0 nm, 651.0 - 715.5 nm and 715.5 - 780.0. The same logic applies to simulations with 27 and 81 channels, where nine and 27 bins, respectively, must be created within the original RGB wavelength intervals. Thereby, Equations 10 to 12 should be adjusted and expanded accordingly.

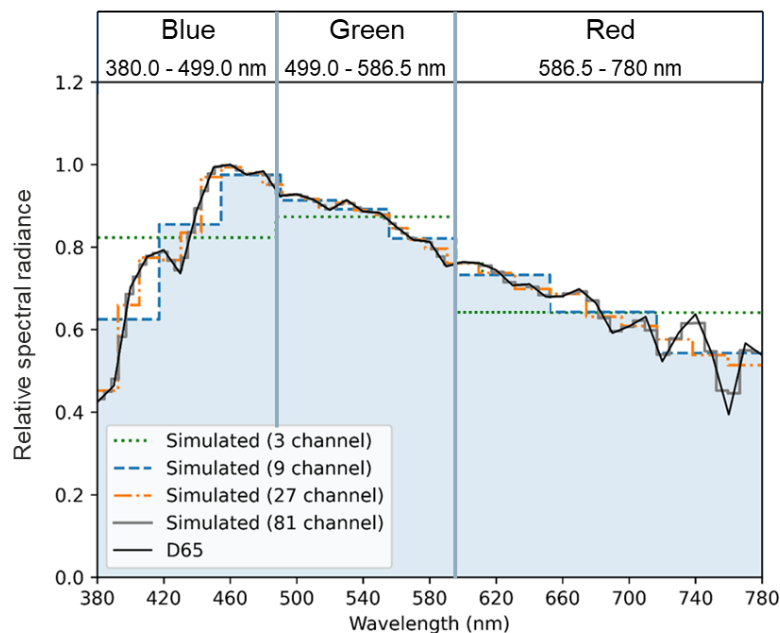


**Figure 12.** Measured (black line) and discretized (colored lines) relative spectral radiance of the D65 illuminant with 6504 K.

Considering that the scaling factor in Equation 13 is valid for a three-channel simulation, the relative average spectral radiance values for the nine, 27 and 81-channel simulations are multiplied by finer coefficients instead. These coefficients are deduced by applying trapezoidal integration to the nine, 27 or 81 intervals of the area-normalized  $V(\lambda)$  curve. The coefficients and intervals for the three, nine, 27 and 81 channels are presented in Appendix A. Figure 12 shows the example of the discretization into  $N$ -channels of the relative spectral radiance of the D65 illuminant with 6504 K.

In the case of nine-channel simulation, three separate spectral sky files are written for wavelength intervals 380 - 499.0 nm, 499.0 - 586.5 nm and 586.5 - 780.0 nm. Each of the sky files has 1,278,960 triplets that describe the respective wavelength interval. “Blue” sky matrix file represents the absolute average spectral radiance of the intervals **380.0** - 419.6 nm, 419.6 - 459.3 nm and 459.3 – **499.0** nm with a set of triplets. “Green” sky matrix file refers to the intervals **499.0** - 528.1 nm, 528.1 - 557.3 nm and 557.3 - **586.5** nm. “Red” sky matrix file described intervals **586.5** - 651.0 nm, 651.0 - 715.5 nm and 715.5 - **780.0**. The spectral sky files are then “fed” to the ASMS.

Regarding the simulation with 27 channels, the original boundaries are divided into nine finer intervals. Nine spectral sky files with absolute average spectral radiance in the respective wavelength bands are produced. Similar steps are done in the simulation with 81 channels, except the original boundaries are divided into 27 channels and produce 27 spectral sky files for the respective parts of the spectrum. The spectral sky files are then “fed” to the ASMS. The ASMS is run one time for three channels, three times for nine channels, nine times for 27 channels and 27 times for 81 channels.

### **3.4 ASMS and post-processing steps**

The ASMS is based on the daylight coefficient method to accommodate the spectral component in the annual simulations. The daylight coefficient method supports the execution of annual daylight simulations without the need to run an individual simulation for each hour of the year, eliminating redundant calculations. The ASMS method extends the daylight coefficient method by enabling spectral simulation with  $N$ -channels.

In a two-phase simulation that relies on the daylight coefficient, the sky matrix is multiplied by the matrix of daylight coefficients. Here, steps that produce a daylight coefficient matrix that considers the spectral properties of the geometry are elaborated. In a conventional three-channel simulation, the first step is creating an octree file from a scene description in Radiance. This is done with the help of the *oconv* program, which combines the geometry of the model with the material description file. In a spectral simulation, the material description file must be edited to contain the spectral information of the surfaces before combining it with geometry via *oconv* program. The spectral reflectance and transmittance values of the materials for wavelength intervals 586.5 - 780.0 nm, 499.0 - 586.5 nm and 380 - 499.0 nm are averaged into three (RGB) bins and written into one material file. If the simulation has more than three channels, the average spectral information is split into

multiple material files for several *oconv* runs. As a result, multiple octree files are generated that represent the reflectance and transmittance values of the surfaces in the respective parts of the visible spectrum.

Once the octree file is obtained, the daylight coefficient matrix can be computed (via *rfluxmtx* program with 10 ambient bounces (-ab), 10000 ambient divisions (-ad) and 0.0001 as limit weight (-lw)). If the simulation with three channels is to be performed, one octree file is “fed” to the *rfluxmtx* program as is. If the simulation is with nine, 27 or 81 channels, then *rfluxmtx* program will be performed three, nine or 27 times with the respective octree file that represents the particular spectral intervals.

In the last step of the ASMS, the generated *spectral* daylight coefficient matrix is multiplied by the *spectral* sky files (presented in Section 3.3.1 to Section 3.3.3). The output of the simulation is the Radiance RGB values. If more than three channels are simulated, then the *spectral* daylight coefficient matrix and the spectral sky files are multiplied, producing multiple output files. Regardless of the number of channels, the simulation output requires post-processing steps. Equations 14 to 16 convert Radiance RGB values to average spectral irradiance in the respective wavelength interval [99]. The equations are expanded to consider more intervals when more than three channels are considered.

$$E_{e,\lambda}^{[586.5, 780.0]} = 179 \times \frac{1}{683} \times \frac{1}{107} \times R \quad (14)$$

$$E_{e,\lambda}^{[499.0, 586.5]} = 179 \times \frac{1}{683} \times \frac{1}{107} \times G \quad (15)$$

$$E_{e,\lambda}^{[380, 499.0]} = 179 \times \frac{1}{683} \times \frac{1}{107} \times B \quad (16)$$

where:

179: luminous efficacy factor for equal-energy white light in Radiance (*lm/W*)

683: photopic luminous efficacy at 555 nm (*lm/W*)

107: area under the curve of the normalized  $V(\lambda)$  function

$E_{e,\lambda}^{[a,b]}$ : spectral irradiance for the *a-b* wavelength interval (*W/m<sup>2</sup>*)

The conversion above yields average spectral irradiance of the discrete wavelength interval from which various quantities can be generated. In this thesis, photopic illuminance and melanopic equivalent daylight illuminance are evaluated. To convert spectral irradiance to

photopic illuminance ( $E_v$ ) and melanopic equivalent daylight illuminance ( $E_{v,mel}^{D65}$ ) Equations 17 and 18 were applied respectively:

$$E_v = 683 \times \left( \int_{586.5}^{780.0} E_{e,\lambda}(\lambda) V(\lambda) d(\lambda) + \int_{499.0}^{586.5} E_{e,\lambda}(\lambda) V(\lambda) d(\lambda) + \int_{380.0}^{499.0} E_{e,\lambda}(\lambda) V(\lambda) d(\lambda) \right) \quad (17)$$

$$E_{v,mel}^{D65} = \left( \int_{586.5}^{780.0} E_{e,\lambda}(\lambda) s_{mel} V(\lambda) d(\lambda) + \int_{499.0}^{586.5} E_{e,\lambda}(\lambda) s_{mel} V(\lambda) d(\lambda) + \int_{380.0}^{499.0} E_{e,\lambda}(\lambda) s_{mel} V(\lambda) d(\lambda) \right) / 1.326 \quad (18)$$

where:

$E_{e,\lambda}(\lambda)$  : spectral irradiance in (W/m<sup>2</sup>/nm or mW/m<sup>2</sup>/nm)

$V(\lambda)$  : photopic spectral sensitivity function

$s_{mel}(\lambda)$ : melanopic spectral sensitivity function

In the three-channel simulation, the RGB bins 586.5-780 nm, 499.0-586.5 nm and 380-499.0 nm have constant spectral irradiance obtained from Equations 14 to 16. In the simulation with nine channels, the above-mentioned bins were equidistantly subdivided into three further channels, thereby resulting in new bins with constant spectral irradiance in the following wavelength bands: **380.0** - 419.6 nm, 419.6 - 459.3 nm, 459.3 - **499.0** nm, **499.0** – 528.1 nm, 528.1 - 557.3 nm, 557.3 - **586.5** nm, **586.5** - 651.0 nm, 651.0 - 715.5 nm, 715.5 - **780.0** nm. The same concept applies to the simulations with 27 and 81 channels.



## Section 4

### ASMS for daylighting

#### 4.1 Reference room

The reference office room previously proposed in [125] is selected as a baseline geometry for comparative analysis. The room represents a typical shoebox model designed for six employees. The room dimensions are as follows: 3.6 m (width), 8.2 m (length) and 2.8 m (height). The total floor area is 29.5 m<sup>2</sup>. The room has a deep floor plan and a south-facing window with 3.0 m width and 1.5 m height. The window-to-wall ratio (WWR) is 40 %. Six work positions are distributed into three groups based on their proximity to the window. Venetian blinds were removed from the original model. The diagram below shows the dimensions of the office room.

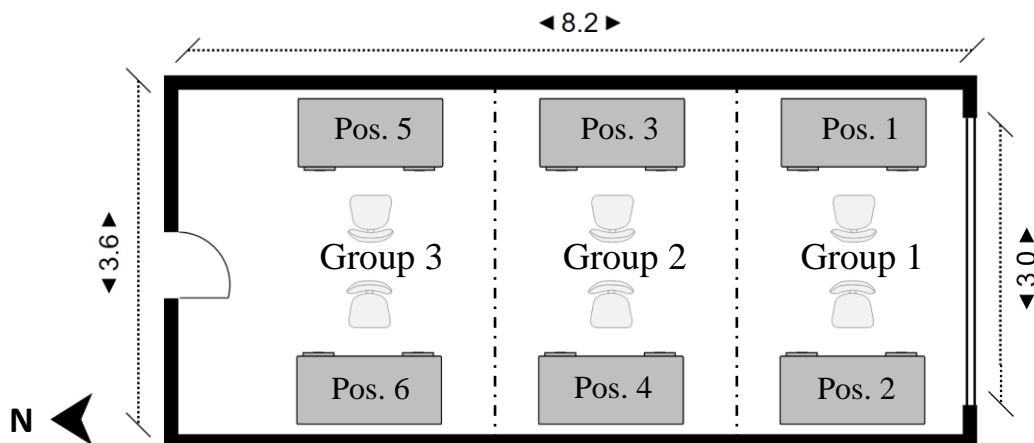


**Figure 13.** Reference office room and the dimensions. The room is divided into three groups based on the proximity to the window. The room has six positions in total. Each group has two positions.

The spectral information for the materials in the office room is selected from an online database [126, 127]. The spectral reflectance of each material was selected according to the typical reflectance values of the surfaces in the office spaces. Double-pane glazing, common for this location and climate, was assembled via Optics software and replaced the original glazing in the reference office room [128]. Table 2 shows the selected materials as well as the reflectance and transmittance values of the surfaces.

**Table 2.** Materials selected for the reference office room with the reflectance and transmittance values presented in percentages.

Surface	Material	Reflectance	Transmittance
Ceiling	White paint	80 %	
Walls	Yellow paint	50 %	
Floor	Wooden parquet	20 %	
Glazing	Double pane low-E		65 %
Ground	Concrete	20 %	

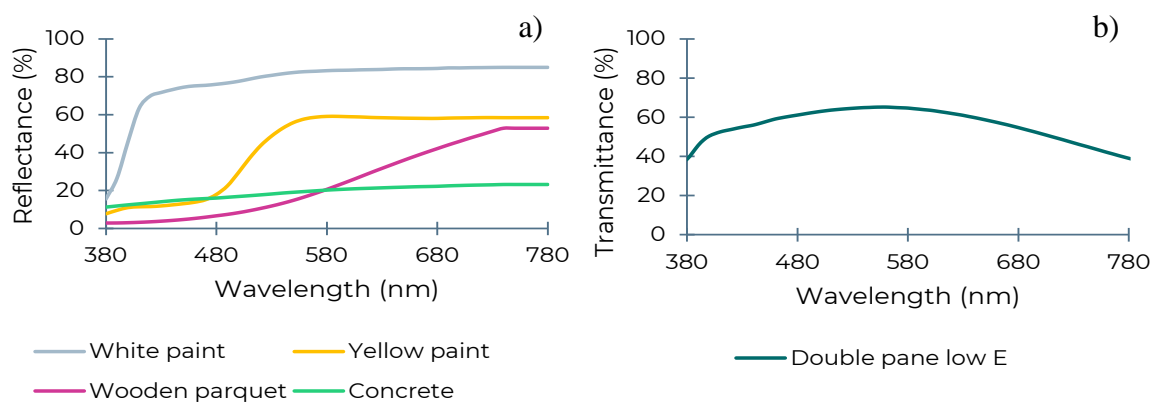


**Figure 14.** a) Spectral reflectance of the white paint (ceiling), yellow paint (walls), wooden parquet (floor) and concrete (ground) from 380 nm to 780 nm. b) Spectral reflectance of the double pane low-E glazing from 380 nm to 780 nm.

## 4.2 Weather data for the ASMS

The weather data of Mannheim, Germany is selected for the analysis. The EPW file (EnergyPlus Weather Format), which is used in the simulations, is based on the weather data from 1982, 1985, 1987, 1988, 1989, 1990. The points on the scatter plots in Figure 15, show hourly values of direct normal radiation on all days of the month [129]. The hourly direct normal radiation exceeds 800 Wh/m<sup>2</sup> in many instances in March, April, May, June, July, August and September. The orange line shows the daily trend for each particular month based on the scattered values. On average, direct normal radiation is the highest in August when it exceeds 400 Wh/m<sup>2</sup>. Figure 16 shows the hourly values of direct normal radiation on the heatmap throughout the year.

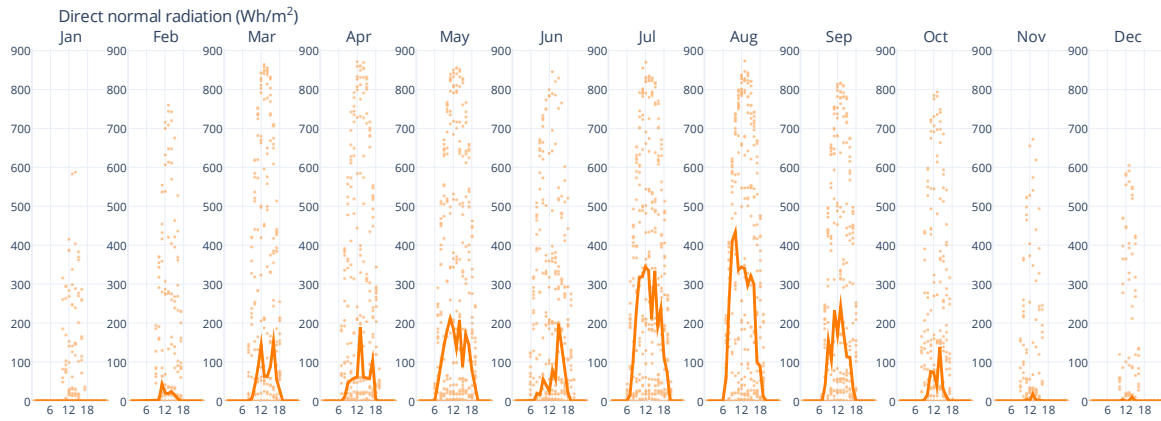


**Figure 15.** The x-axis represents 24 hours of the day. The y-axis shows the magnitude of direct normal radiation in Wh/m<sup>2</sup>. Orange points indicate hourly values of direct normal radiation for each month extracted from the weather data. The orange line is the trend line based on the hourly values. Source: CBE Clima Tool [129].

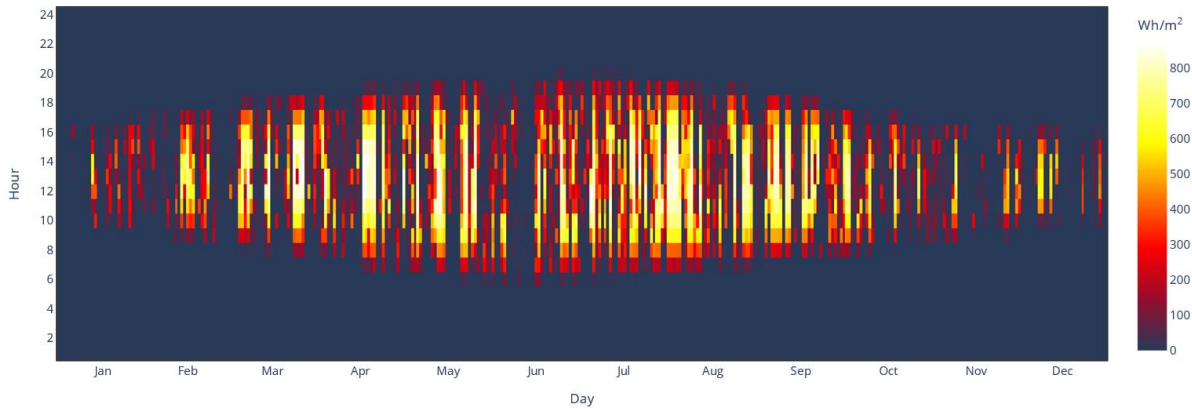


**Figure 16.** Hourly values of direct normal radiation represented as heatmap. The x-axis represents months. The y-axis shows hours of the day. The magnitude of direct normal radiation is color-coded and presented in Wh/m<sup>2</sup>. Source: CBE Clima Tool [129].

Figure 17 and Figure 18 represent diffuse horizontal radiation in Mannheim. Figure 17 shows that hourly diffuse horizontal radiation exceeds 400 Wh/m<sup>2</sup> in April, May, June, July and August. The maximum daily average diffuse horizontal radiation is beyond 300 Wh/m<sup>2</sup> in April, May, June and July. In order to run the daylighting simulation, the hourly direct normal and diffuse horizontal radiation values are extracted from the EPW weather file via the *epw2wea* program in Radiance. The program produces a WEA file, which can be passed directly to other Radiance programs, such as *gendaymtx*, for the generation of the discretized sky (as elaborated in Section 3.3). Figure 19 presents the annual profile of diffuse horizontal and direct normal radiation that is used as the input in the ASMS.

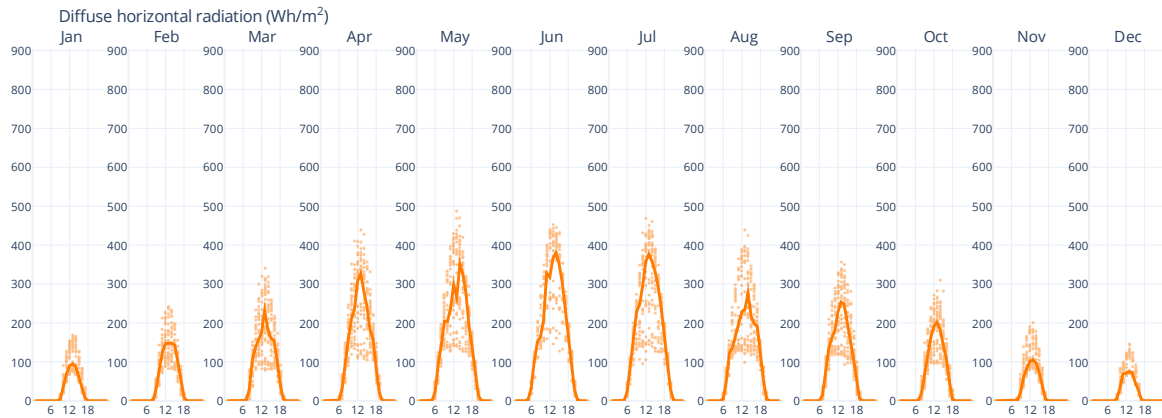


**Figure 17.** The x-axis represents 24 hours of the day. The y-axis shows the magnitude of diffuse horizontal radiation in Wh/m<sup>2</sup>. The orange points indicate hourly values of diffuse horizontal radiation for each month extracted from the weather data. The orange line is the trend line based on the hourly value. Source: CBE Clima Tool [129].

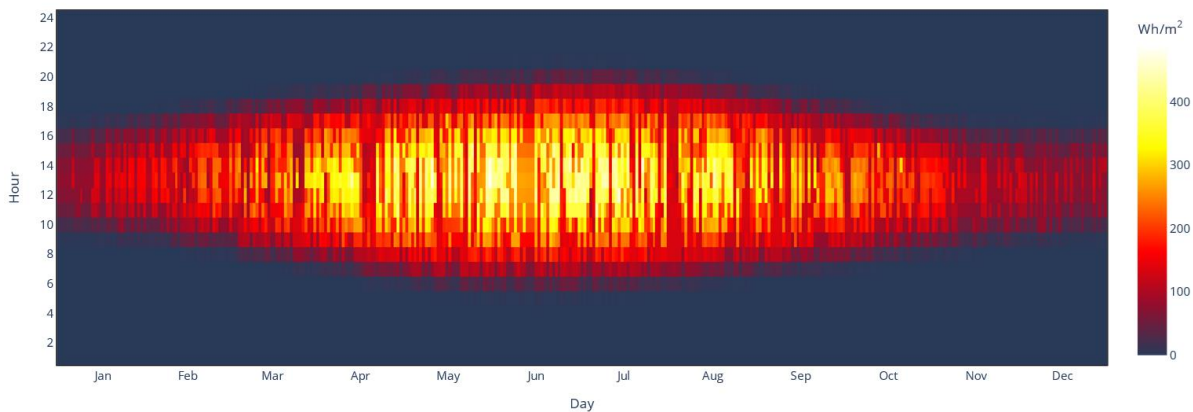


**Figure 18.** Hourly values of diffuse horizontal radiation represented as heatmap. The x-axis represents months. The y-axis shows hours of the day. The magnitude of diffuse horizontal radiation is color-coded and presented in Wh/m<sup>2</sup>. Source: CBE Clima Tool [129].

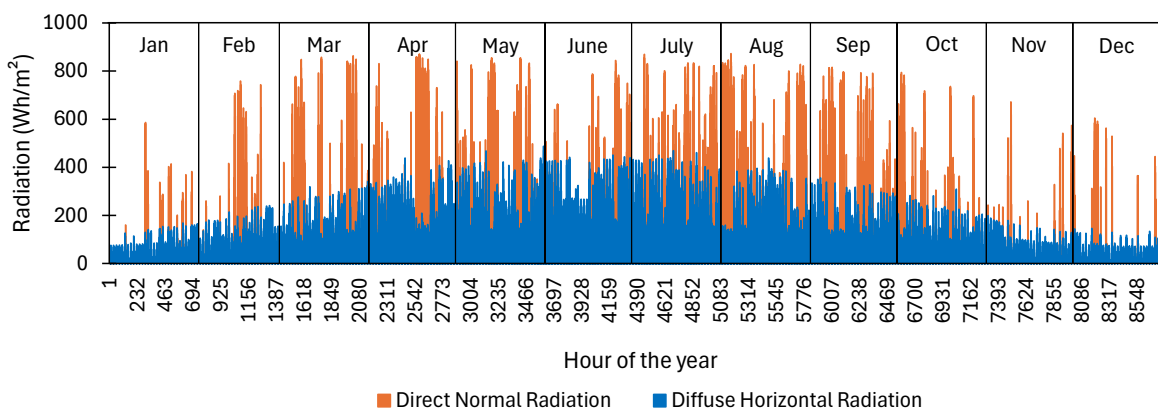


**Figure 19.** The annual profile of the diffuse horizontal and direct normal radiation in Mannheim as the output of epw2wea Radiance program and input for the ASMS. The x-axis represents hours. The y-axis shows the magnitude of radiation in Wh/m<sup>2</sup>.

### 4.3 Variability in the simulation of daylight

Based on the random nature of hemispherical sampling in Radiance, illuminance predictions can vary even between identical simulation runs (refer to Section 3.1). Therefore, the effect of random sampling on the variability of the results is investigated in this section. The variability between simulations is analyzed via the standard deviation of the hourly integral irradiance in the visible spectrum between 380 nm and 780 nm (further denoted by  $E_e^{380-780}$ ). This analysis is done for all six positions in the room and all the channels considered in this thesis. Equation 19 is used to derive the standard deviation of one hourly value, here referred to as  $y$ :

$$y = \sqrt{\frac{\sum (E_e^{380-780}_i - \bar{E}_e^{380-780})^2}{N - 1}} \quad (19)$$

where:

$y$  : the standard deviation of  $E_e^{380-780}$  for one hourly value based on ten simulation runs

$\bar{E}_e^{380-780}$  : the mean  $E_e^{380-780}$  of ten simulation runs for one hourly value

$E_e^{380-780}_i$  : individual  $E_e^{380-780}$  values in ten simulation runs for one hourly value ( $i = 1 \dots 10$ )

$N$  : the size of the sample i.e., ten simulation runs ( $N = 10$ )

The coefficient of determination, also known as  $R^2$ , represents the proportion of variance of the dependent variable, the standard deviation of ten simulation runs. In other words,  $R^2$  describes how close the values of standard deviation are to the gradient line of the regression model. This value is calculated assuming the origin at zero and presented in scatterplot in Figure 20 and Figure 21 according to Equation 20:

$$R^2 = 1 - \frac{\sum (y_j - \hat{y}_j)^2}{\sum (y_j)^2} \quad (20)$$

where:

$y_j$  : actual standard deviation of ten simulation runs for hourly  $E_e^{380-780}$  ( $j = 1 \dots 3265$ )

$\hat{y}_j$  : predicted standard deviation according to the linear regression model of ten simulation runs for hourly  $E_e^{380-780}$  ( $j = 1 \dots 3265$ )

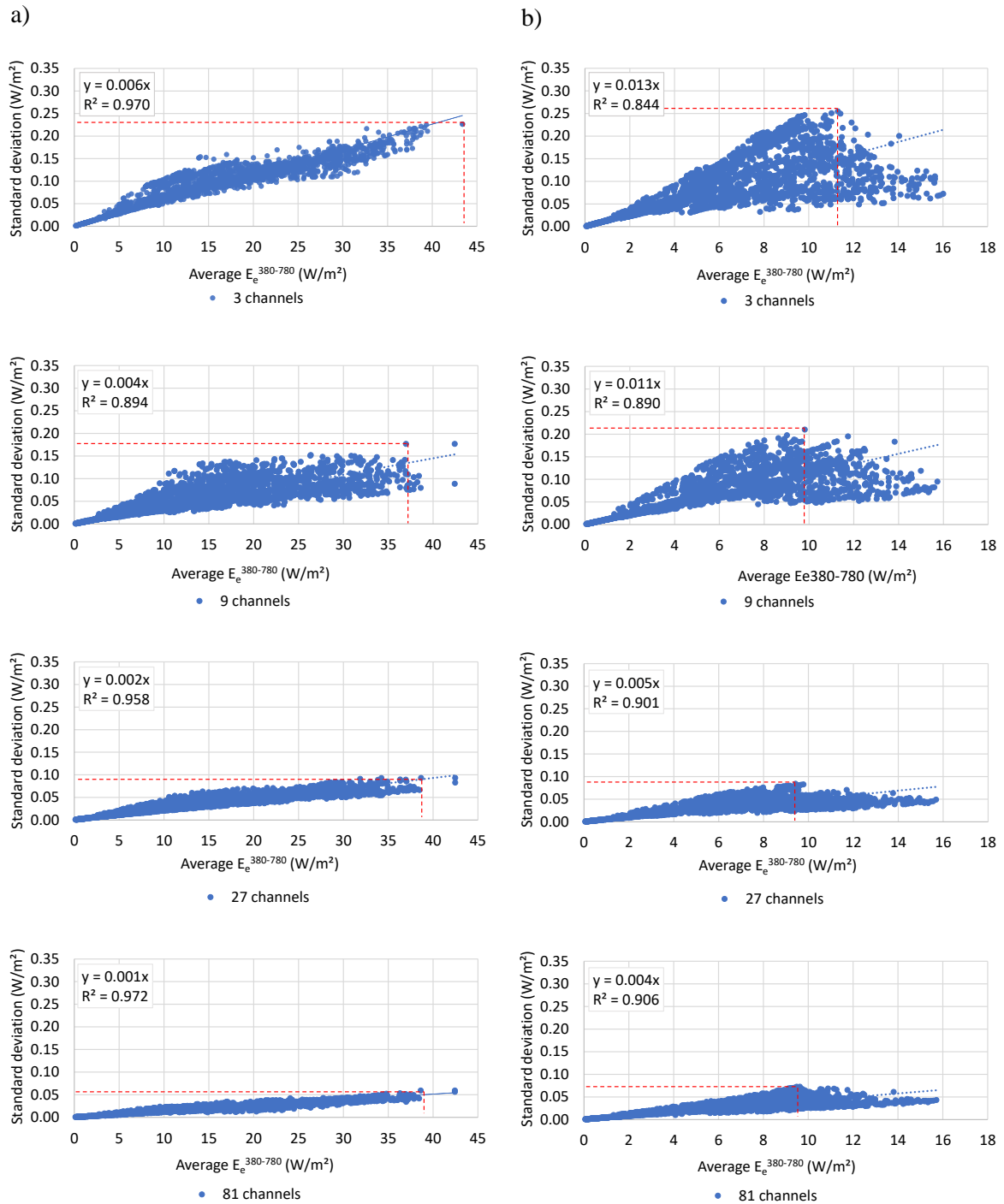


**Figure 20.** Scatterplots show standard deviation (y-axis) plotted against the average  $E_e^{380-780}$  (x-axis) for positions 1. Row (a) presents the results at the horizontal desk level (0.80 m) and row (b) at the vertical eye level (1.20 m) for simulations with three, nine, 27 and 81 channels. Average  $E_e^{380-780}$  refers to ten simulation runs. The red dashed line represents the maximum standard deviation at the respective  $E_e^{380-780}$  in each scatter plot.

Figure 20 (a) shows scatterplots of position 1 with three-, nine-, 27- and 81-channel discretization at the horizontal desk level (0.80 m). Figure 20 (b) shows the same information recorded at the vertical eye level at 1.20 m. The scatterplots represent the relationship between the standard deviation (y-axis) and the average  $E_e^{380-780}$  of ten simulation runs (x-axis). The dotted blue line represents the regression line that passes through the origin of each plot. The gradient of the regression line provides information on the strength of the relationship and indicates how fast the dependent variable (standard deviation) increases as a function of the independent variable (average  $E_e^{380-780}$ ). All scatterplots show moderate to strong, positive, linear relationship between the standard deviation and  $E_e^{380-780}$  of ten simulation runs. The scatterplots for positions 3 to 6 are presented in Appendix B.

It is noteworthy that the maximum standard deviation is consistently lower in the simulations that have a higher number of channels. Figure 20 (a) shows that the maximum standard deviation at the horizontal desk level is +/- 0.23 W/m<sup>2</sup> (at 43.4 W/m<sup>2</sup>) in the simulations with three channels, +/- 0.18 W/m<sup>2</sup> (at 37.0 W/m<sup>2</sup>) in the simulations with nine channels, +/- 0.10 W/m<sup>2</sup> (at 38.7 W/m<sup>2</sup>) in the simulations with 27 channels and +/- 0.06 W/m<sup>2</sup> (at 38.6 W/m<sup>2</sup>) in the simulations with 81 channels

The maximum standard deviation at the vertical eye level is shown in Figure 20 (b). The maximum standard deviation is +/- 0.25 W/m<sup>2</sup> (at 11.3 W/m<sup>2</sup>) in the simulations with three channels, +/- 0.21 W/m<sup>2</sup> (at 9.8 W/m<sup>2</sup>) in the simulations with nine channels, +/- 0.09 W/m<sup>2</sup> (at 9.4 W/m<sup>2</sup>) in the simulations with 27 channels and +/- 0.07 W/m<sup>2</sup> (at 9.6 W/m<sup>2</sup>) in the simulations with 81 channels.

Figure 21 (a) shows that the maximum standard deviation at the horizontal desk level is +/- 0.27 W/m<sup>2</sup> (at 39.3 W/m<sup>2</sup>) in the simulations with three channels, +/- 0.18 W/m<sup>2</sup> (at 36.9 W/m<sup>2</sup>) in the simulations with nine channels, +/- 0.15 W/m<sup>2</sup> (at 35.0 W/m<sup>2</sup>) in the simulations with 27 channels and +/- 0.08 W/m<sup>2</sup> (at 32.3 W/m<sup>2</sup>) in the simulations with 81 channels for position 2.

The maximum standard deviation at the vertical eye level is shown in Figure 21 (b). The maximum standard deviation is +/- 0.27 W/m<sup>2</sup> (at 9.2 W/m<sup>2</sup>) in the simulations with three channels, +/- 0.19 W/m<sup>2</sup> (at 10.2 W/m<sup>2</sup>) in the simulations with nine channels, +/- 0.11 W/m<sup>2</sup> (at 10.3 W/m<sup>2</sup>) in the simulations with 27 channels and +/- 0.06 W/m<sup>2</sup> (at 8.7 W/m<sup>2</sup>) in the simulations with 81 channels.

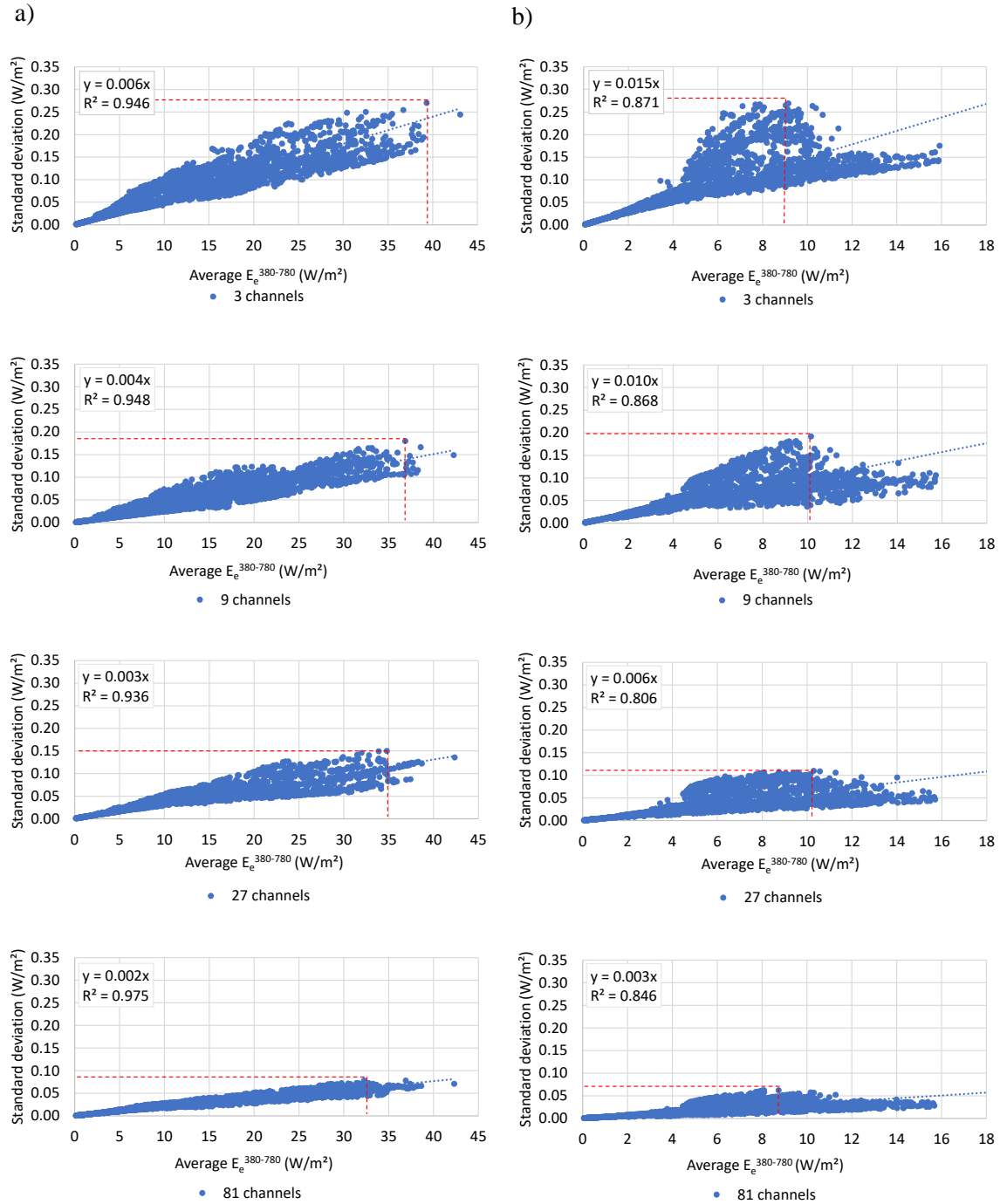


**Figure 21.** Scatterplots show standard deviation (y-axis) plotted against the average  $E_e^{380-780}$  (x-axis) for positions 2. Row (a) presents the results at the horizontal desk level (0.80 m) and row (b) at the vertical eye level (1.20 m) for simulations with three, nine, 27 and 81 channels. Average  $E_e^{380-780}$  refers to ten simulation runs. The red dashed line represents the maximum standard deviation at the respective  $E_e^{380-780}$  in each scatter plot.

The initial hypothesis that increasing the number of channels would consistently decrease the gradient of the linear regression model, thereby reducing the standard deviation, is confirmed. A short analysis is done for the horizontal and vertical  $E_e^{380-780}$  of 10 W/m<sup>2</sup>



based on the linear regression models for positions 1 to 6. Tables 3 and 4 show the standard deviation in  $W/m^2$  based on the average of ten simulation runs for the simulation with three, nine-, 27- and 81-channels.

**Table 3.** *Standard deviation that occurs on positions 1-3 on the vertical and horizontal planes for the simulation with three, nine, 27 and 81 channels. The regression model is based on ten Radiance simulation runs with three, nine, 27 and 81 channel discretization.*

Number of channels	Standard deviation ( $W/m^2$ )					
	Position 1		Position 2		Position 3	
	Horiz.	Vert.	Horiz.	Vert.	Horiz.	Vert.
3	0.06	0.13	0.06	0.15	0.21	0.34
9	0.04	0.11	0.04	0.10	0.17	0.31
27	0.02	0.05	0.03	0.06	0.09	0.14
81	0.01	0.04	0.02	0.03	0.05	0.09

**Table 4.** *Standard deviation that occurs on positions 4-6 on the vertical and horizontal planes for the simulation with three, nine, 27 and 81 channels. The regression model is based on ten Radiance simulation runs with three, nine, 27 and 81 channel discretization.*

Number of channels	Standard deviation ( $W/m^2$ )					
	Position 4		Position 5		Position 6	
	Horiz.	Vert.	Horiz.	Vert.	Horiz.	Vert.
3	0.20	0.32	0.47	0.88	0.34	0.62
9	0.13	0.32	0.23	0.33	0.33	0.51
27	0.10	0.17	0.21	0.23	0.14	0.25
81	0.07	0.01	0.07	0.14	0.07	0.14

#### 4.4 Results of ASMS for daylighting

The following section presents the results of the ASMS for daylighting. The results presented for each  $N$ -channel are based on the average of five simulation runs. Figure 22 and Figure 23 present scatter plots for positions 1 to 6. The x-axis represents the average photopic or melanopic equivalent daylight illuminance of the 81-channel simulation obtained by performing five simulation runs. The y-axis represents the absolute difference of the photopic or melanopic equivalent daylight illuminance in lx. Each point in the scatter plot represents the absolute difference in photopic or melanopic equivalent daylight illuminance of three-, nine- or 27-channel simulation compared to 81 channels, representing the baseline.

#### 4.4.1 Results of photopic illuminance

Figure 22 shows the difference in photopic illuminance in relation to the baseline simulation with 81 channels for positions 1 to 6. Figures show that the simulation with three channels has the highest absolute difference in photopic illuminance compared to the baseline. The difference increases with the increase of the magnitude of the photopic illuminance. For example, the highest baseline photopic illuminance is approximately 9797 lx (SD = +/- 25.5 lx) for position 1. This means that an identical analysis with a three-channel simulation would produce a result of approximately 9372 lx (SD = +/- 66.5 lx).

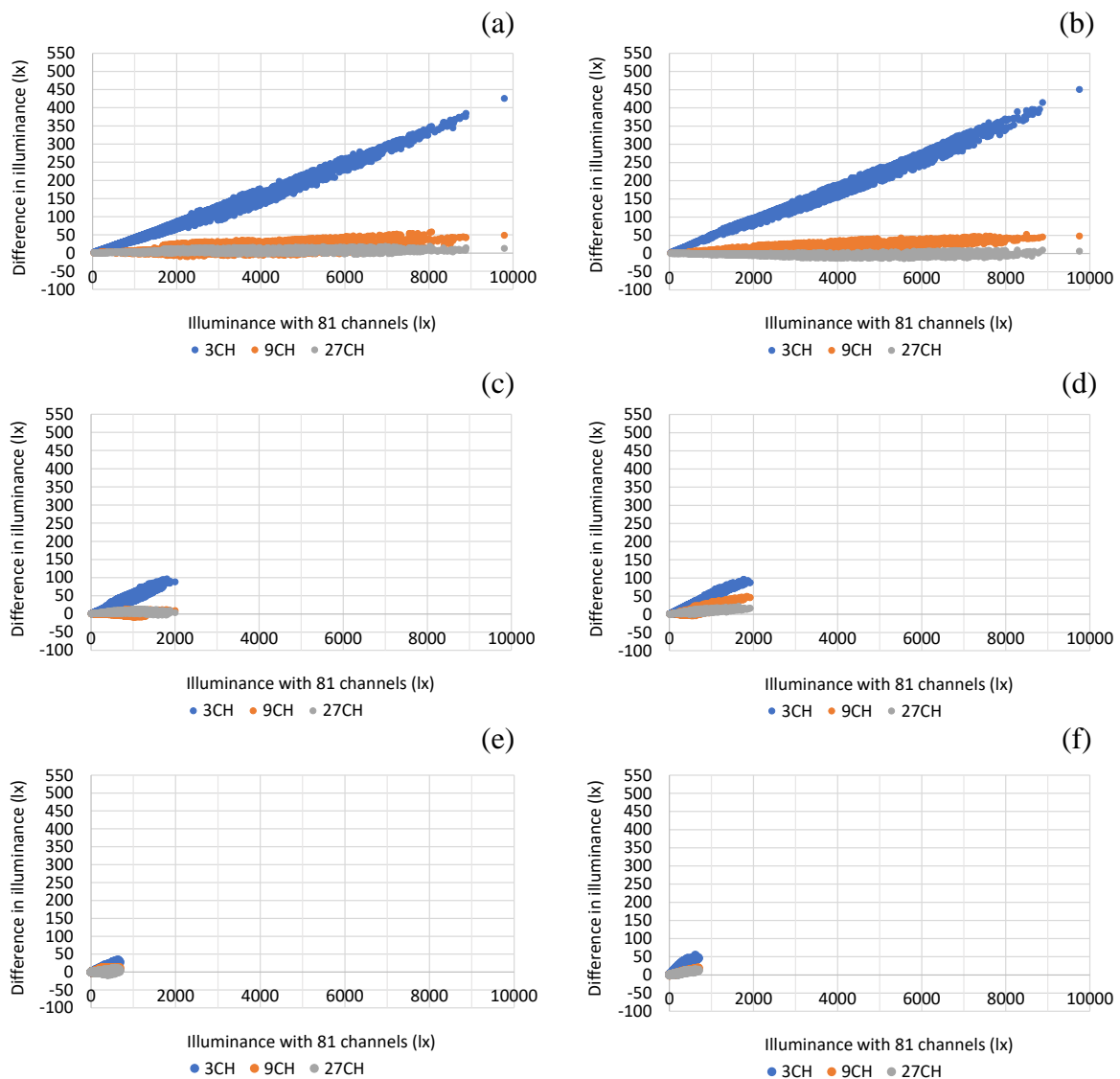


**Figure 22.** The absolute difference in photopic illuminance for the simulations with three, nine and 27 channels in comparison to the baseline illuminance with 81 channels for positions 1 (a) to 6 (f). The x-axis represents the baseline illuminance in the simulation with 81 channels. The y-axis represents the absolute difference from the baseline simulation for the rest of the N-channel simulations in lx.

Table 5 presents the difference in percent for the maximum baseline photopic illuminance on positions 1 to 6 for the simulations with three, nine and 27 channels.

**Table 5.** *The difference in photopic illuminance presented in percent for the simulations with three, nine, 27 and 81 channels compared to the maximum baseline illuminance for positions 1 to 6.*

Number of channels	$\Delta$ in photopic illuminance for maximum baseline illuminance in percent					
	Position 1	Position 2	Position 3	Position 4	Position 5	Position 6
3	4.3	4.6	4.4	4.5	4.3	4.4
9	0.4	0.7	0.8	0.9	1.1	1.0
27	0.1	0.1	0.2	0.8	0.7	0.6

#### 4.4.2 Results of melanopic equivalent daylight illuminance

The same analysis is performed for melanopic equivalent daylight illuminance. According to Figure 23, the simulations with three channels have the highest absolute difference in melanopic equivalent daylight illuminance in comparison to the baseline with 81 channels. As established previously, the absolute difference increases with the increase of the magnitude. The highest baseline melanopic equivalent daylight illuminance is approximately 3216 lx (SD = +/- 16.1 lx) for position 1. Whereas the highest melanopic equivalent daylight illuminance in the three-channel simulation is 2937 lx (SD = +/- 17.0 lx). The difference in melanopic equivalent daylight illuminance compared to the maximum baseline for positions 1 to 6 is presented in Table 6.

**Table 6.** *The difference in melanopic equivalent daylight illuminance presented in percent for the simulations with three, nine, 27 and 81 channels compared to the maximum baseline illuminance for positions 1 to 6.*

Number of channels	$\Delta$ in melanopic equivalent daylight illuminance for maximum baseline illuminance in percent					
	Position 1	Position 2	Position 3	Position 4	Position 5	Position 6
3	8.7	8.8	5.5	6.0	5.6	4.9
9	1.3	1.1	3.4	2.7	3.5	3.5
27	0.7	0.3	1.0	1.4	1.2	1.1

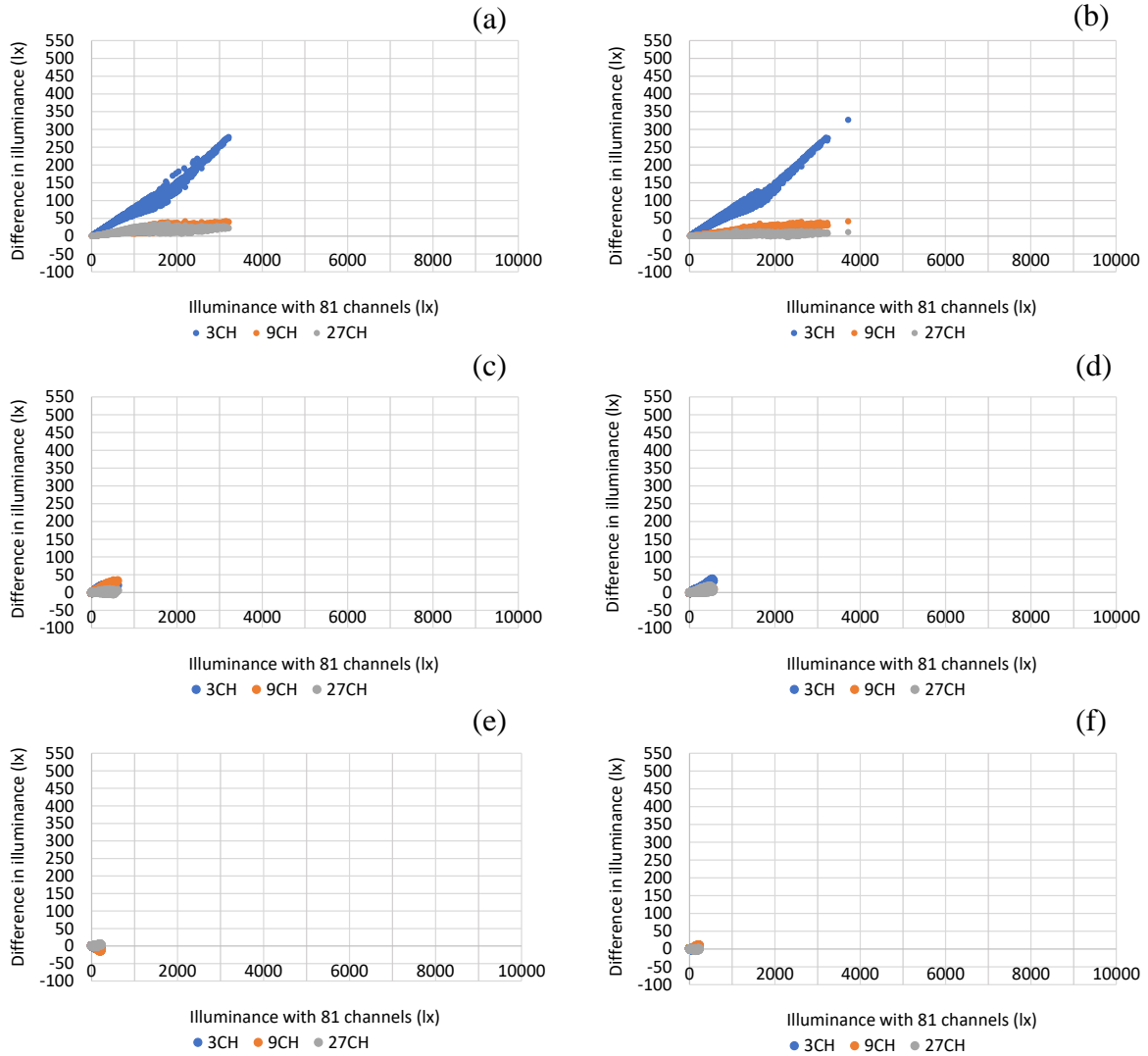


**Figure 23.** The absolute difference in melanopic equivalent daylight illuminance for the simulations with three, nine and 27 channels in comparison to the baseline illuminance with 81 channels for positions 1 (a) to 6 (f). The x-axis represents the baseline illuminance in the simulation with 81 channels. The y-axis represents the absolute difference from the baseline simulation for the rest of the  $N$ -channel simulations in lx.

#### 4.5 Discussion of the ASMS results

The following section discusses the results of photopic and melanopic equivalent daylight illuminance produced by the ASMS. Notably, the difference between the three-channel simulation and the rest of the multichannel simulations is slightly more pronounced with the melanopic equivalent daylight. For example, the absolute difference between the baseline and three-channel simulation is approximately 150 lx for photopic illuminance with 3000 lx. In contrast, the absolute difference is about 250 lx for melanopic equivalent daylight illuminance of the same magnitude (refer to Figures 22 and 23).

Figures 24 and 25 show all hours when the photopic and melanopic equivalent daylight illuminance in positions 1 and 2 are below the respective thresholds (500 lx for photopic illuminance and 250 lx for melanopic equivalent daylight illuminance). These hours serve as the basis for evaluating electric lighting demand. Therefore, accurate prediction of illuminance is especially critical for these hours. The comparison for all hours of the year, irrespective of the illuminance threshold, is presented in Appendix C.

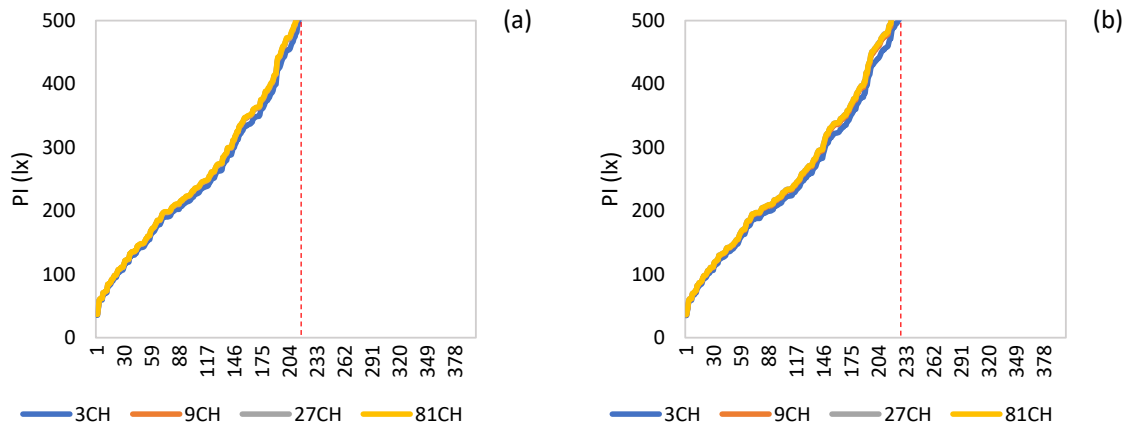


**Figure 24.** Hours when the photopic illuminance is below the 500-lx threshold on the horizontal desk level for position 1 (a) and position 2 (b). The x-axis represents hours. The y-axis presents the illuminance range. The red dashed lines represent hours when photopic illuminance is between zero and 500 lx, corresponding to the threshold of photopic illuminance. PI = photopic illuminance in lx.

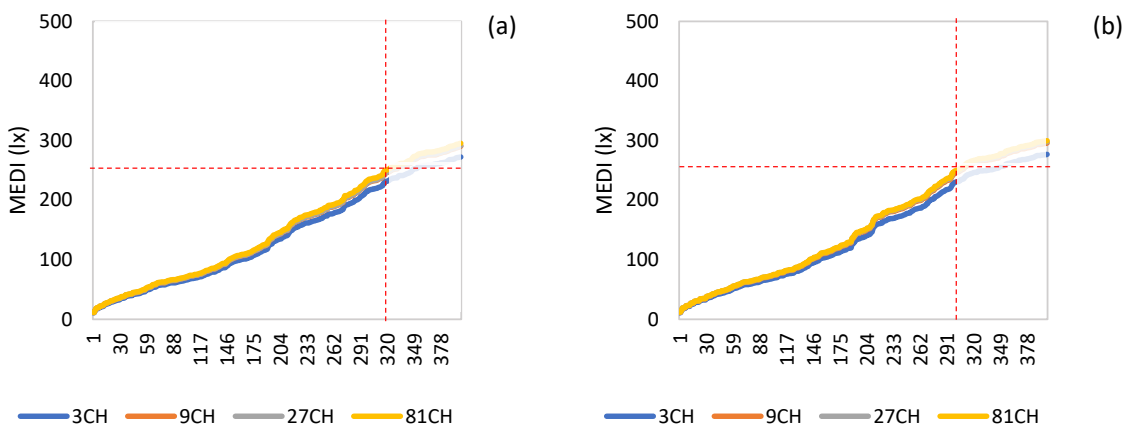


**Figure 25.** Hours when the melanopic equivalent daylight illuminance is below the 250-lx threshold on the vertical eye level for position 1 (a) and position 2 (b). The x-axis represents hours. The y-axis presents the illuminance range. The red dashed lines represent hours when melanopic equivalent daylight illuminance is between zero and 250 lx, corresponding to the threshold of melanopic equivalent daylight illuminance. MEDI = melanopic equivalent daylight illuminance in lx.

Figure 26 elaborates on the previously-mentioned finding by depicting the spectral irradiance at the desk (a) and the eye level (b) on 01.01 at 15:30 in relation to the respective sensitivity curves. To calculate photopic or melanopic equivalent daylight illuminance, the photopic or melanopic sensitivity curve is multiplied by the spectral irradiance at the desk or the eye level. The area under the resultant curve is then scaled by the corresponding factor (see exact steps in Section 3.4)

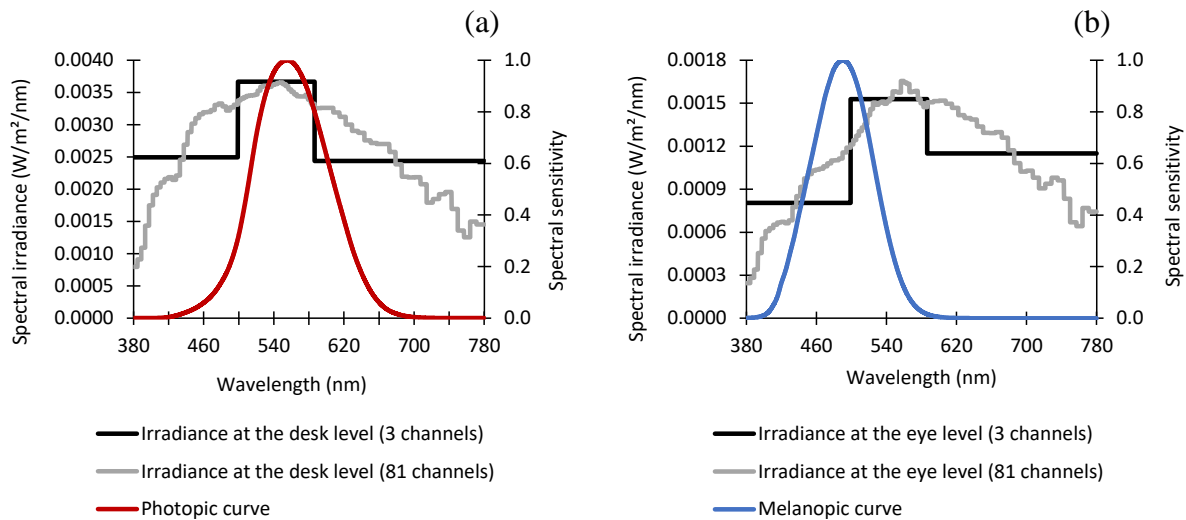


**Figure 26.** Photopic (a) and melanopic (b) sensitivity curves along with the spectral irradiance for the three-channel and 81-channel simulation for position 1 on the horizontal desk level (a) and vertical eye level (b) on 01.01 at 15:30. The x-axis represents the visible spectrum from 380 nm to 780 nm. The left y-axis shows the spectral irradiance in W/m<sup>2</sup>/nm. The right y-axis refers to the relative spectral sensitivity of photopic and melanopic curves.

To explain the larger deviation in the melanopic equivalent daylight illuminance, one should refer to the peaks of the sensitivity curves. The peak of the melanopic sensitivity curve occurs at approximately 490 nm, very close to the boundary between blue and green spectral bins at 499 nm, contributing to the higher underestimation of melanopic equivalent daylight illuminance. On the other hand, the peak of the photopic sensitivity curve occurs at 555 nm, far from the abrupt bin boundaries at 499.0 nm and 586.5 nm.

The photopic illuminance on 01.01 at 15:30 is 238.3 lx (SD = +/- 1.7) in the simulation with three channels and 248.6 lx (SD = +/- 0.6) in the baseline simulation with 81 channels for position 1. This difference corresponds to approximately 4 %. The melanopic equivalent daylight illuminance is 72.0 lx (SD = +/- 0.4) in the simulation with three channels and 77.8 lx (SD = +/- 0.4) in the baseline simulation for position 1. This results in a 7 % difference. These findings are relevant for the evaluation of lighting energy demand since

they propose that a simulation with three channels will predict daylight illuminance, especially melanopic equivalent daylight illuminance, with lower accuracy in comparison to the simulations with higher resolution.

## Section 5

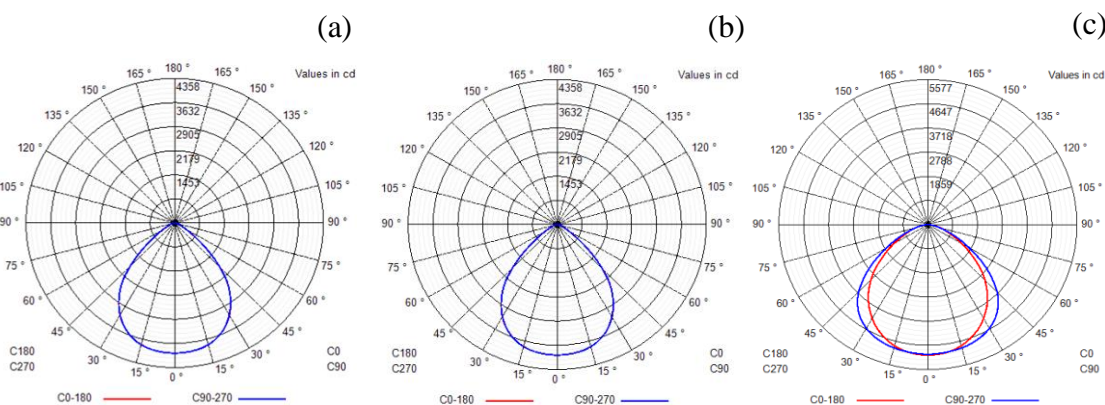
# ASMS and point-in-time spectral simulation with electric light

### 5.1 Photopic and spectral properties of the luminaires

Since daylight is not always sufficient to maintain the required lighting for office activities, electric light is predicted via spectral point-in-time simulation. The following section presents the framework and the results of the spectral simulations. Two LED and one fluorescent luminaires are selected for the analysis:

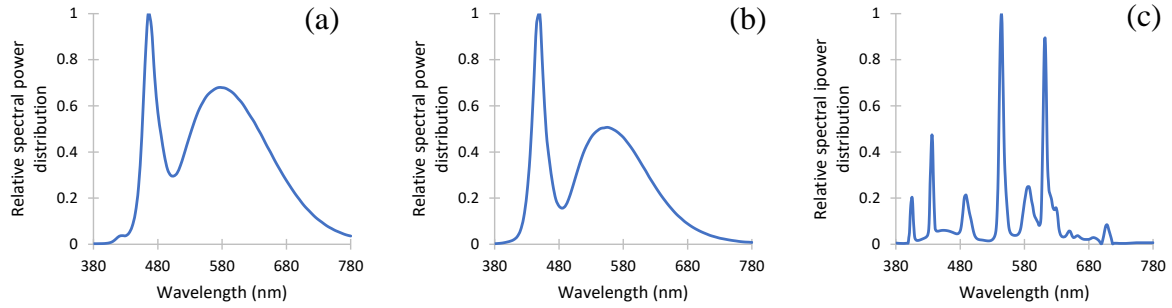
1. LED luminaire with 4000 K (64 W)
2. LED luminaire with 6500 K (64 W)
3. Fluorescent luminaire with 3500 K (216 W)

Figure 27 shows polar luminous intensity graphs of the three luminaires. The distribution of luminous intensity is plotted in candelas for two planes: the frontal plane (C0/180) and the side plane (C90/270). The graph helps determine the expected distribution from the luminaire in addition to intensity. Figures 27 (a) and (b) show symmetrical luminous intensity distribution for LED downlight. Figure 27 (c) shows slightly asymmetrical distribution of fluorescent downlight between the frontal and side planes.



**Figure 27.** Polar luminous intensity graphs of LED with 4000 K (a), LED with 6500 K (b) and fluorescent luminaire with 3500 K (c). The distribution of luminous intensity is in candelas for frontal plane (C0/180) and the side plane (C90/270).





**Figure 28.** Relative spectral power distribution of LED with 4000 K (a), LED with 6500 K (b) and fluorescent luminaire with 3500 K (c). The x-axis represents the visible spectrum from 380 nm to 780 nm. The y-axis shows the spectral power distribution normalized to one.

LEDs with 4000 K and 6500 K represent luminaires with a relatively continuous spectrum. However, the LED luminaire with 6500 K presents a sharper peak in the blue wavelength region of the visible spectrum. The fluorescent luminaire depicts a discontinuous spectrum with several peaks and extreme fluctuations (see Figure 28 (c)).

## 5.2 Maintenance factors of the luminaires

To account for the decrease in illuminance over the entirety of the service life of the luminaire, the maintenance factor (MF) must be considered in the electric simulation according to DIN EN 12464-1 [130]. The maintenance factor is calculated according to the Equation 21:

$$MF = LSF \times LLMF \times LMF \times RSMF \quad (21)$$

where:

**LSF:** Lamp survival factor. It describes the probability of lamp failure over its service life. Considering that the replacement of faulty systems takes place directly in order to maintain the appropriate light levels, this factor is assumed to be 1.0.

**LLMF:** Lamp luminous flux maintenance factor. This factor represents the depreciation in luminous flux of a lamp over its service life. According to the specifications of the manufacturers, this factor is 0.90 for the selected LED luminaires and 0.70 for the fluorescent luminaire.

**LMF:** Luminaire maintenance factor. It expresses the influence of dirt on optical properties of the luminaires. This value is typically 0.93 for direct-distribution luminaires [131].

*RSMF*: Room surface maintenance factor. This factor refers to the depreciation of the reflectance of surfaces that occurs over time. Considering a clean room with a yearly cleaning schedule, the factor is 0.97 for direct-distribution luminaires [131].

The illuminance of the analyzed luminaires is multiplied by the respective maintenance factor to account for the loss that occurs over time. Following Equation 21, the maintenance factors are listed below:

**Table 7.** Factors needed to calculate luminaire-specific maintenance factors according to Equation 21. The resulting maintenance factor is presented in bold font. FL = fluorescent.

Luminaire	LSF	LLMF	LMF	RSMF	<b>MF</b>
LED 4000 K	1.00	0.90	0.93	0.97	<b>0.81</b>
LED 6500 K	1.00	0.90	0.93	0.97	<b>0.81</b>
FL 3500 K	1.00	0.70	0.93	0.97	<b>0.63</b>

### 5.3 Luminaire groups in the office room

Since the office room is relatively deep (8.2 m), positions 1 to 6 get a different amount of natural light. Positions 1 and 2 get the most daylight hours throughout the year and require the least amount of electric lighting. However, even these positions cannot entirely rely on daylight to maintain an appropriate level of illuminance in the room. On the other hand, positions 5 and 6 receive the least amount of daylight and rely on electric lighting the most. Therefore, electric light has to be used for most of the working hours to maintain photopic illuminance and melanopic equivalent daylight illuminance beyond 500 lx and 250 lx respectively, for the positions that are located the farthest from the window. Accordingly, the positions are categorized into three groups to enable independent lighting control:

- Group 1: positions adjacent to the window
- Group 2: positions in the middle of the office room
- Group 3: positions the farthest away from the window

In Figure 29, green and blue dots represent imaginary sensors that record illuminance. The green dots denote the photopic illuminance sensor, which records illuminance at the desk level (0.80 m) on the horizontal plane. The blue dots represent imaginary sensors that

record melanopic equivalent daylight illuminance at eye level (1.20 m) on the vertical plane. The yellow glow lines show that there are two luminaires in each zone.

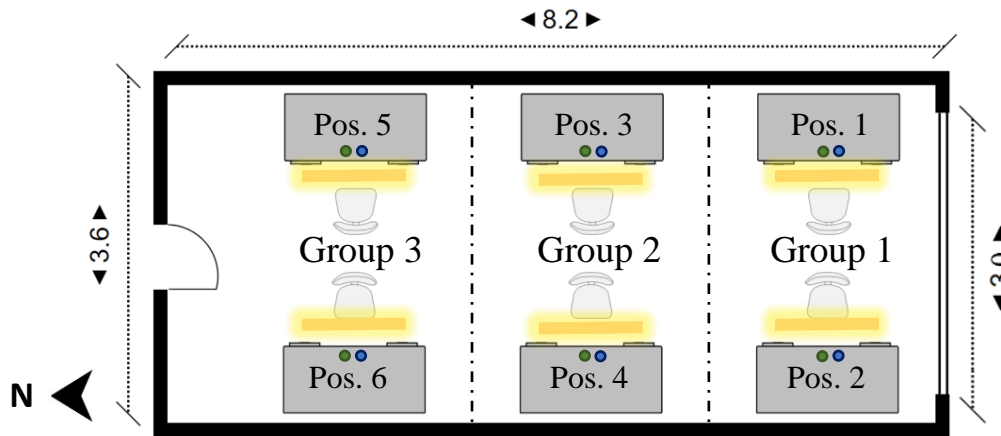


**Figure 29.** Three groups for independent lighting control in the office room. Group 1 represents the positions near the window that receive the most daylight, group 2 depicts the middle positions that receive less daylight and group 3 shows the positions that are located the farthest from the window and have the least amount of daylight. Photopic illuminance, shown by the green dot, is a theoretical sensor for illuminance at the desk level on the horizontal plane (0.80 m). The blue dots represent theoretical sensors that record melanopic equivalent daylight illuminance at eye level on a vertical plane (1.20 m). Pos. = position.

## 5.4 Simulation framework of electric lighting in Radiance

The point-in-time spectral simulation with the electric light is done separately from the ASMS, as commonly done in Radiance simulations when supplementary electric light is required. The sky is generated using *gendaylit* program that utilizes Perez model to generate daylight description in Radiance. To ensure that the sky has no impact on the simulation, the direct-normal-irradiance and diffuse-horizontal-irradiance are assigned zero, creating a dark sky.

As described previously, the transmittance and reflectance of the materials are discretized into three bins where Red, Green, Blue corresponded to wavelength-bands 586.5-780 nm, 499.0-586.5 nm and 380-499.0 nm respectively. Each bin is subsequently divided into finer bins depending on the necessary number of channels. A similar procedure is described in Section 3.3.3 that serves as a pre-processing step for ASMS.

A photometric (IES) file that describes the luminous intensity of luminaires is necessary to simulate electric light. In order to be able to use IES file in Radiance, the file must be converted to Radiance format using *ies2rad* program. To include the previously described

maintenance factor (see Section 5.2), the *-m option* in the *ies2rad* program is used to scale the brightness of the LED and fluorescent luminaires. The color of the luminaire can be specified according to its actual spectral power distribution using the *-c option* in the *ies2rad* program. It is noteworthy that energy balance must be preserved when assigning the color of the luminaire, as is done with the sky in Section 3.3.3. As described in that section, several simulations defined by the total number of channels are needed to depict the visible spectrum of light from 380 nm to 780 nm.

An array of six luminaires is created on top of respective positions (using *-xform* program in Radiance). Dark sky, room geometry, material descriptions and the array of luminaires are combined into one octree file (using *-oconv* program) that represents the 3D room. Finally, a spectral point-in-time simulation is performed (via *-rtrace* command). Post-processing steps are necessary to obtain photopic and melanopic equivalent daylight illuminance from the spectral irradiance on the imaginary sensors at the desk and eye level for each position. These steps are described in Section 3.4. Figure 30 shows the relative spectral irradiance at the eye level from position 1 in a room with LED with 4000 K (a), LED with 6500 K (b) and fluorescent with 3500 K (c) luminaires in a three, nine, 27- and 81-channel simulation.

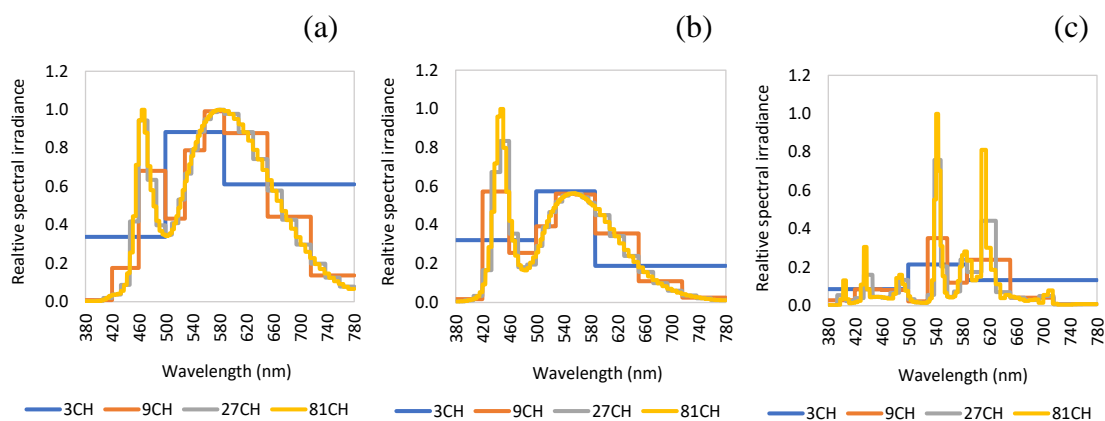


**Figure 30.** Relative spectral irradiance of LED with 4000 K (a), LED with 6500 K (b) and fluorescent luminaire with 3500 K (c) in a three, nine, 27, and 81-channel simulation at the eye level from position 1. CH = channels.

## 5.5 Variability in the simulation of electric light

The variability of the daylight simulation results is highlighted due to the random sampling in the Monte-Carlo raytracing method in Section 4.3. Since electric light relies on deterministic sampling in Radiance, a lower standard deviation is expected between

multiple simulation runs than that presented in the scatter plots in Section 4.3. Tables 8 and 9 show the standard deviation of irradiance based on five simulation runs with LED luminaire with 4000 K. The results represent positions 1 to 6.

**Table 8.** *Standard deviation for irradiance at the desk level (horizontal plane at 0.80 m) for three-channel, nine-channel, 27-channel, and 81-channel discretization based on five simulation runs. The results are presented for each position in the office room with LED luminaire with 4000 K.*

Number of channels	Standard deviation (W/m <sup>2</sup> )					
	Pos. 1	Pos. 2	Pos. 3	Pos. 4	Pos. 5	Pos. 6
3	$1.74 \times 10^{-3}$	$1.66 \times 10^{-3}$	$6.67 \times 10^{-4}$	$6.22 \times 10^{-4}$	$1.44 \times 10^{-3}$	$1.03 \times 10^{-3}$
9	$5.49 \times 10^{-4}$	$4.83 \times 10^{-4}$	$5.21 \times 10^{-4}$	$1.90 \times 10^{-4}$	$7.45 \times 10^{-4}$	$5.36 \times 10^{-4}$
27	$2.88 \times 10^{-4}$	$3.81 \times 10^{-4}$	$2.32 \times 10^{-4}$	$1.85 \times 10^{-4}$	$1.99 \times 10^{-4}$	$2.82 \times 10^{-4}$
81	$1.45 \times 10^{-4}$	$2.10 \times 10^{-4}$	$1.13 \times 10^{-4}$	$1.82 \times 10^{-4}$	$1.70 \times 10^{-4}$	$1.25 \times 10^{-4}$

**Table 9.** *Standard deviation for irradiance at the eye level (vertical plane at 1.20 m) for three-channel, nine-channel, 27-channel, and 81-channel discretization based on five simulation runs. The results are presented for each position in the office room with LED luminaire with 4000 K.*

Number of channels	Standard deviation (W/m <sup>2</sup> )					
	Pos. 1	Pos. 2	Pos. 3	Pos. 4	Pos. 5	Pos. 6
3	$2.14 \times 10^{-3}$	$1.24 \times 10^{-3}$	$1.15 \times 10^{-4}$	$8.25 \times 10^{-4}$	$3.76 \times 10^{-4}$	$6.00 \times 10^{-4}$
9	$6.82 \times 10^{-4}$	$6.51 \times 10^{-4}$	$3.08 \times 10^{-4}$	$4.14 \times 10^{-4}$	$2.67 \times 10^{-4}$	$5.09 \times 10^{-4}$
27	$2.35 \times 10^{-4}$	$2.32 \times 10^{-4}$	$2.17 \times 10^{-4}$	$4.01 \times 10^{-4}$	$2.63 \times 10^{-4}$	$3.02 \times 10^{-4}$
81	$1.76 \times 10^{-4}$	$8.26 \times 10^{-5}$	$1.92 \times 10^{-4}$	$2.86 \times 10^{-4}$	$1.11 \times 10^{-4}$	$2.04 \times 10^{-4}$

The maximum standard deviation occurs in the three-channel simulation and equals to  $1.74 \times 10^{-3}$  W/m<sup>2</sup> for horizontal irradiance and  $2.14 \times 10^{-3}$  W/m<sup>2</sup> for vertical irradiance. The standard deviation for the vertical irradiance, which makes up only  $8.3 \times 10^{-4}$  % of the irradiance magnitude on position 1, is slightly higher than the horizontal irradiance, although both deviations are relatively insignificant.

## 5.6 Illuminance in the prototypical room provided by luminaires

The following section investigates the illuminance in the office room before group-dependent dimming is applied to the luminaires. The purpose of the section is to illustrate the impact of spectral discretization of the luminaires on illuminance. Figure 31 shows

absolute spectral irradiance at the desk and eye level simulated for position 1 with LED with 4000 K, LED with 6500 K and fluorescent luminaire with 3500 K. The spectral irradiance is plotted alongside photopic (a) and melanopic (b) sensitivity curves. Appendix D presents the photopic and melanopic equivalent daylight illuminance produced by the luminaires when they are discretized into three, nine, 27 and 81 channels for positions 1 to 6 based on one simulation run.

**Table 10.** Deviation of photopic and melanopic equivalent daylight illuminance from the baseline simulation with 81 channels for the three-, nine- and 27-channel discretization in percent for position 1. Negative values present overestimation. Lumin. = Luminaires; Chann. = Channels; 4000 K = LED with 4000 K; 6500 K = LED with 6500 K; 3500 K = Fluorescent with 3500 K.

Analysis Lumin. Chann.	Photopic illuminance (%)			Melanopic equivalent daylight illuminance (%)		
	4000 K	6500 K	3500 K	4000 K	6500 K	3500 K
3	0.6	0.7	1.6	-5.8	-12.2	-52.6
9	0.1	0.0	0.9	-3.0	-0.9	-7.4
27	0.0	0.0	0.5	-0.6	-0.7	-2.4

According to Table 10, the difference in photopic illuminance when three-channel simulation is compared to the baseline is 7 lx (0.6 %), 8 lx (0.7 %) and 18 lx (1.6 %) for both LED luminaires and the fluorescent luminaire respectively. When comparing the nine-channel simulation to the baseline, the difference in photopic illuminance is 1 lx (0.1 %) and 11 lx (0.9 %) for LED with 4000 K and fluorescent luminaire, respectively. There is a difference of 5 lx (0.5 %) when comparing the photopic illuminance of the simulation with fluorescent light at 27-channel to the baseline with 81 channels.

When melanopic equivalent daylight illuminance is regarded, the three-channel simulation overestimates the illuminance by 23 lx (- 5.8 %) for the LED with 4000 K, 52 lx (- 12.2 %) for the LED with 6500 K and by 131 lx (- 52.6 %) for the fluorescent luminaire in comparison to the baseline with 81 channels. The overestimation is 12 lx (- 3.0 %) for the LED with 4000 K, 4 lx (- 0.9 %) for the LED with 6500 K, and 18 lx (-7.4 %) for the fluorescent luminaire in the simulation with nine channels in comparison to the baseline.

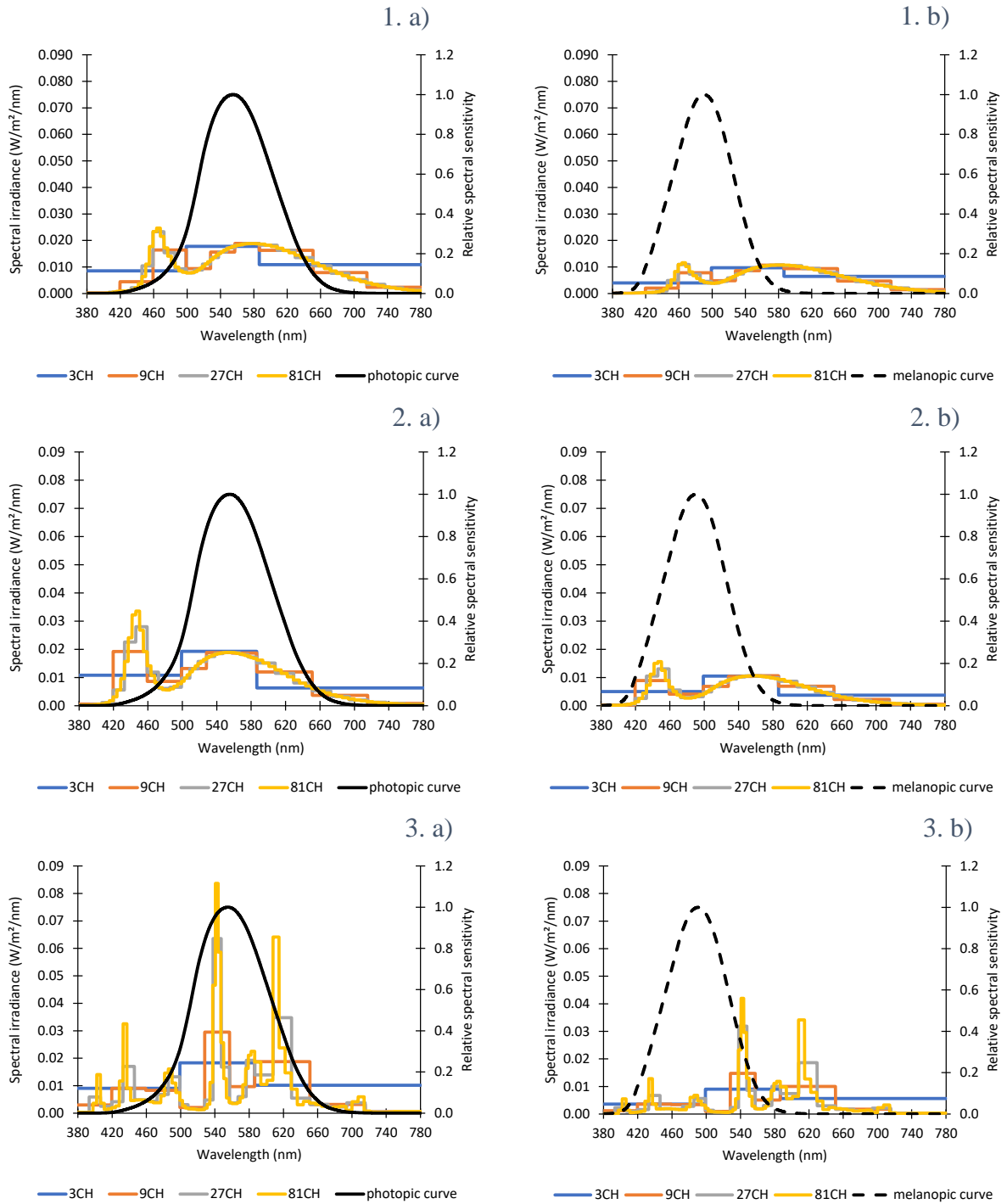


**Figure 31.** Absolute spectral irradiance in a three, nine, 27 and 81-channel simulation with LED with 4000 K (1), LED with 6500 K (2) and fluorescent light with 3500 K on position 1 at the desk level alongside the photopic sensitivity curve (a) and at the eye level alongside the melanopic sensitivity curve (b). CH = channels.

The overestimation is 2 lx (- 0.6 %) for LED with 4000 K, 3 lx (- 0.7 %) for LED with 6500 K and 6 lx (- 2.4 %) for the fluorescent luminaire in comparison to the baseline with 81 channels.

The number of channels affects prediction accuracy more significantly in the case of melanopic equivalent daylight illuminance than photopic illuminance. The improvement in prediction is especially noteworthy when comparing the result of the three-channel simulation to the baseline with 81 channels. The deviation is the highest for fluorescent light, which has many peaks in the visible spectrum. It is followed by the LED with 6500 K, which has a sharper peak in the blue wavelength region and then by the LED with 4000 K, which has the most continuous spectrum among the presented luminaires.

## 5.7 Group-dependent dimming of the luminaires

Photopic and melanopic equivalent daylight illuminance obtained from a point-in-time simulation represents the output of the luminaires when no dimming is applied. However, during many hours, only a fraction of the luminaire output is necessary to reach the prescribed threshold for illuminance. For this reason, a linear dimming function is applied to the luminaires.

The lighting control or the final dimming is determined based on the four imaginary sensors within each group in Figure 29 in Section 5.3. During post-processing steps, the supplementary illuminance, provided by the electric light source to maintain the required level of illuminance, is calculated by subtracting the daylight readings of imaginary sensors from the photopic and melanopic thresholds. Equations 22 and 23 define dimming when photopic and melanopic equivalent daylight illuminance are considered independently. Equation 24 presents the resultant dimming.

$$DF_{photo} = \frac{500 - Daylight_{photo}}{Luminaire_{photo}} \quad (22)$$

$$DF_{mel} = \frac{250 - Daylight_{mel}}{Luminaire_{mel}} \quad (23)$$

where:

$DF_x$ : Dimming factor based on photopic or melanopic equivalent daylight illuminance



*Daylight:* Photopic or melanopic equivalent daylight illuminance provided by daylight ( $lx$ )

*Luminaire<sub>x</sub>:* Maximum photopic or melanopic equivalent daylight illuminance provided by luminaire before dimming ( $lx$ )

The resultant dimming factor is derived through the following calculation:

$$DF_{resultant} = DF_{photo} \text{ if } DF_{photo} > DF_{mel} \text{ or } DF_{mel} \text{ if } DF_{mel} > DF_{photo} \quad (24)$$

where:

*DF<sub>resultant</sub>:* Resultant dimming factor based the dominant dimming factor value

The total output of the luminaire occurs when the dimming factor is 1. For example, during a hypothetical hour X the required supplementary illuminance for positions 1 and 2 within Group 1 are presented in Table 11:

**Table 11.** A hypothetical example of supplementary electric illuminance during hour X for Group 1 in a three-channel simulation. PI = photopic illuminance; MEDI = melanopic equivalent daylight illuminance.

Illuminance	Position 1	Position 2
PI	107.0	102.9
MEDI	51.4	47.5

Highlighted photopic and melanopic values show that position 1 requires more supplementary light than position 2 during hypothetical hour X. Table 12 shows the maximum illuminance output of the LED luminaire with 4000 K in Group 1 at the desk and eye level in a three-channel simulation prior to dimming. These values are the average photopic and melanopic equivalent daylight illuminance for positions 1 and 2 produced by the respective luminaire, which can be found in Appendix D.

Table 13 shows two dimming factors that vary based on the unit of interest. The highest dimming factor in Table 13 will be selected. In this case, the dimming factor of 0.12 is selected and applied to the luminaires in Group 1 as the dimming factor 0.10 would not be sufficient to reach the threshold of melanopic equivalent daylight illuminance. Similar steps are executed for Groups 2 and 3.

**Table 12.** Maximum illuminance output of the LED luminaire with 4000 K for Group 1. The values are an average of illuminance on positions 1 and 2. PI = photopic illuminance; MEDI = melanopic equivalent daylight illuminance.

Illuminance	Group 1
PI	1121
MEDI	412

**Table 13.** Maximum dimming factor during hour X for Group 1 in a three-channel simulation. PI = photopic illuminance; MEDI = melanopic equivalent daylight illuminance.

Illuminance	Group 1
PI-based dimming factor	0.10
MEDI-based dimming factor	0.12

## 5.8 Discussion of the spectral simulation with electric light

It is noteworthy that the standard deviation is significantly higher when daylighting is considered compared to the electric luminaires due to the Monte Carlo sampling. In Section 5.5, the maximum standard deviation of the electric luminaire is only  $\pm 2.14 \times 10^{-3} \text{ W/m}^2$  when irradiance is approximately  $2.6 \text{ W/m}^2$  at the vertical plane. Considering the linear regression model for the same position (position 1) and discretization (three channels), the standard deviation for daylight is  $\pm 0.04 \text{ W/m}^2$  at the same irradiance magnitude. The standard deviation of daylighting is over 18 times higher than that of electric lighting. This finding is consistent with the explanation provided in Section 3.1 that the random nature of the Monte Carlo approach yields a higher standard deviation than the deterministic approach.

Furthermore, according to Section 5.6, spectral discretization significantly affects the prediction accuracy of melanopic equivalent daylight illuminance. This finding is the most evident in the example with fluorescent luminaire with discontinuous spectrum, where melanopic equivalent daylight illuminance is overpredicted by 131 lx (up to - 52.6 %) in the simulation with three channels compared to the simulation with 81 channels. The prediction is overestimated by 52 lx (- 12.2) % and 23 lx (- 5.8 %) for the LED with 6500 K and 4000 K respectively when a spectral three-channel simulation is compared to the simulation with 81 channels. The reason behind lower accuracy in the prediction of

melanopic equivalent daylight illuminance is attributed to the peak of the melanopic sensitivity curve that occurs at 490 nm, very close to the boundary between blue (380.0 nm - 499.0 nm) and green spectral bins (499.0 nm - 586.5 nm), which contributes to the lower prediction accuracy of melanopic equivalent daylight illuminance, as previously described in Section 4.5. Finer discretization has also improved the accuracy of the prediction of photopic illuminance. However, it is noteworthy that the underestimation of photopic illuminance in the simulation with three channels is comparatively less significant. Namely, 7 lx (0.6 %) for LED with 4000 K, 8 lx (0.7 %) for LED with 6500 K and 18 lx (1.6 %) for the fluorescent luminaire when compared to the baseline simulation.

## Section 6

### Lighting energy demand and dimming factor

#### 6.1 Lighting energy demand with photopic- and melanopic-based dimming

The following section presents the annual lighting energy demand of the three different luminaire types in the office room based on the following:

1. photopic and melanopic dimming: dimming of the luminaire based on maintaining illuminance according to the photopic and melanopic equivalent daylight illuminance thresholds; and
2. photopic dimming: dimming of the luminaire based on maintaining illuminance according to the photopic illuminance threshold.

The power of the luminaire is multiplied by the dimming factor for each hour of the year, which requires supplementary electric lighting. The resultant hourly values are then added to calculate the annual lighting demand of the reference room.

$$LE \text{ in the group} = \sum_{i=1}^{3265} DF_i \cdot Power \cdot \Delta t \cdot N \quad (25)$$

where:

*LE*: lighting energy (*Wh*)

*DF*: dimming factor calculated according to the steps described in Section 5.7

*Power*: power of the luminaire (*W*)

$\Delta t$ : time increment in the simulation (h)

*N*: total number of luminaires per group

The annual lighting energy demand kWh/m<sup>2</sup>a is obtained by:

$$\begin{aligned} & \text{Lighting energy demand} \\ & = \frac{(LE \text{ in the group 1} + LE \text{ in the group 2} + LE \text{ in the group 3}) / 1000}{\text{Area of the office room}} \quad (26) \end{aligned}$$

Figure 32 presents the dimming factor in a simulation with 81 channels based on triggering caused by photopic (a), melanopic equivalent daylight illuminance (b) or both (c). For the latter, the resultant signal is determined based on the higher dimming factor, as elaborated in Section 5.7. The dimming behavior in the simulations with the rest of the  $N$ -channels is presented in Appendix E.

Since a higher dimming signal is mostly frequently triggered by melanopic equivalent daylight illuminance, the resultant dimming adopted signals from Figure 32 (b). This finding is highlighted by the significant resemblance of Figures 32 (b) and (c).

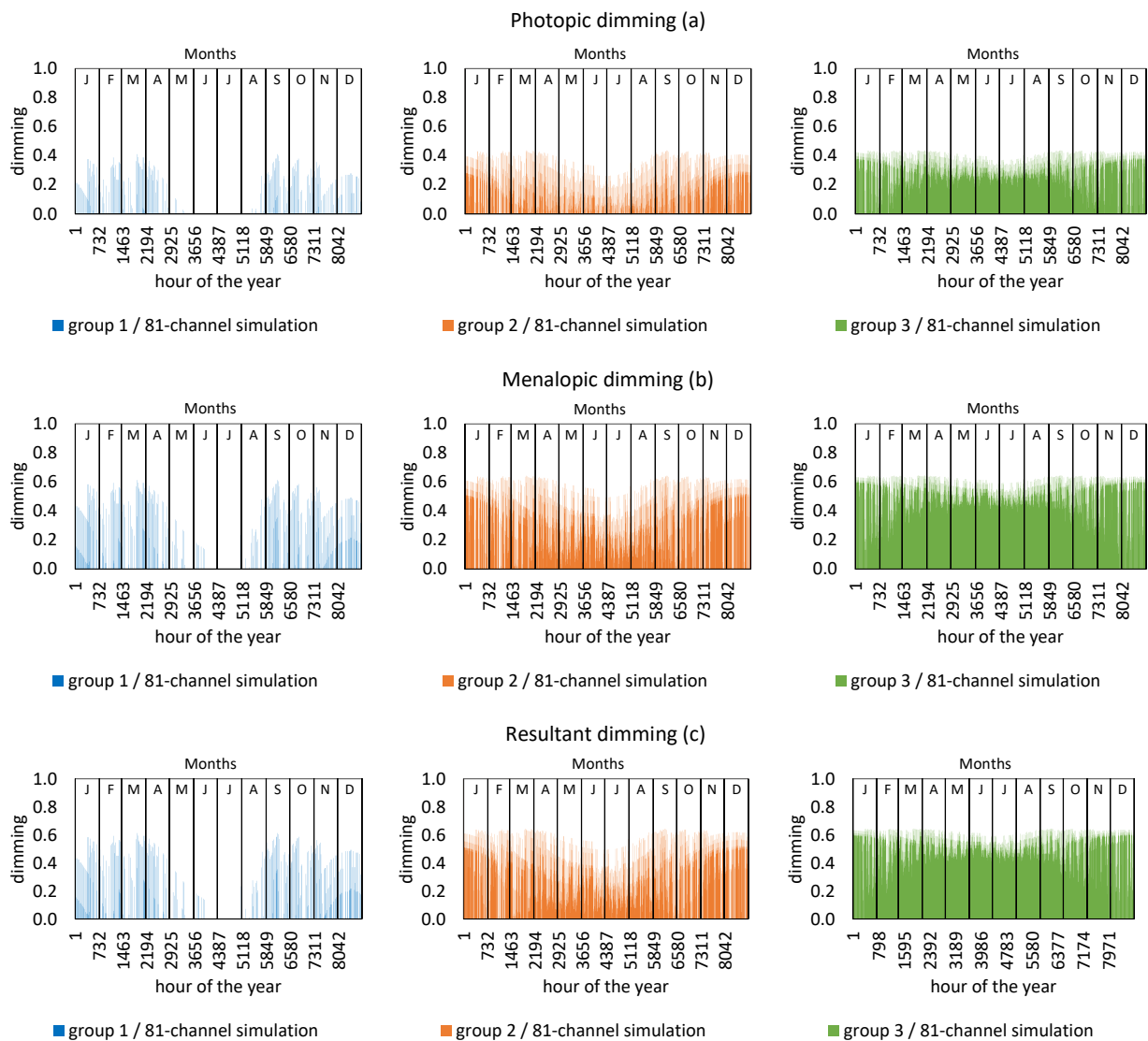


**Figure 32.** Dimming behavior based on photopic illuminance (a), melanopic equivalent daylight illuminance (b) and both (c). The dimming factor is presented for the three groups in the office room for the simulations 81 channels. Luminaire = LED with 4000 K. The lower x-axis represents the hours of the year; the upper x-axis shows the months of the year; the y-axis is the dimming magnitude.

Furthermore, Figure 33 (a) shows annual absolute dimming for photopic and melanopic equivalent daylight illuminance. It highlights that dimming occurs more frequently for melanopic equivalent daylight illuminance than for photopic illuminance. This leads to the conclusion that insufficient levels of melanopic equivalent daylight illuminance are more prevalent in the office room.

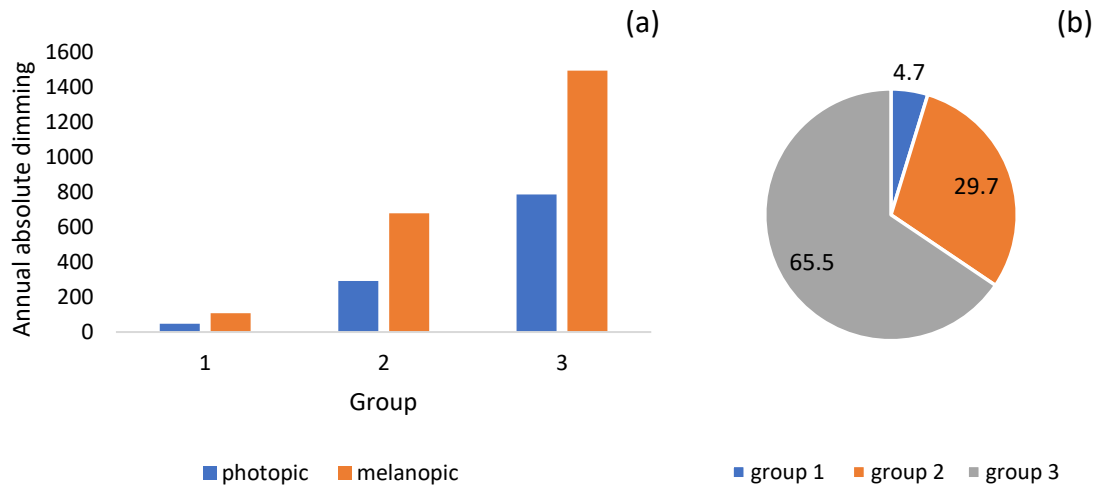


**Figure 33.** (a) Annual absolute dimming triggering based on the thresholds for photopic illuminance and melanopic equivalent daylight illuminance in Groups 1, 2 and 3 in the office room with LED with 4000 K. (b) Pie chart of the photopic and melanopic dimming factor distribution among the three groups in the office room. The results are presented as percentages. Luminaire = LED with 4000 K.

Figure 33 (b) presents a pie chart of the photopic and melanopic dimming factor distribution among the three groups in the office room for a simulation with 81 channels. The percentages are calculated according to Equation 27:

$$\begin{aligned}
 & \text{Dimming percentage}_{\text{Group } x} \\
 &= \frac{\sum_{i=1}^{3265} DF_{i \text{ Group } x}}{\sum_{i=1}^{3265} DF_{i \text{ Group } 1} + \sum_{i=1}^{3265} DF_{i \text{ Group } 2} + \sum_{i=1}^{3265} DF_{i \text{ Group } 3}} \quad (27)
 \end{aligned}$$

$DF_{i \text{ Group } x}$ : resultant dimming factor during hour  $i$  in arbitrary Group  $x$

The dimming factor distribution is consistent with the layout of the office room. The pie chart shows that the dimming in Group 1, which is located near the window, is equivalent to only 4.7 % of the overall dimming in the office room. Dimming in Group 2, the center of the room is equivalent to 29.7 % of the total dimming. Finally, the highest dimming signal occurs in Group 3, located the furthest away from the window. Here, the dimming

ratio is 65.5 %. These percentages correspond to the distribution of the lighting energy demand in the room.

Figures 34 to 36 show the annual lighting demand in the office room with LED and fluorescent luminaires. The figures show variations in lighting demand depending on the number of channels that are considered in the daylight and electric light simulations. The group of the first four bars presents annual lighting demand in the office room considering three-channel simulation for daylighting and three-, nine-, 27- and 81-channel simulation for electric lighting. The following three groups of four bars present the results when daylight is simulated with nine, 27 and 81 channels, serving as the basis for the evaluation of electric lighting demand.

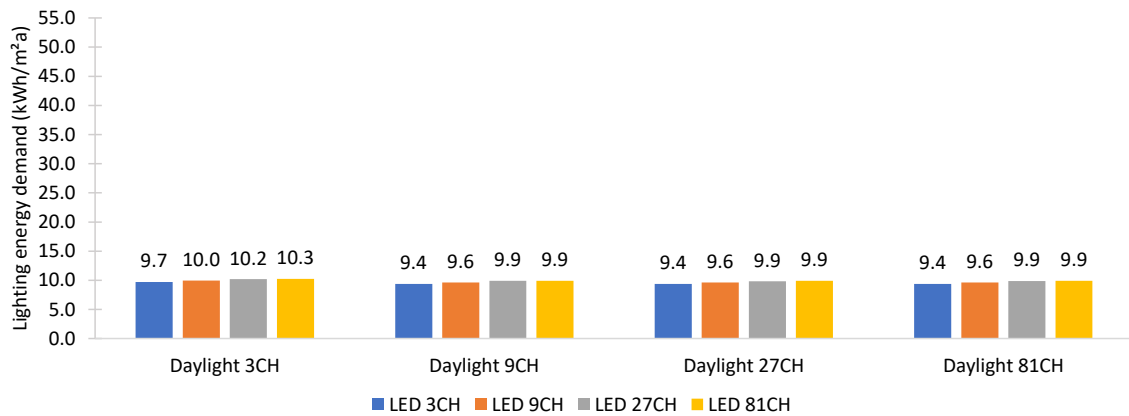


**Figure 34.** Annual lighting energy demand in the office room with LED luminaires with 4000 K with respect to number of channels in the simulations. The results are presented for the simulations with three, nine, 27 and 81 channels to one decimal place.

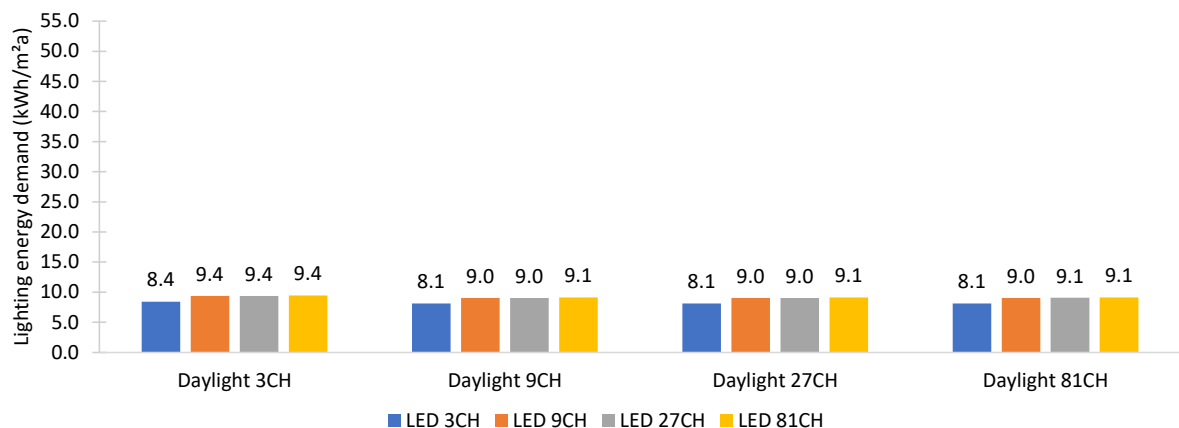


**Figure 35.** Annual lighting energy demand in the office room with LED luminaires with 6500 K with respect to number of channels in the simulations. The results are presented for the simulations with three, nine, 27 and 81 channels to one decimal place.

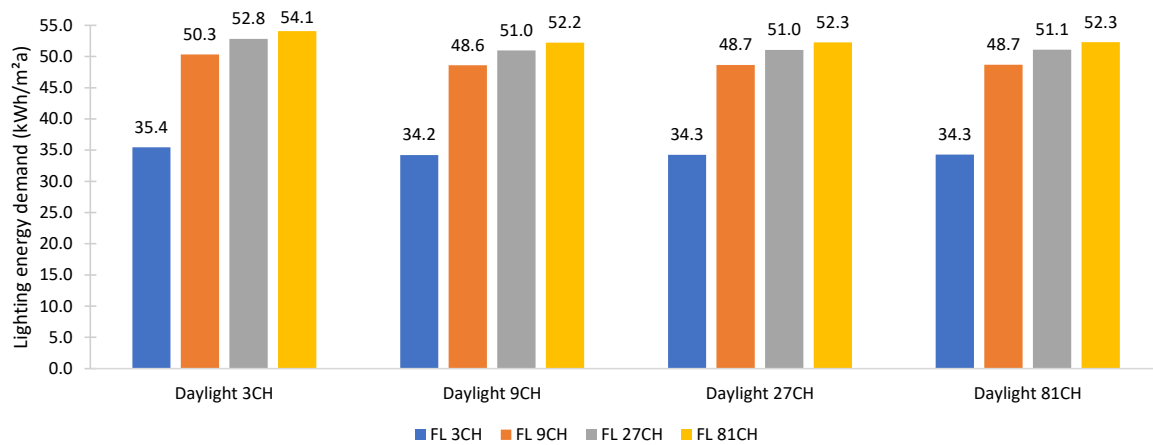


**Figure 36.** Annual lighting energy demand in the office room with fluorescent luminaires with 3500 K with respect to number of channels in the simulations. The results are presented for the simulations with three, nine, 27 and 81 channels to one decimal place.

### 6.1.1 Impact of the number of channels in daylight simulation

This section investigates the effect of daylight discretization on the annual lighting energy demand in isolation. Since the complexity of the simulation framework is predominantly attributed to the ASMS framework that is developed to consider spectral skies for each timestep, this analysis strives to reflect the impact of discretization in the ASMS on the evaluation of electric lighting demand.

The lighting energy demand of the simulations where only the channels of the daylight simulation are increasing is investigated. The same colored bars within Figures 34, 35, and 36 are compared. Considering the daylight simulation with 81 channels as the baseline, Table 14 shows the deviation in percent for the simulations with three, nine, and 27 channels. Negative values represent overprediction of electric lighting demand.

According to the table, a daylight simulation with three channels underpredicts the photopic and melanopic equivalent daylight illuminance (also shown in Appendix C). Therefore, the supplementary electric light is overpredicted by 3.4 %, irrespective of the number of channels in the electric simulation to reach the required illuminance thresholds.

The absolute difference in electric lighting demand differs according to the luminaire of selection. However, the overprediction of lighting energy demand can reach up to 1.1 kWh/m<sup>2</sup>a in a three-channel simulation. This value is deduced by subtracting the electric lighting energy demand of the three-channel simulation with daylight and fluorescent light from the electric lighting demand of daylight and fluorescent light simulated with 81 channels and three channels, respectively. The difference is 0.3 kWh/m<sup>2</sup>a



when LED luminaires are considered. Below are the calculations of the maximum improvement in lighting energy demand. Negative values represent overprediction.

- LED 4000 K:  $9.4 \text{ kWh/m}^2\text{a} - 9.7 \text{ kWh/m}^2\text{a} = - 0.3 \text{ kWh/m}^2\text{a}$
- LED 6500 K:  $8.1 \text{ kWh/m}^2\text{a} - 8.4 \text{ kWh/m}^2\text{a} = - 0.3 \text{ kWh/m}^2\text{a}$
- Fluorescent 3500 K:  $34.3 \text{ kWh/m}^2\text{a} - 35.4 \text{ kWh/m}^2\text{a} = - 1.1 \text{ kWh/m}^2\text{a}$

**Table 14.** *Difference in electric lighting demand of both LED and fluorescent luminaires in percent considering a baseline with 81 channels. Negative values represent overprediction. CH = channels.*

Luminaire	Daylight 3CH	Daylight 9CH	Daylight 27CH
3CH			
9CH			
27CH	-3.4 %	0.2 %	0.1 %
81CH			

### 6.1.2 Impact of the number of channels in electric light simulation

This section discusses the effect of discretization of electric light simulation on lighting energy demand. It addresses the question of whether increasing the number of channels only in the simulation with electric light would significantly affect the lighting energy demand. Considering the electric light with 81-channel simulation as the baseline for assessment, Tables 15 to 17 present the difference in electric lighting demand in percent for the simulations with three, nine and 27 channels.

The difference from the baseline simulation with 81 channels reaches up to 5.3 % with LED with 4000 K, 10.8% with LED with 6500 K and 34.4% with fluorescent luminaire with 3500 K when simulation with only three channels is considered. This finding is similar irrespective of the number of channels in the daylight simulations. The difference between the simulation with three channels and the baseline is significantly more pronounced for the fluorescent luminaire due to the nature of the discontinuous spectrum of this type of illuminant.

The absolute difference in electric lighting demand for fluorescent luminaire is  $18.7 \text{ kWh/m}^2\text{a}$  ( $54.1 \text{ kWh/m}^2\text{a} - 35.4 \text{ kWh/m}^2\text{a}$ ) when comparing a simulation with 81 channels (electric light) and a three-channel (daylight) with a three-channel simulation (daylight + electric light). The absolute difference is  $0.6 \text{ kWh/m}^2$  for LED with 4000 K ( $10.3 \text{ kWh/m}^2\text{a} - 9.7 \text{ kWh/m}^2\text{a}$ ) and  $1.0 \text{ kWh/m}^2\text{a}$  for LED with 6500 K ( $9.4 \text{ kWh/m}^2\text{a} -$

8.4 kWh/m<sup>2</sup>a) when a three-channel (daylight) and 81-channel (electric light) simulation is compared to a three-channel simulation (daylight + electric light).

**Table 15.** *The difference in electric lighting demand of LED luminaires with 4000 K in percent considering the 81-channel simulation of electric light to be the baseline. Negative values represent overprediction. CH = channels.*

LED 4000 K	Daylight 3CH	Daylight 9CH	Daylight 27CH	Daylight 81CH
3CH			5.3 %	
9CH			2.9 %	
27CH			0.5 %	

**Table 16.** *The difference in electric lighting demand of LED luminaires with 6500 K in percent considering the 81-channel simulation of electric light to be the baseline. Negative values represent overprediction. CH = channels.*

LED 6500 K	Daylight 3CH	Daylight 9CH	Daylight 27CH	Daylight 81CH
3CH			10.8 %	
9CH			0.8 %	
27CH			0.7 %	

**Table 17.** *The difference in electric lighting demand of fluorescent luminaires with 3500 K in percent considering the 81-channel simulation of electric light to be the baseline. Negative values represent overprediction. CH = channel, FL = fluorescent.*

FL 3500 K	Daylight 3CH	Daylight 9CH	Daylight 27CH	Daylight 81CH
3CH			34.4 %	
9CH			6.9 %	
27CH			2.3 %	

### 6.1.3 Impact of the number of channels in electric and daylight simulation

In the following section, the combined effect of the discretization of daylight and electric light on lighting energy is presented. Table 18 shows the difference in the prediction of lighting energy demand compared to the reference baseline, a simulation with 81 channels for daylight and electric light. A counterintuitive finding shows a smaller deviation in a three-channel simulation than in a nine-channel simulation. This finding is elaborated next.

**Table 18.** *The difference in lighting energy demand in comparison to the baseline, a simulation with 81 channels for daylighting and electric lighting. In italic bold font: counterintuitive finding that shows lower deviation from the baseline in a three-channel simulation in comparison to a nine-channel simulation. Negative values show an overprediction of the electric lighting demand. Electric light = LED with 4000 K.*

<i>LED 4000 K</i>	Daylight 3CH	Daylight 9CH	Daylight 27CH	Daylight 81CH
3CH	<b>2.1 %</b>	5.5 %	5.4 %	5.3 %
9CH	-0.4 %	<b>3.0 %</b>	2.9 %	2.9 %
27CH	-2.8 %	0.7 %	<b>0.6 %</b>	0.5 %
81CH	-3.4 %	0.2 %	0.1 %	<b>Baseline</b>

As presented in Section 4.5 (also refer to Appendix C), photopic and melanopic equivalent daylight illuminance are more significantly underpredicted in the daylight simulation with three channels compared to the rest of the  $N$ -channel simulations. Since the illuminance of the daylight is consistently underpredicted in a three-channel simulation, the amount of lighting energy needed to reach the necessary threshold of illuminance is overestimated.

At the same time, melanopic equivalent daylight illuminance, which governs the dimming of the luminaires, is consistently and more significantly overpredicted in the electric simulation with three channels. The overprediction depends on the spectrum of the luminaire, as elaborated in Section 5.6 (also refer to Appendix D). For this reason, the annual lighting energy demand is underpredicted in the three-channel simulation compared to the nine-channel simulation for the LED with 4000 K.

Since the three-channel simulation simultaneously overpredicts (due to daylight simulation) and underpredicts (due to electric light simulation) electric lighting demand, the resultant underprediction of only 2.1 % occurs due to the compensation. Compared to the nine-channel simulation (3.0 %), the lower value (2.1 %) is a coincidental result of underestimation and overestimation that occurs in the simulation and is not an indicator of better accuracy.

Because the results are spectrum-dependent, the deviation is different with the LED luminaire with 6500 K. Given that coarse spectral discretization with three channels has a more significant overprediction of melanopic equivalent illuminance with this type of LED luminaire (refer to Table 10 in Section 5.6), which leads to a higher underprediction of the needed lighting energy in a three-channel simulation. This results in the underestimation of

lighting energy demand by 7.8 % in a simulation with three channels in comparison to the baseline simulation, as shown in Table 19.

**Table 19.** *The difference in lighting energy demand in comparison to the baseline, which is a simulation with 81 channels for daylighting and electric lighting. Negative values show an overprediction of the electric lighting demand. Electric light = LED with 6500 K.*

<i>LED 6500 K</i>	Daylight 3CH	Daylight 9CH	Daylight 27CH	Daylight 81CH
3CH	<b>7.8 %</b>	10.9 %	10.9 %	10.8 %
9CH	-2.5 %	<b>1.0 %</b>	0.9 %	0.8 %
27CH	-2.6 %	0.9 %	<b>0.8 %</b>	0.7 %
81CH	-3.4 %	0.2 %	0.1 %	<b>Baseline</b>

Considering that spectral discretization has the biggest impact on fluorescent light due to its discontinuous spectrum (refer to Table 10 in Section 5.6), the underprediction of lighting energy is the highest in comparison to the rest of the luminaires. Table 20 shows that the underprediction of electric light energy is 32.2 % with three channels compared to the baseline.

**Table 20.** *The difference in lighting energy demand in comparison to the baseline, which is a simulation with 81 channels for daylighting and electric lighting. Negative values show overprediction of the electric lighting demand. Electric light = fluorescent with 3500 K.*

<i>FL 3500 K</i>	Daylight 3CH	Daylight 9CH	Daylight 27CH	Daylight 81CH
3CH	<b>32.2 %</b>	34.6 %	34.5 %	34.4 %
9CH	3.7 %	<b>7.0 %</b>	7.0 %	6.9 %
27CH	-1.0 %	2.5 %	<b>2.4 %</b>	2.3 %
81CH	-3.4 %	0.2 %	0.1 %	<b>Baseline</b>

## 6.2 Lighting energy demand with photopic-based dimming

Currently, maintaining an appropriate level of melanopic equivalent daylight illuminance is not prescribed for either simulation-based analysis or real spaces. For this reason, the following section assesses the annual lighting energy demand where only a photopic illuminance threshold of 500 lx at the desk level is maintained. This analysis aims to investigate the lighting energy demand needed for photopic-based simulation only. The purpose is to compare the results to those obtained in Section 6.1, where electric lighting is intended to satisfy photopic (500 lx at the horizontal desk level) and melanopic equivalent daylight illuminance (250 lx at the vertical eye level) requirements.

Figures 37 to 39 show the annual lighting energy demand for the office room with LED and fluorescent luminaires when the electric light is dimmed according to the photopic threshold for illuminance only. As in Section 6.1, the first four bars show the annual lighting demand in a three-channel daylighting simulation and an  $N$ -channel simulation for electric lighting. The other three groups of four bars show when daylight with nine, 27 and 81 channels served as the basis.

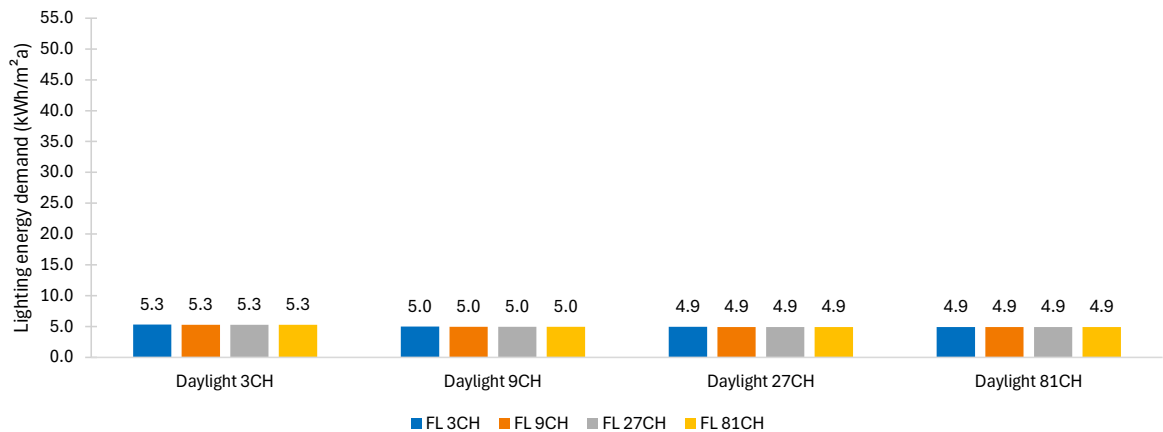


**Figure 37.** Variations in the annual lighting energy demand in the office room with LED luminaires with 4000 K that is controlled based on the threshold for photopic illuminance (500 lx at the horizontal desk level) with three, nine, 27 and 81-channel simulations of daylight and electric light. The results are presented to one decimal place.

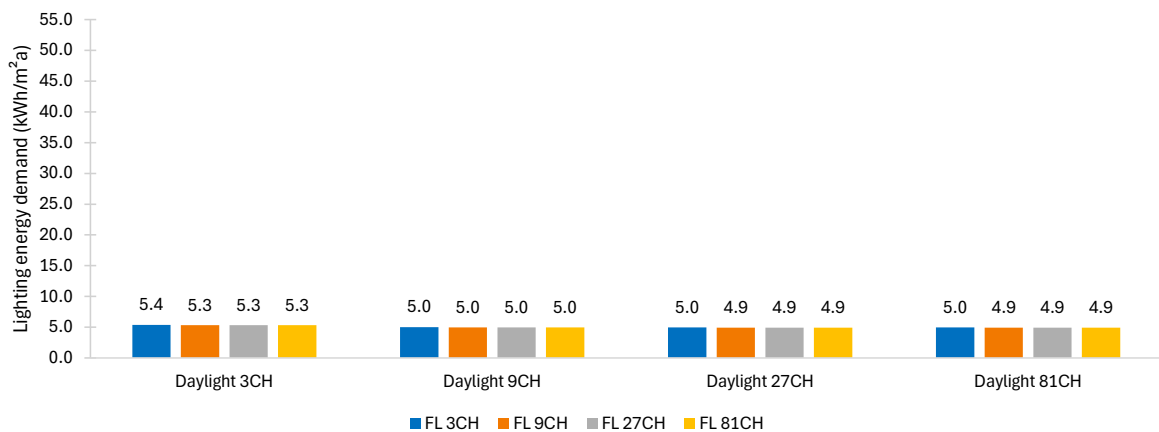


**Figure 38.** Variations in the annual lighting energy demand in the office room with LED luminaires with 6500 K that is controlled based on the threshold for photopic illuminance (500 lx at the horizontal desk level) with three, nine, 27 and 81-channel simulations of daylight and electric light. The results are presented to one decimal place.

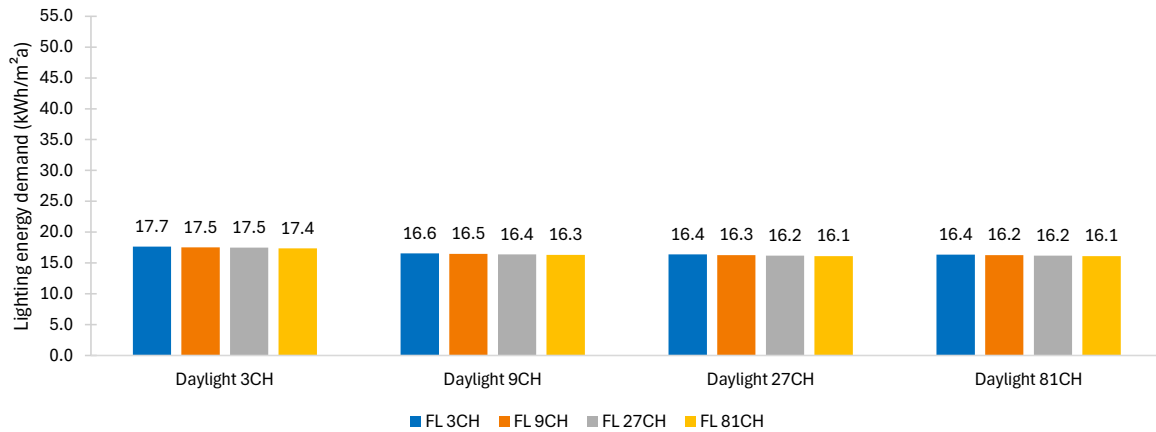


**Figure 39.** Variations in the annual lighting energy demand in the office room with fluorescent luminaires with 3500 K that is controlled based on the threshold for photopic illuminance (500 lx at the horizontal desk level) with three, nine, 27 and 81-channel simulations of daylight and electric light. The results are presented to one decimal place.

Tables 21 to 23 show the difference in the prediction of lighting energy demand with three, nine or 27 channels in comparison to the baseline, which is the simulation with 81 channels for daylighting and electric lighting. According to the tables, the spectral simulation with three channels overestimates the annual lighting energy demand by 8.6 % for LED luminaires with 4000 K, by 8.8 % for LED luminaires with 6500 K, and by 9.7 % for fluorescent luminaires in comparison to the baseline.

Tables 24 to 26 show the difference in annual lighting energy demand in percent between the values presented in Figures 34-36 and Figures 37-39 for LED and fluorescent luminaires. On average, when only photopic illuminance is considered, the annual lighting energy demand is only 48.6 % (LED 4000 K), 43.3% (LED 6500 K) and 63.6 % (fluorescent 3500 K) of the demand where melanopic equivalent daylight illuminance threshold is also maintained.

The figures and tables in this section show that consideration of only photopic illuminance leads to significantly lower annual lighting energy demand in comparison to the values presented in Section 6.1. Furthermore, the effect of discretization on annual lighting energy demand is less evident when only photopic illuminance is considered, as already indicated in Table 10 in Section 5.6, which presents the luminaire output for  $N$ -channels.

**Table 21.** Difference in lighting energy demand in comparison to the baseline, which is a simulation with 81 channels for daylighting and electric lighting. Negative values show an overprediction of the electric lighting demand. Electric light = LED with 4000 K.

<i>Difference in percent (%)</i>				
<i>LED 4000 K</i>	Daylight 3CH	Daylight 9CH	Daylight 27CH	Daylight 81CH
3CH	<b>-8.6</b>	-1.9	-0.7	-0.6
9CH	-8.1	<b>-1.4</b>	-0.2	-0.1
27CH	-8.0	-1.3	<b>-0.1</b>	0.0
81CH	-7.9	-1.2	-0.1	<b>Baseline</b>

**Table 22.** Difference in lighting energy demand in comparison to the baseline, which is a simulation with 81 channels for daylighting and electric lighting. Negative values show an overprediction of the electric lighting demand. Electric light = LED with 6500 K.

<i>Difference in percent (%)</i>				
<i>LED 6500 K</i>	Daylight 3CH	Daylight 9CH	Daylight 27CH	Daylight 81CH
3CH	<b>-8.8</b>	-2.1	-0.9	-0.8
9CH	-8.0	<b>-1.3</b>	-0.1	0.0
27CH	-7.9	-1.2	<b>-0.1</b>	0.0
81CH	-7.9	-1.2	-0.1	<b>Baseline</b>

**Table 23.** Difference in lighting energy demand in comparison to the baseline, which is a simulation with 81 channels for daylighting and electric lighting. Negative values show an overprediction of the electric lighting demand. Electric light = fluorescent light with 3500 K.

<i>Difference in percent (%)</i>				
<i>FL 3500 K</i>	Daylight 3CH	Daylight 9CH	Daylight 27CH	Daylight 81CH
3CH	<b>-9.7</b>	-2.9	-1.8	-1.7
9CH	-9.0	<b>-2.2</b>	-1.0	-1.0
27CH	-8.5	-1.8	<b>-0.6</b>	-0.6
81CH	-7.9	-1.2	-0.1	<b>Baseline</b>

**Table 24.** Underestimation of lighting energy demand in percent when only photopic illuminance is maintained in comparison to the light energy demand when both photopic and melanopic equivalent daylight illuminance thresholds are maintained. Electric light = LED with 4000 K.

<i>Difference in percent (%)</i>				
<i>LED 4000 K</i>	Daylight 3CH	Daylight 9CH	Daylight 27CH	Daylight 81CH
3CH	45.2	46.7	47.4	47.5
9CH	46.8	48.3	49.0	49.1
27CH	48.1	49.6	50.2	50.3
81CH	48.4	49.9	50.5	50.6

**Table 25.** Underestimation of lighting energy demand in percent when only photopic illuminance is maintained in comparison to the light energy demand when both photopic and melanopic equivalent daylight illuminance thresholds are maintained. Electric light = LED with 6500 K.

<i>Difference in percent (%)</i>				
<i>LED 6500 K</i>	Daylight 3CH	Daylight 9CH	Daylight 27CH	Daylight 81CH
3CH	36.4	38.2	39.0	39.1
9CH	43.2	44.8	45.5	45.6
27CH	43.3	44.9	45.6	45.7
81CH	43.7	45.3	46.0	46.1

**Table 26.** Underestimation of lighting energy demand in percent when only photopic illuminance is maintained in comparison to the light energy demand when both photopic and melanopic equivalent daylight illuminance thresholds are maintained. Electric light = fluorescent (FL) with 3500 K.

<i>Difference in percent (%)</i>				
<i>FL 3500 K</i>	Daylight 3CH	Daylight 9CH	Daylight 27CH	Daylight 81CH
3CH	50.2	51.6	52.2	52.3
9CH	65.2	66.2	66.6	66.6
27CH	66.9	67.9	68.3	68.3
81CH	67.9	68.8	69.2	69.2

### 6.3 Analysis of the dimming factor

The dimming of the luminaire is triggered for each hour separately, depending on the required photopic and melanopic equivalent daylight illuminance. Here, dimming based on photopic and melanopic equivalent daylight illuminance and photopic-only dimming is discussed. The following sections present the dimming of the LED luminaire with 6500 K, which is simulated with 81 channels, in groups 1, 2 and 3.

#### 6.3.1 Photopic- and melanopic-based dimming

Figures 40 to 45 show the carpet plots for the dimming for each hour of the year between 8:30 and 18:30. The depth of color represents the dimming of the luminaire. White represents the hours when the luminaire is off and the dimming factor is 0; the most saturated orange color means that the luminaire is on with the full output, i.e., the dimming factor is 1. The light blue shading represents the hours when spectral simulation is not possible due to constrictions in the sky generation (refer to Section 3.3.2). Those hours are left out of the overall analysis.



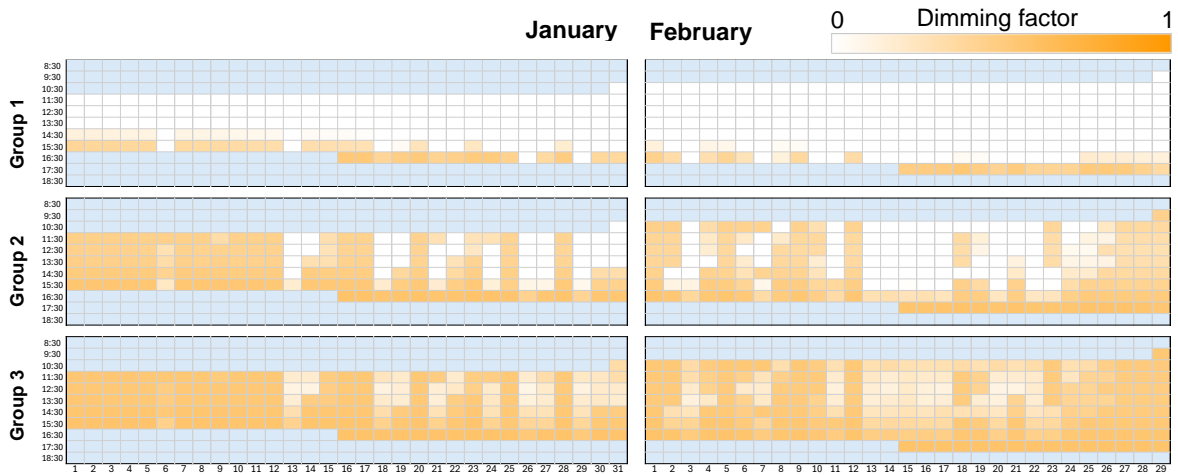


**Figure 40.** Hourly dimming behavior in Group 1, Group 2 and Group 3 in January and February. Pale blue color represents hours of the year for which spectral simulation is not possible due to limitation of spectral sky generation. White color represents no electric light. Shades of orange represent the use of luminaires, where pale color represents a low dimming factor (i.e., luminaire on but with a low intensity) and the saturated orange color represents luminaire on with full output.

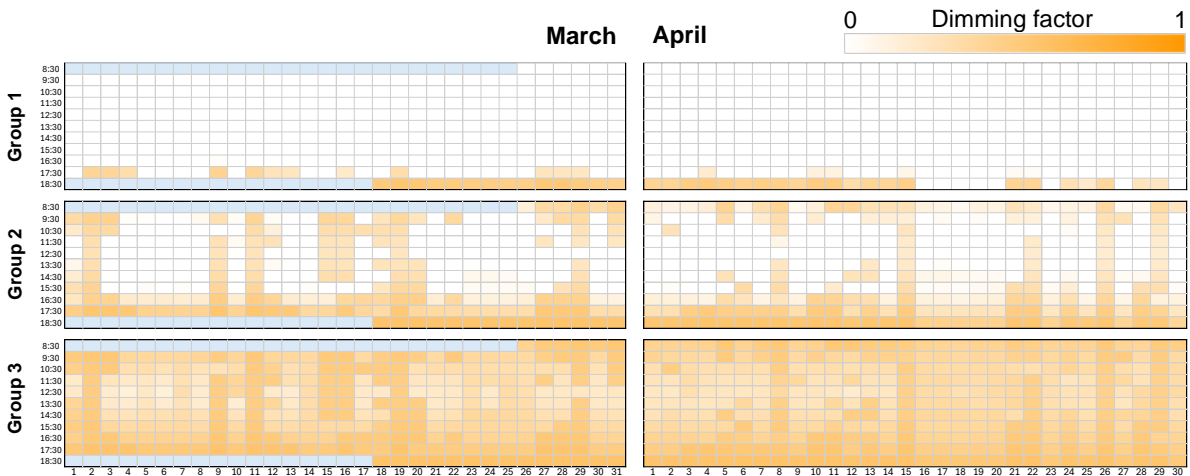


**Figure 41.** Hourly dimming behavior in Group 1, Group 2 and Group 3 in March and April. Pale blue color represents hours of the year for which spectral simulation is not possible due to limitation of spectral sky generation. White color represents no electric light. Shades of orange represent the use of luminaires, where pale color represents a low dimming factor (i.e., luminaire on but with a low intensity) and the saturated orange color represents luminaire on with full output.

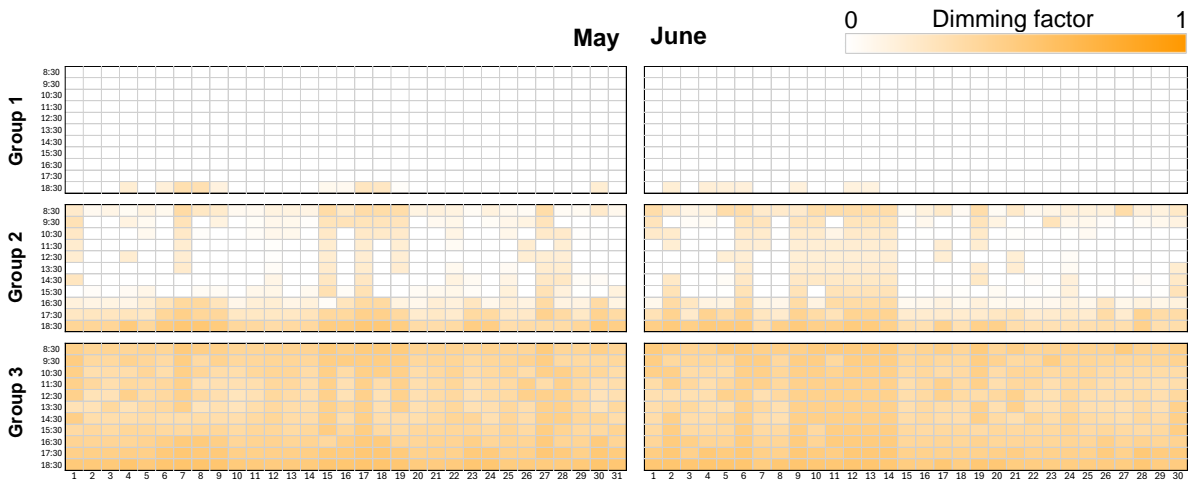


**Figure 42.** Hourly dimming behavior in Group 1, Group 2 and Group 3 in May and June. Pale blue color represents hours of the year for which spectral simulation is not possible due to limitation of spectral sky generation. White color represents no electric light. Shades of orange represent the use of luminaires, where pale color represents a low dimming factor (i.e., luminaire on but with a low intensity) and the saturated orange color represents luminaire on with full output.

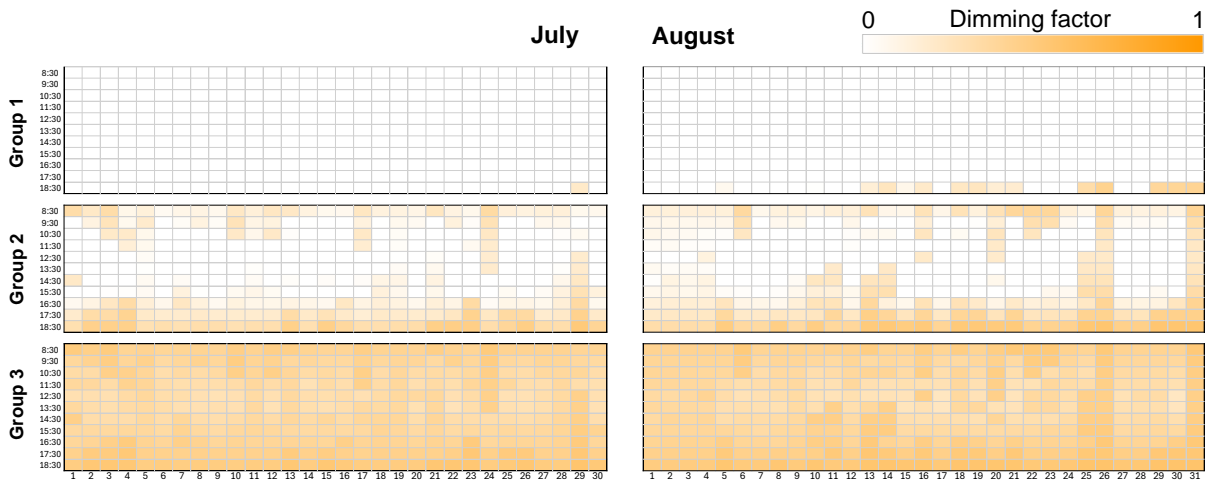


**Figure 43.** Hourly dimming behavior in Group 1, Group 2 and Group 3 in July and August. Pale blue color represents hours of the year for which spectral simulation is not possible due to limitation of spectral sky generation. White color represents no electric light. Shades of orange represent the use of luminaires, where pale color represents a low dimming factor (i.e., luminaire on but with a low intensity) and the saturated orange color represents luminaire on with full output.

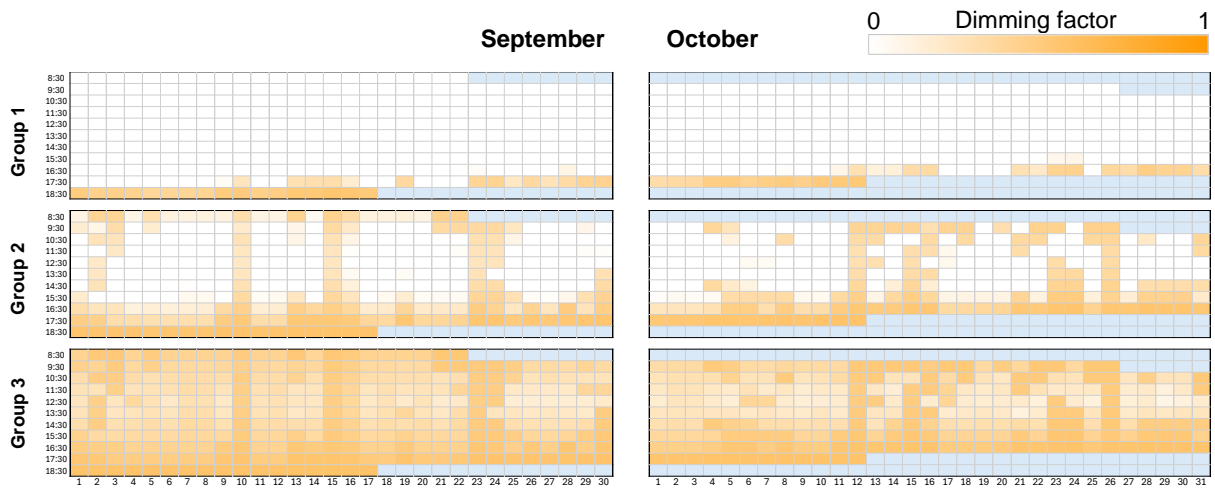


**Figure 44.** Hourly dimming behavior in Group 1, Group 2 and Group 3 in September and October. Pale blue color represents hours of the year for which spectral simulation is not possible due to limitation of spectral sky generation. White color represents no electric light. Shades of orange represent the use of luminaires, where pale color represents a low dimming factor (i.e., luminaire on but with a low intensity) and the saturated orange color represents luminaire on with full output

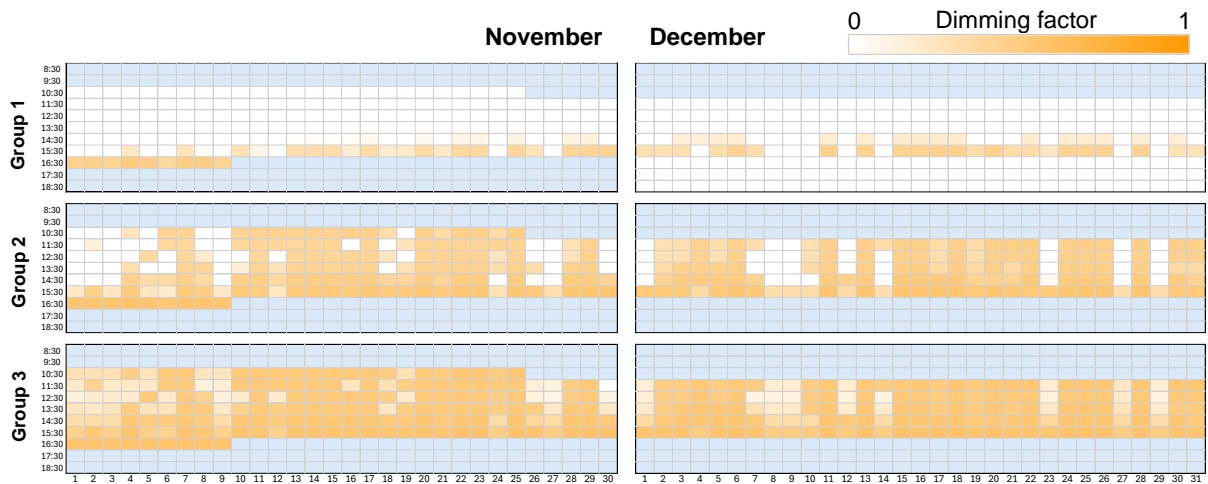


**Figure 45.** Hourly dimming in Group 1, Group 2 and Group 3 in November and December. Pale blue color represents hours of the year for which spectral simulation is not possible due to limitation of spectral sky generation. White color represents no electric light. Shades of orange represent the use of luminaires, where pale color represents a low dimming factor (i.e., luminaire on but with a low intensity) and the saturated orange color represents luminaire on with full output

According to Figures 40 to 45, luminaires in Group 3 activate more frequently than those in Group 1 and Group 2. This is previously mentioned in Section 6.1 and is an expected outcome due to the proximity of the workplaces to the window in Group 1. While months such as March, April, May, June, July, August, September and October display more frequent use of luminaires (due to the ability to generate more spectral skies for more hours for those months), the dimming factor of the luminaires is higher for winter months, such as November, December, January and February, when lower levels of photopic and melanopic equivalent daylight illuminance are expected from daylight.

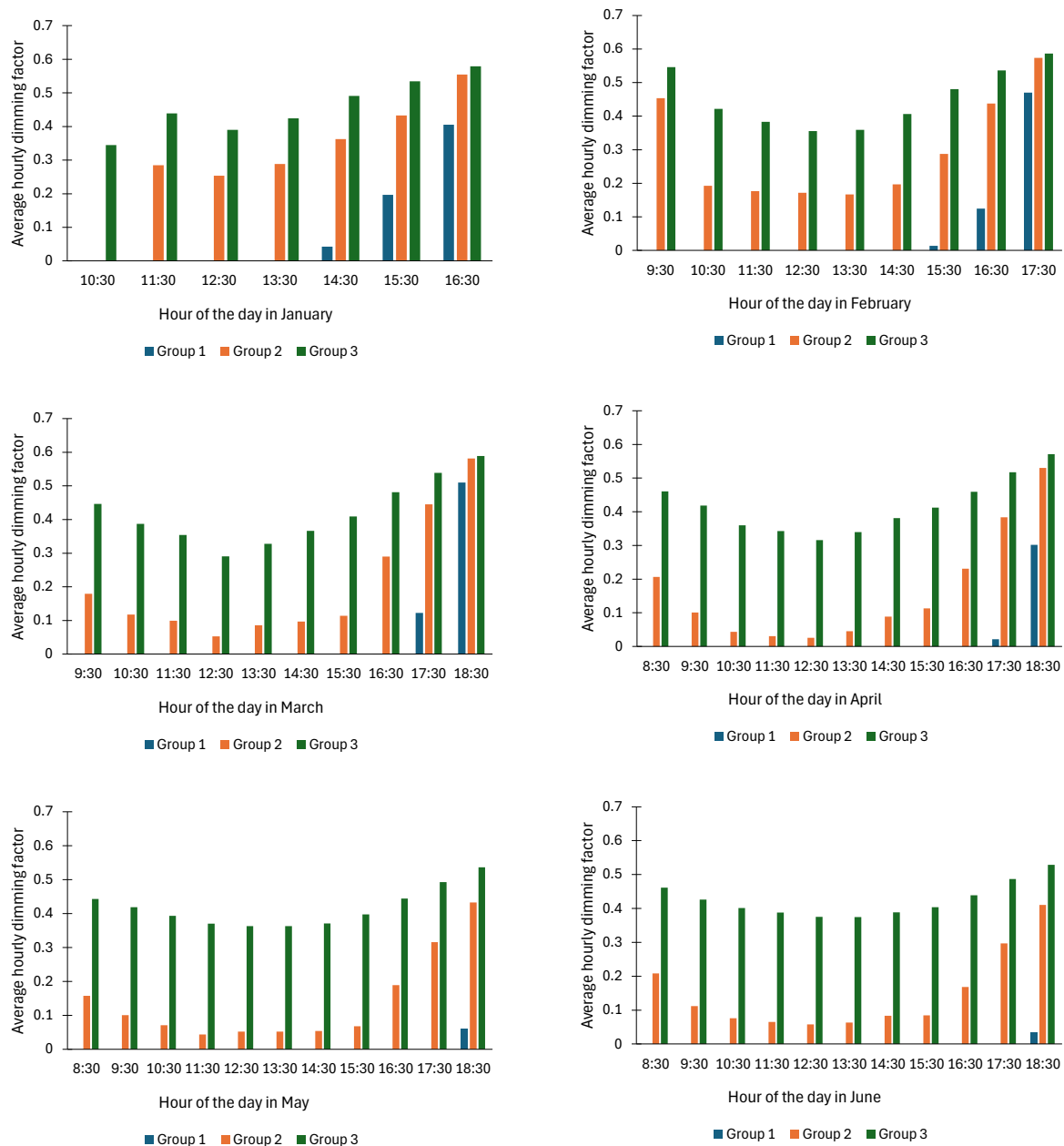


**Figure 46.** Average hourly dimming factor from January to June for group 1, group 2 and group 3 based on the 81-channel simulation and LED luminaire with 6500 K.

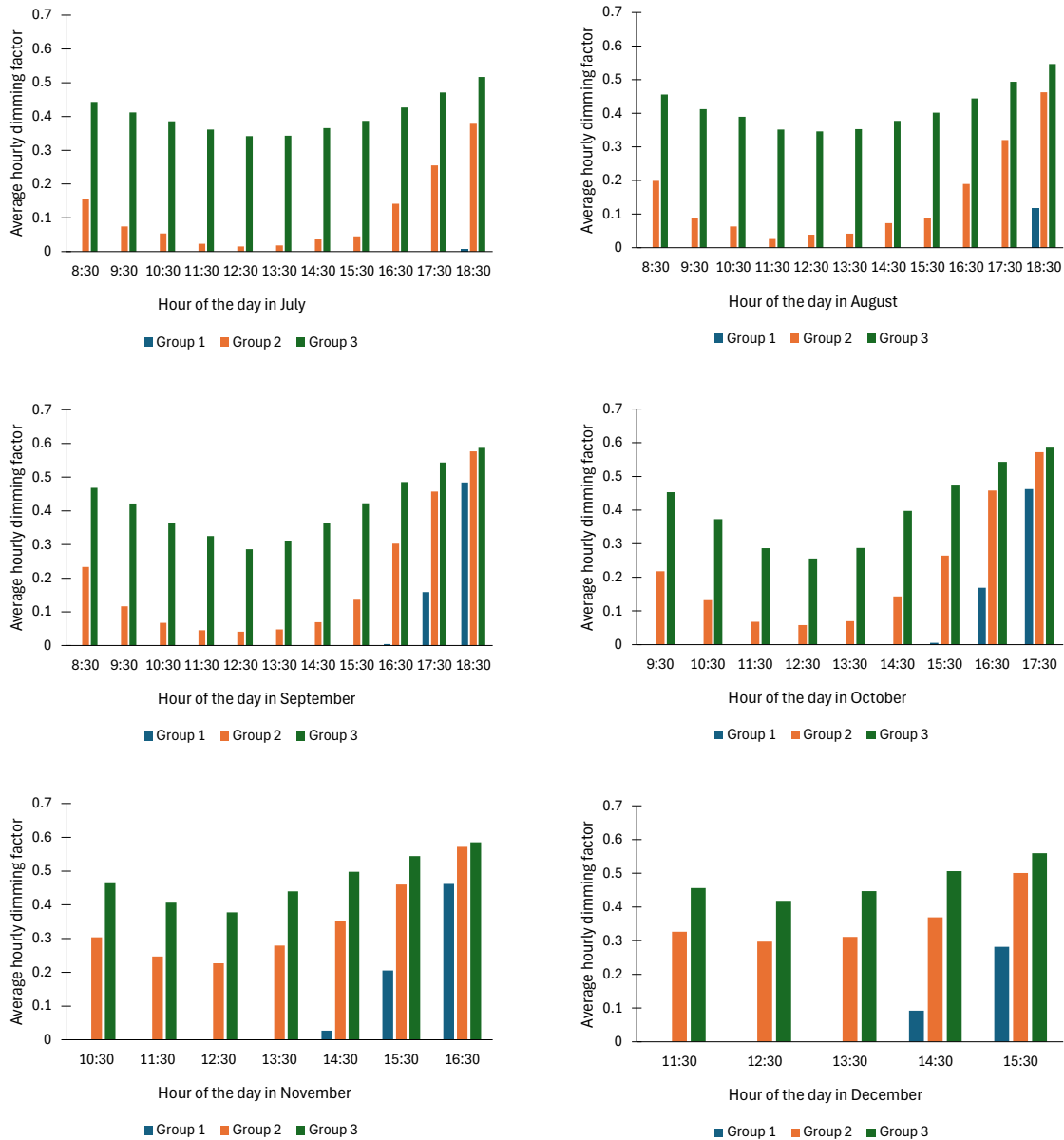


**Figure 47.** Average hourly dimming factor from July to December for Group 1, group 2 and group 3 based on the 81-channel simulation and LED luminaire with 6500 K.

Figure 46 and Figure 47 show the average hourly dimming factor for Group 1, Group 2 and Group 3 from January to December. In this analysis, the dimming factor is based on the 81-channel simulation of the LED luminaire with 6500 K. The luminaires are frequently activated in Group 2 and Group 3 to maintain melanopic equivalent daylight illuminance for positions 3 to 6.

In Group 1, the luminaires are activated less frequently due to the proximity of the work positions to the window. Nevertheless, the luminaires in Group 1 are activated during the

winter months, starting at 14:30 in November, December and January and at 15:30 in February and October.

The dimming factor generally does not exceed 0.6 since this scaling is equivalent to 250 lx of melanopically equivalent daylight illuminance that satisfies the non-visual threshold. It is noteworthy that the average dimming factor is at least 0.3 for Group 3 at all times, which is equivalent to approximately 125 lx.

The above-presented finding highlights the disadvantage of room geometry that on average provides only 50 % of the required lighting on positions 5 and 6 to maintain visual and non-visual requirements through daylighting.

### **6.3.2 Photopic-based dimming**

This section presents photopic-only dimming. The luminaires are dimmed independently within each group to supplement daylight and maintain the appropriate level of photopic illuminance at the horizontal level for positions 1 to 6.

Figures 48 to 53 show the carpet plots from January to December for Group 1, Group 2 and Group 3. As shown in Section 6.3.1, Group 3 receives the least daylight and requires more electric light to maintain an appropriate level of illuminance. However, the carpet plots for November, December, January, and February show that the luminaires are not continuously on in Group 3 as they were in Section 6.3.1. This is because the solar altitude angle is lower in winter months, so daylight can be provided deep into the office and meet the requirements for illuminance at the desk level.

Figures 54 and 55 show the average hourly photopic-based dimming factor during working hours. The average dimming factor is never significantly less than 0.1 in Group 3 (except in October at 12:30), equating to approximately 50 lx. Provided that the dimming factor is at least 0.3 in Group 3 when melanopic threshold of illuminance is considered (refer to Section 6.3.1), this finding suggests that it is more challenging to maintain an appropriate level of melanopic equivalent daylight illuminance than photopic illuminance in the office room when relying on daylight exclusively.

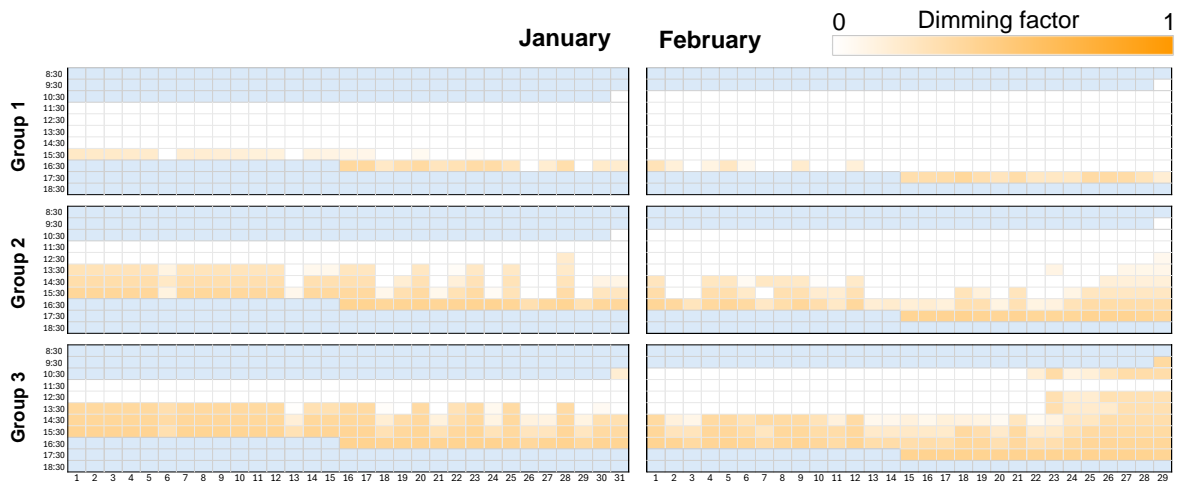


**Figure 48.** Hourly photopic-based dimming in Group 1, Group 2 and Group 3 in January and February. Pale blue color represents hours of the year for which spectral simulation is not possible due to limitation of spectral sky generation. White color represents no electric light. Shades of orange represent the use of luminaires, where pale color represents a low dimming factor (i.e., luminaire on but with a low intensity) and the saturated orange color represents luminaire on with full output.

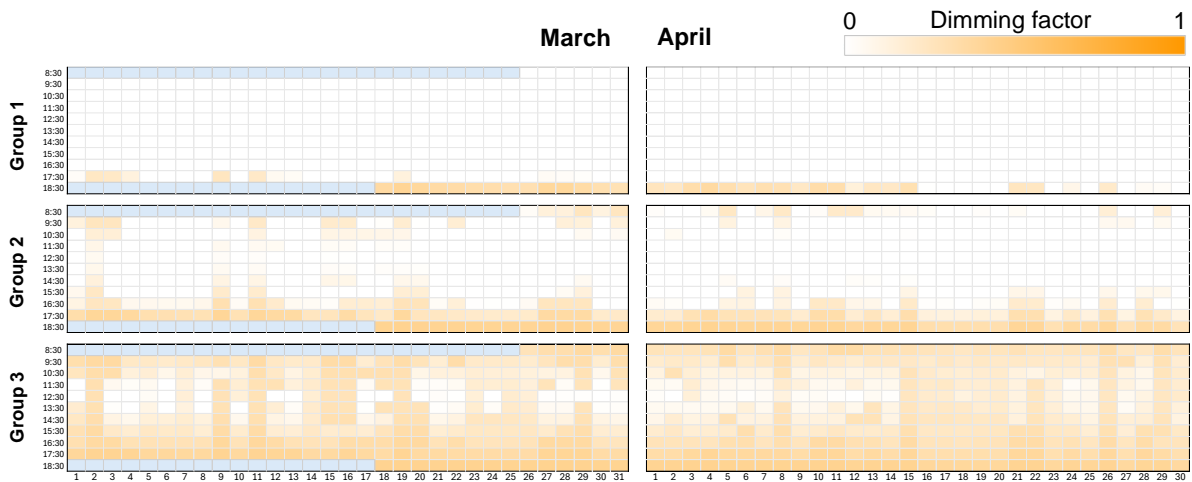


**Figure 49.** Hourly photopic-based dimming in Group 1, Group 2 and Group 3 in March and April. Pale blue color represents hours of the year for which spectral simulation is not possible due to limitation of spectral sky generation. White color represents no electric light. Shades of orange represent the use of luminaires, where pale color represents a low dimming factor (i.e., luminaire on but with a low intensity) and the saturated orange color represents luminaire on with full output.

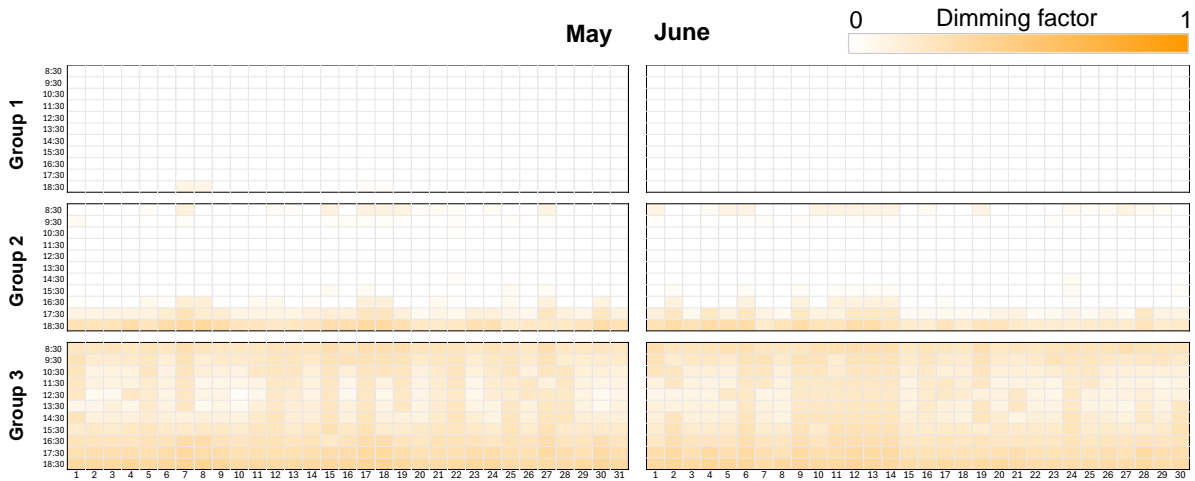


**Figure 50.** Hourly photopic-based dimming in Group 1, Group 2 and Group 3 in May and June. Pale blue color represents hours of the year for which spectral simulation is not possible due to limitation of spectral sky generation. White color represents no electric light. Shades of orange represent the use of luminaires, where pale color represents a low dimming factor (i.e., luminaire on but with a low intensity) and the saturated orange color represents luminaire on with full output.

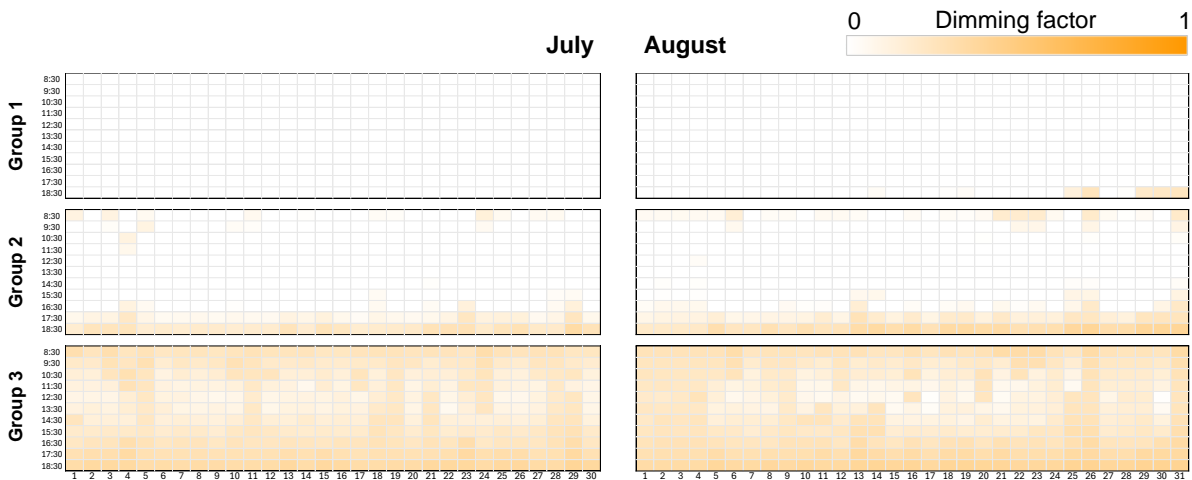


**Figure 51.** Hourly photopic-based dimming in Group 1, Group 2 and Group 3 in July and August. Pale blue color represents hours of the year for which spectral simulation is not possible due to limitation of spectral sky generation. White color represents no electric light. Shades of orange represent the use of luminaires, where pale color represents a low dimming factor (i.e., luminaire on but with a low intensity) and the saturated orange color represents luminaire on with full output.



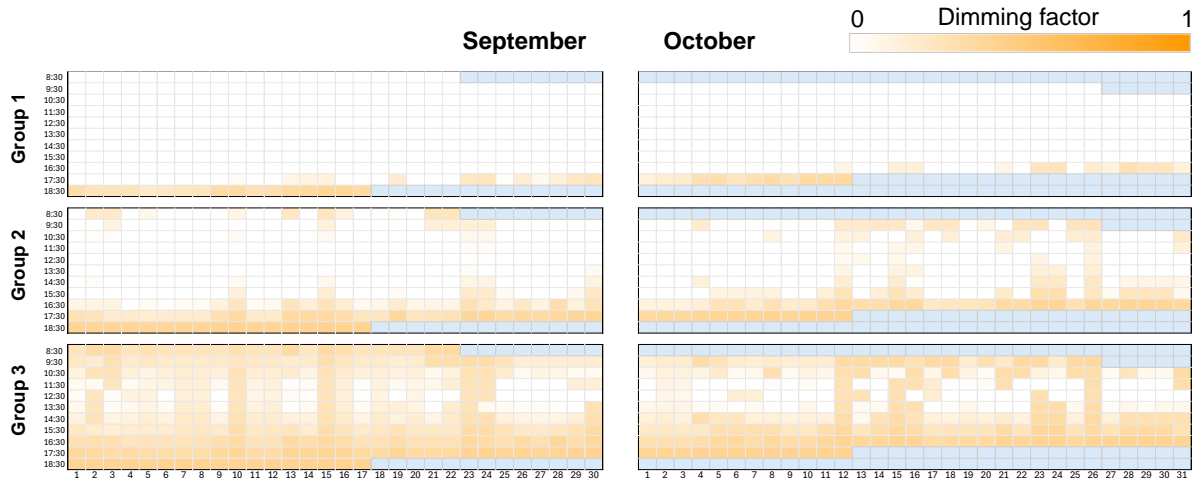


**Figure 52.** Hourly photopic-based dimming in Group 1, Group 2 and Group 3 in September and October. Pale blue color represents hours of the year for which spectral simulation is not possible due to limitation of spectral sky generation. White color represents no electric light. Shades of orange represent the use of luminaires, where pale color represents a low dimming factor (i.e., luminaire on but with a low intensity) and the saturated orange color represents luminaire on with full output.

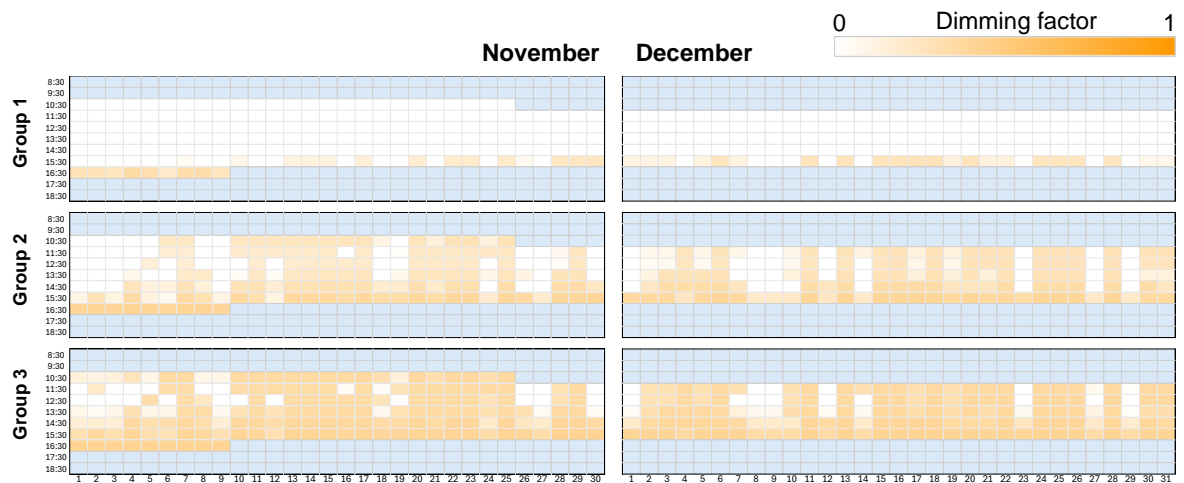


**Figure 53.** Hourly photopic-based dimming in Group 1, Group 2 and Group 3 in November and December. Pale blue color represents hours of the year for which spectral simulation is not possible due to limitation of spectral sky generation. White color represents no electric light. Shades of orange represent the use of luminaires, where pale color represents a low dimming factor (i.e., luminaire on but with a low intensity) and the saturated orange color represents luminaire on with full output.

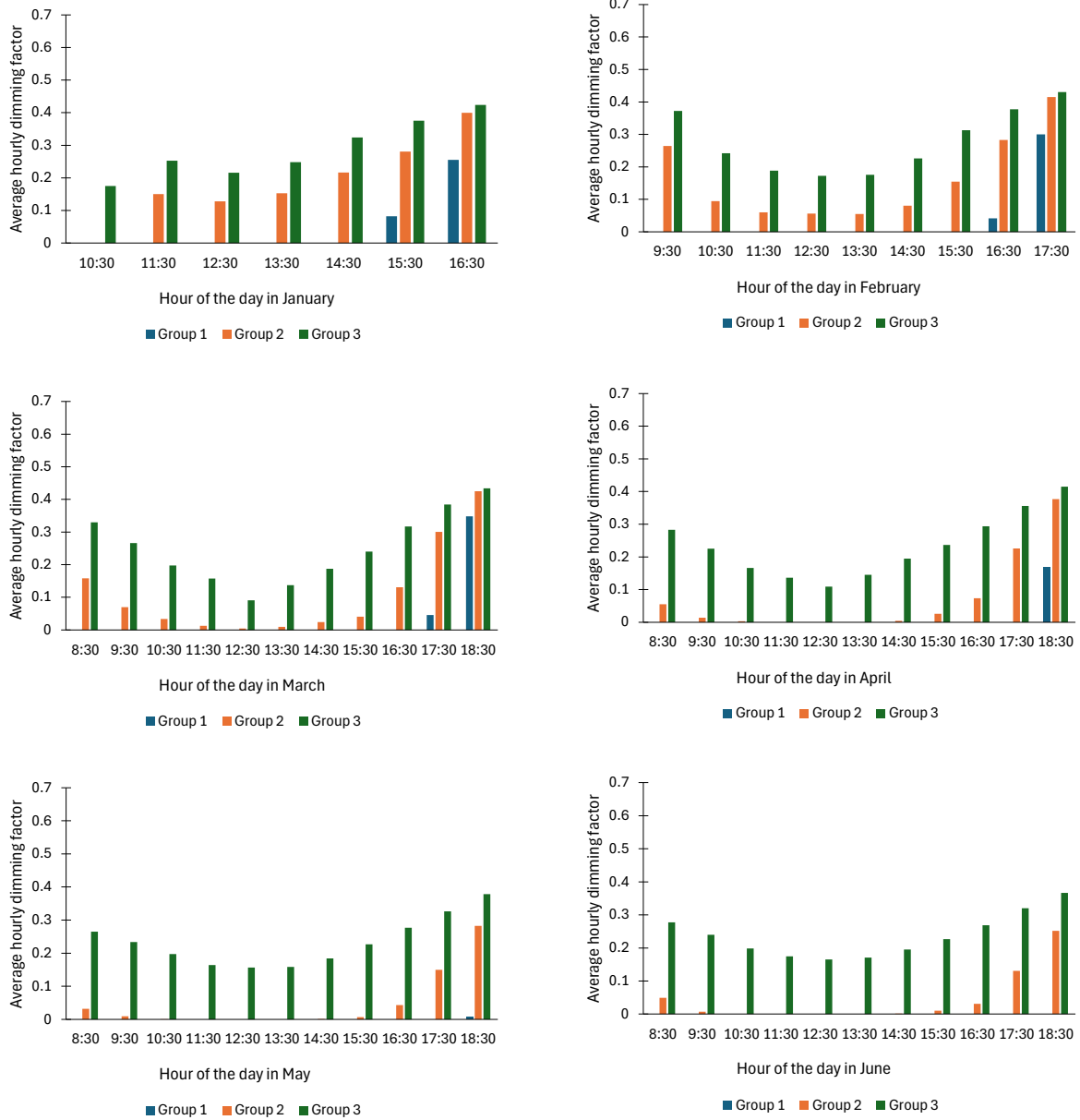


**Figure 54.** Average hourly photopic-based dimming factor from January to June for Group 1, Group 2 and Group 3 based on the 81-channel simulation and LED luminaire with 6500 K.

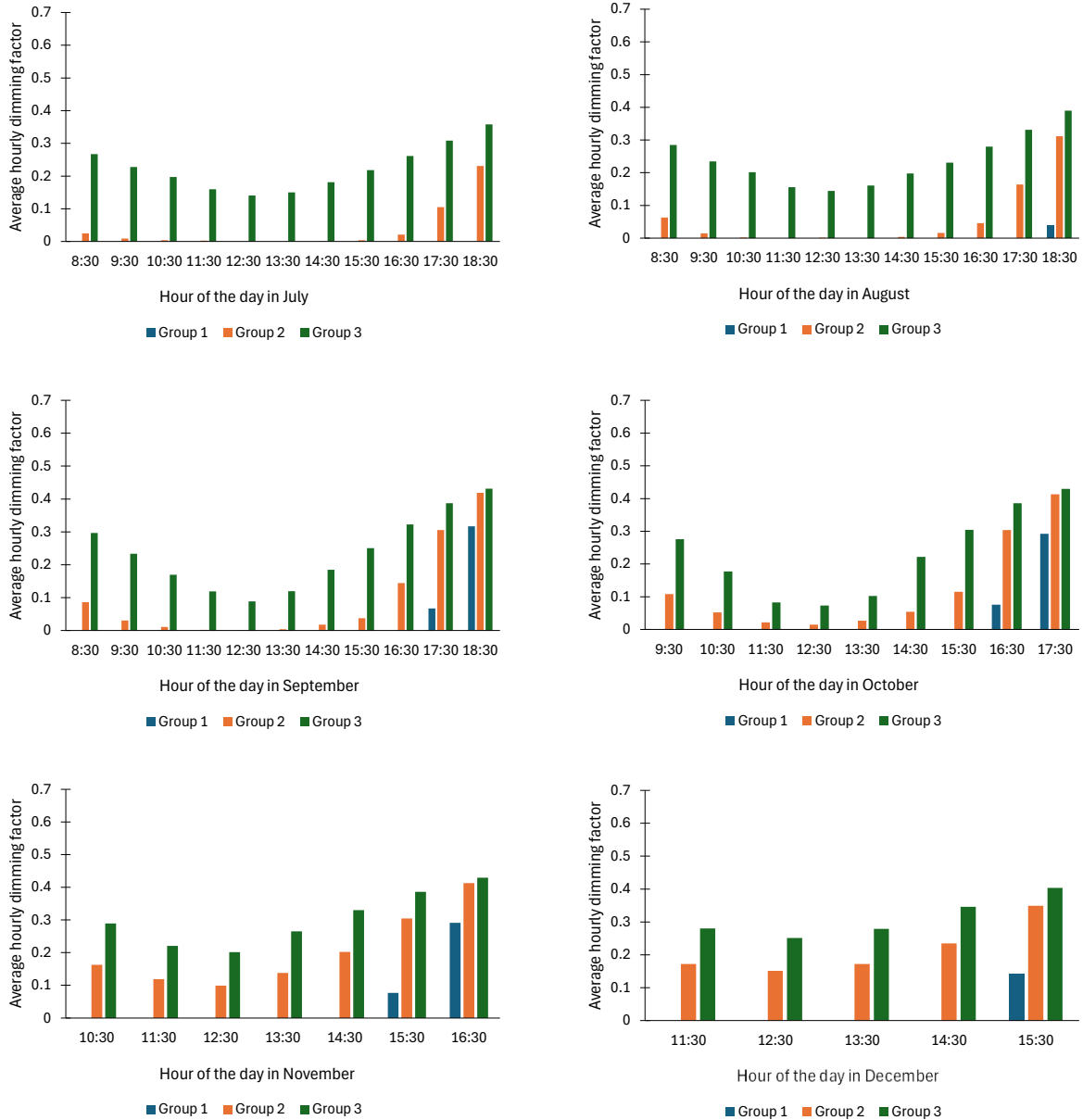


**Figure 55.** Average hourly photopic-based dimming factor from July to December for Group 1, Group 2 and Group 3 based on the 81-channel simulation and LED luminaire with 6500 K.

## 6.4 Discussion of the electric lighting energy

According to the results presented in Section 6, several conclusions can be made regarding the effect of spectral discretization on annual lighting energy demand, depending on analysis criteria. For example, when the number of channels is increased to 81 only in the daylighting part of the simulation, the prediction improvement of annual lighting energy demand reaches up to 3.4 % in comparison to the three-channel simulation. In terms of absolute values, increasing the number of channels to 81 in the daylight simulation prevents the overprediction of lighting energy demand by **1.1 kWh/m<sup>2</sup>a** or **0.3 kWh/m<sup>2</sup>a** that otherwise occurs in a three-channel simulation with daylighting and fluorescent luminaire or with daylighting and LED luminaires, respectively.

When focusing on the discretization of the electric light exclusively and considering the daylighting part of the simulation with three channels constantly, the improvement in the prediction of the annual lighting energy demand is more considerable. Namely, the three-channel simulation underpredicts the annual lighting energy demand between 5.3 % and 34.4 %. These percentages translate to the following absolute annual lighting energy demand:

- **0.6 kWh/m<sup>2</sup>a** with LED with 4000 K
- **1.0 kWh/m<sup>2</sup>a** with LED with 6500 K
- **18.7 kWh/m<sup>2</sup>a** with fluorescent luminaire with 3500 K

When discretization of daylight and electric light is considered, the three-channel simulation underpredicts the annual lighting energy demand in comparison to fine discretization with 81 channels between 2.1 % and 32.2 %, by:

- **0.2 kWh/m<sup>2</sup>a** with LED luminaires with 4000 K
- **0.7 kWh/m<sup>2</sup>a** with LED luminaires with 6500 K
- **16.9 kWh/m<sup>2</sup>a** with fluorescent luminaires with 3500 K

It is noteworthy that nine-channel discretization maintained the underprediction of the electric lighting demand between 1.0 % and 7.0% compared to the simulation with 81 channels. The simulation with 27 channels retained the underprediction between 0.6 % and 2.4 % in comparison to the baseline.

The activation of the luminaires is governed by the non-visual threshold (250 lx of melanopic equivalent daylight illuminance) since the photopic illuminance threshold

appears to be maintained within the acceptable levels by lower luminaire output. Especially noteworthy is that the average hourly melanopic equivalent daylight illuminance on the work positions 5 and 6 in Group 3 of the office room is, at best, 125 lx when daylight is the only means of illumination. Therefore, those positions needed a lot more electric lighting, which points out the disadvantages of deep floor plans in office spaces, especially in terms of provision of sufficient melanopic equivalent daylight illuminance.

Currently, maintaining melanopic equivalent daylight illuminance in spaces is not a requirement. Instead, various standards and recommendations focus on maintaining the photopic properties of light. For this reason, a separate analysis of annual lighting energy demand is done in Section 6.3.2. On the one hand, the results showed that the impact of discretization on the accuracy of the prediction of annual lighting energy demand is less spectrum-dependent when only photopic illuminance is considered; this has been previously highlighted in Section 5.6. In comparison to the conclusions summarised in Section 6.3.1, increasing the number of channels to 81 in the daylight and electric component corrects the overprediction of photopic illuminance that occurs in a three-channel simulation between 8.6 % and 9.7 %, or by:

- **0.4 kWh/m<sup>2</sup>a** with LED luminaires with 4000 K
- **0.4 kWh/m<sup>2</sup>a** with LED luminaires with 6500 K
- **1.6 kWh/m<sup>2</sup>a** with fluorescent luminaires with 3500 K

The annual lighting energy demand overprediction is between 1.3 % and 2.2 % in the simulation with nine channels and between 0.1 % and 0.6 % in the simulation with 27 channels compared to the baseline, depending on the spectral properties of the luminaire.

On the other hand, it was found that the annual lighting energy demand is significantly lower in comparison to the analysis that additionally considered maintaining the required threshold of melanopic equivalent daylight illuminance. When comparing simulations with 81 channels, the underestimation of annual lighting energy demand in the analysis that only regarded photopic illuminance is between 4.2 kWh/m<sup>2</sup>a and 36.2 kWh/m<sup>2</sup>a, depending on the luminaire considered in the office room.

## Section 7

### Discussion

#### 7.1 Summary

Light affects humans in a non-visual way. This relatively new discovery has been the focus of multiple disciplines over the past couple of decades. Even though research on the relationship between light and non-image-forming effects is ongoing, architects and light designers have recently been more proactive in considering non-visual aspects of light in buildings. While there is no concrete consensus about the effect of light on humans today, there are some suggestions in the literature regarding the level of light that should be maintained throughout the day to support physiology, sleep and wakefulness. What is certain is that the spectral composition of light, which is the main component of the non-visual metrics, must be regarded in real spaces and in simulations.

With a few exceptions, most lighting simulation tools do not account for the spectral component of light. Furthermore, a tool that can produce matrix-based annual spectrally resolved simulations is yet to be proposed. Conventional lighting simulation tools present the visible spectrum in one, or at best, three channels: red, green and blue. However, even if the reflectance and transmittance of surfaces from 380 nm to 480 nm are averaged into three channels, much information is lost due to the coarse resolution. The resolution of the discretization in a spectral simulation and in which cases more channels significantly impact the prediction remain to be determined. Presumably, increasing the number of channels can affect the accuracy of illuminance and energy assessment. Especially in rooms with light sources with discontinuous spectral power distribution or surfaces with discontinuous spectral reflectance and transmittance.

This thesis proposes an ASMS framework combined with point-in-time electric light simulation for annual spectral simulation with various levels of discretization for a more accurate assessment of photopic and melanopic equivalent daylight illuminance and, consequently, lighting energy demand. The developed framework proposes the steps to perform annual matrix simulations, which consider the spectral properties of the model and the distinct spectral composition of the sky for each simulated timestep. This framework is based on the daylight coefficient approach. The sky matrix in ASMS is adjusted to include

the spectral component for each individual sky patch, while the geometrical model contains the spectral description of the surfaces. The ASMS method is presented with the possibility of running simulations with three, nine, 27, and 81 channels. The post-processing steps to obtain spectral irradiance, photopic and melanopic equivalent daylight illuminance are described in Section 3.4.

Based on the random nature of hemispherical sampling in the Radiance-based ASMS framework, illuminance predictions can vary even between identical simulation runs (refer to Section 3.1). To investigate the impact of variability, the standard deviation of ten simulation runs is derived based on the irradiance (in the visible spectrum) for each time step. This information produced linear regression models for the simulations with three, nine, 27 and 81 channels for different positions on vertical and horizontal planes. It is found that increasing the number of channels reduces the standard deviation for irradiance. Section 4.3 presented standard deviation that occurs on positions 1 to 6 when only daylight is simulated. Nevertheless, the annual photopic and melanopic equivalent daylight illuminance results are presented based on the average of five simulation runs to reduce the relatively low impact of variability in daylight simulations.

The annual results of photopic and melanopic equivalent daylight illuminance serve as the basis for the simulation of electric light to establish the necessary activation of the luminaires to maintain appropriate illumination in the office space. A point-in-time simulation with a dark sky and electric luminaires is run to establish the output of three luminaires: LED with 4000 K, LED with 6500 K and fluorescent light with 3500 K. The output of the luminaires is scaled using a dimming factor for each hour of the year, according to the needed electric lighting at the desk and eye levels.

The output of the luminaires is controlled differently by adjusting the dimming for each group in the office room based on the theoretical sensors at the desk and eye level. The luminaires are conditioned to supplement the sensor with the lowest photopic or melanopic equivalent daylight illuminance in each group. This ensures that the minimum threshold of photopic and melanopic equivalent daylight illuminance is maintained in the entire group. Group 1, which is closest to the glazing, requires the lowest percentage of electric lighting, namely, 4.7 %, as shown in Figure 33 in Section 6.1. However, during some of the hours of the winter months, the luminaires in Group 1 are on as early as 14:30 or 15:30. Groups 2 and 3 required 29.7 % and 65.5 % of the lighting energy, respectively.

When the simulation was performed with 81 channels, the prediction of annual lighting energy demand in comparison to the spectral simulation with three channels is increased by:

- 2.1 % or 0.2 kWh/m<sup>2</sup>a for 4000 K LED luminaires
- 7.8 % or 0.7 kWh/m<sup>2</sup>a for 6500 K LED luminaires
- 32.2 % or 16.9 kWh/m<sup>2</sup>a for 3500 K fluorescent luminaires

Depending on the luminaire, increasing the channels to nine or 27 maintained the underprediction of the electric lighting demand between 1.0 % and 7.0 % or 0.6 % and 2.4 %, respectively, compared to the baseline simulation. This finding highlights that increasing the number of channels impacts the annual lighting energy demand prediction and is especially significant in the case of luminaires with a discontinuous spectrum.

Further analysis focused on evaluating annual lighting energy demand when the luminaire dimming is only based on maintaining the photopic illuminance threshold (500 lx at the horizontal desk level) in the office room. The simulation with three channels overestimated annual lighting energy demand in comparison to the simulations with higher discretization. It was found that increasing the number of channels from three to 81 reduces the prediction of annual lighting energy demand by:

- 8.6 % or 0.4 kWh/m<sup>2</sup>a for 4000 K LED luminaires
- 8.8 % or 0.4 kWh/m<sup>2</sup>a for 6500 K LED luminaires
- 9.7 % or 1.6 kWh/m<sup>2</sup>a for 3500 K fluorescent luminaires

The simulation with nine or 27 channels overpredicts the annual lighting energy demand between 1.3 % and 2.2 % or 0.1 % and 0.6 %, respectively, compared to the baseline simulation with 81 channels. The exact percentage depends on the spectral properties of the luminaire in the office room.

Notably, the total annual energy demand is significantly lower when only photopic-based dimming is applied to the luminaires. Additionally, the effect of finer discretization on the annual lighting energy demand prediction is less evident when only photopic-based dimming is used to control the luminaires.

## **7.2 Recommendations**

This thesis investigates the effect of spectral discretization of daylight and electric light on annual lighting energy demand in a shoebox model that presents typical features of an



office room. The room has a deep floor plan designed for six occupants executing sedentary tasks, presenting a problematic yet ordinary office layout. The room has six luminaires arranged by pairs into three groups that differ based on their proximity to the window. Three luminaire types were investigated: neutral-white LED light with 4000 K, cool-white LED light with 6500 K, and warm-white fluorescent light with 3500 K. While the results of the analysis are not universally transferrable to other office scenarios, general recommendations for architects and light designers can be derived based on the work presented in this thesis. The following section presents three recommendations:

Recommendation 1:

*Appropriate level of melanopic equivalent daylight illuminance must be maintained in spaces and considered for the assessment of annual lighting energy demand.*

According to the results presented in this thesis, considering only photopic illuminance leads to a significant deficiency of melanopic equivalent daylight illuminance that is otherwise necessary for people to receive throughout the daytime to sustain healthy physiology, sleep and wakefulness. Accordingly, when only the photopic threshold of illuminance is maintained, the prediction of annual lighting energy demand is significantly lower. This leads to the false assumption that less energy is required to sustain illumination in office spaces. This recommendation is valid irrespective of the channel discretization since there is a significant difference in the predicted annual lighting energy demand even in simulations with low resolution.

Recommendation 2:

*Finer spectral discretization leads to more accurate prediction of illuminance and annual lighting energy demand.*

In general, photopic and melanopic equivalent daylight illuminance are underpredicted in the three-channel **daylight simulation** compared to higher-resolution simulations. On the other hand, photopic illuminance is underestimated, while melanopic equivalent daylight illuminance is overestimated in the three-channel **electric light simulation**. The magnitude of overestimation and underestimation is related to the spectrum of the light source. For the reasons mentioned above, a finer discretization ensures a more accurate assessment of illuminance and annual lighting energy demand.

- a) Luminaires with continuous spectrum

This work examined two nearly identical LED luminaires that only differed in their spectral power distribution. At the highest resolution, the annual lighting energy demand was 0.8 kWh/m<sup>2</sup>a higher for the 4000 K LED luminaire because it delivered lower levels of melanopic equivalent daylight illuminance than the 6500 K LED luminaire with the same amount of energy. This difference constitutes 8.8% percent of the annual lighting energy demand of the 6500 K LED luminaire. The difference in photopic illuminance between the two LED luminaires was nearly non-perceivable, which highlights the importance of Recommendation 1. While the numerical findings are specific to the investigated case, it is recommended to consider the spectral power distribution even in subtly different LED luminaires for the highest prediction accuracy.

#### b) Luminaires with discontinuous spectrum

It has been demonstrated that the spectral characteristics and the level of spectral discretization in the model determine the potential accuracy improvement. Thus, a simulation of the model with non-neutral spectral illuminant and surface properties is more likely to profit from fine spectral discretization. This work has confirmed that the finer spectral resolution of luminaires with discontinuous spectral power distribution significantly affects the prediction of illuminance and annual lighting energy demand. The high-resolution discretization of fluorescent luminaires improved the prediction of annual lighting energy demand by over 30 % compared to the spectral simulation with three channels. While this thesis focused on neutral surfaces in the office room, it can be assumed that finer discretization will be equally necessary for surfaces with discontinuous spectral transmittance or reflectance.

#### Recommendation 3:

*The appropriate level of light must be provided for the entire space. Avoiding deep floor plans and including materials that foster light reflection can potentially reduce annual lighting energy demand.*

The analysis showed that providing an acceptable level of melanopic equivalent daylight illuminance is particularly complicated in rooms with deep floor plans where some workplaces locate far from the windows. In the investigated example, it was shown that workplaces in the back of the room, on average, received less than 50 % of the required melanopic equivalent daylight illuminance and needed steady supplementation with electric light to maintain an appropriate level of light. Avoiding deep floor plans at the

conceptual design stage can prevent the disadvantageous light distribution that leads to high lighting energy demand. If such an option is impossible, planning spaces with passive solutions such as light shelves or improving reflectance of the relevant surfaces may contribute to better-lit spaces to some degree. Annual matrix spectral simulation combined with point-in-time spectral simulation of electric light will help predict the potential improvement granted by the passive measures.

## Section 8

### Conclusion

#### 8.1 Conclusion

This thesis proposes an annual spectral matrix simulation (ASMS) framework for multichannel daylight simulations with spectral sky modeling for each timestep. A point-in-time multichannel simulation of electric light completes the framework for hours that require supplementary illumination, based on which the annual lighting energy demand of the luminaires is determined. This thesis investigates whether finer spectral discretization provides more accurate results of illuminance and annual lighting energy demand in a typical office room. The discretization with three, nine, 27 and 81 channels are examined.

It is noteworthy that spectral simulation with three channels does not represent the current practices. Simulations are still often performed with just one channel, assuming a non-spectral, grey environment. In this sense, comparing a one-channel simulation against an 81-channel simulation would result in the most remarkable accuracy improvement. However, since one-channel simulation assumes a flat spectrum from 380 nm to 780 nm, annual illuminance and lighting energy demand predictions do not require the use of the developed ASMS method. For this reason, simulation with one channel is not a part of the analysis. Nevertheless, in the context of the lighting simulation practices, the three-channel spectral simulation does not represent the actual worst-case scenario.

Reflecting on the research questions from Section 1.3, the improvement of the photopic and melanopic equivalent daylight illuminance depends on the spectral complexity of the model. Nevertheless, fine spectral discretization improves the prediction accuracy of photopic and melanopic equivalent daylight illuminance, even for daylight with a relatively continuous spectrum. The accuracy improvement is also significant in the simulation of electric light, especially for luminaires with a discontinuous spectrum, such as the fluorescent luminaire.

It is noteworthy that including metrics that consider the non-visual aspect of light in the assessment shows that higher lighting energy demand is required to sustain the necessary threshold of illumination. Additionally, spectral discretization is especially relevant when

melanopic equivalent daylight illuminance is considered in the assessment. Finer spectral discretization prevents inaccuracies that otherwise occur due to coarse band resolution of the blue and green spectral bins right near the peak of the melanopic sensitivity curve. Finer spectral discretization also improves the accuracy of prediction of photopic illuminance but to a lesser degree.

With regard to lighting energy, spectral simulation with three channels underestimates the actual demand compared to the rest of the  $N$ -channel simulations when the assessment involves photopic and melanopic equivalent daylight illuminance. In contrast, the annual lighting energy demand is slightly overestimated in a three-channel simulation compared to multichannel simulations when only the photopic illuminance is considered. However, the annual lighting energy demand is significantly lower when only photopic illuminance is maintained. In such cases, the minimum threshold of melanopic equivalent daylight illuminance is not met for most of the occupied hours.

As with the illuminance predictions, the magnitude of over- and underestimation of annual lighting energy demand depends on the spectral complexity of the model. However, the underprediction of annual lighting energy demand in a three-channel simulation reaches 16.9 kWh/m<sup>2</sup>a with fluorescent luminaires. For LED luminaires with correlated color temperature of 4000 K and 6500 K, the difference between three- and 81-channel simulations is 0.2 kWh/m<sup>2</sup>a and 0.7 kWh/m<sup>2</sup>a, respectively.

The need for spectral discretization is highlighted when examining the absolute annual lighting energy demand of both LED luminaires. The annual lighting energy demand is 0.8 kWh/m<sup>2</sup>a higher for the 4000 K luminaire at the highest resolution due to distinct spectral power distribution despite otherwise having similar properties. While this thesis presented a relatively typical office room, the results emphasize the importance of including the spectral component in the assessment of illuminance and lighting energy demand, even in spaces with neutral properties.

Lastly, the geometry of the office room has a significant effect on the overall annual lighting energy demand. The disadvantage of the deep floor plan, where some areas heavily rely on the electric light to maintain the required level of illuminance, is an issue that can be addressed in the initial design phases. In already erected buildings, the problem can be improved through passive measures, such as intentional choice of wall paint or reduction of surfaces that obstruct daylight. For the above-mentioned endeavors, the framework

presented in this thesis can aid architects and light designers in making intentional and sustainable choices.

## **8.2 Limitations**

### Generation of the spectral sky

It is plausible that the work presented a few limitations. Section 3.3.2 explains that the ASMS relies on the previously validated conversion of luminance to correlated color temperature. However, the conversions are validated for clear and overcast skies only. While the predominant sky type in Mannheim is intermediate, it is treated as overcast in this work because of the lack of validated conversions in the literature due to the complexity of this sky type. Presumably, the annual lighting energy demand would be different if such conversion existed for the intermediate sky.

Furthermore, the conversion between the sky luminance and correlated color temperature is validated for the German climate and is unlikely to fit other, for example, tropical locations. Another limitation is that the conversion between luminance and correlated color temperature is not validated for hours when the solar altitude is below  $10^\circ$ . Therefore, these hours were not considered in the analysis of electric lighting energy demand, even though they occur in the morning and evening of the winter months.

### Visual and non-visual comfort assessment

This work considered photopic and melanopic equivalent daylight illuminance for the assessment of annual lighting energy demand. The glare evaluation and prevention are currently not integrated into the ASMS. Since ASMS is based on the two-phase method (i.e., daylight coefficient), a matrix-based simulation of dynamic fenestration systems, such as Venetian blinds, is impossible in the current framework. However, the ASMS framework can be potentially extended for use with the three-phase method that includes flux transfer inside the fenestration.

Potentially, it is possible to integrate glare prevention with electrochromic glazing in the current framework. During relevant hours, the most transparent electrochromic glazing state that counters the risk of glare should be selected. For this, a separate simulation for each electrochromic glazing state must be simulated in advance. Nonetheless, the use of electrochromic glazing often presents additional challenges regarding color quality indoors that can be potentially corrected by preserving non-tinted glazing sections and appropriate

spectral composition of electric light. The color quality can be monitored via a color rendering index. The exact implications of glare prevention and maintenance of indoor color quality on the annual lighting energy demand are yet to be explored.

### Non-neutral surfaces

The results presented in this thesis show that the proposed framework is especially beneficial for luminaires with discontinuous spectral characteristics, such as fluorescent luminaires. While the neutral properties of the materials selected for the geometry are typical for an office room, the selection of relatively continuous spectral reflectance and transmittance of the surfaces did not fully challenge the potential of the developed tool. The inclusion of tinted glazing and accent walls could add complexity to the simulated scene to explore the capability of the multichannel spectral simulation tool. The addition of such surfaces to the scene would likely show a higher accuracy improvement when increasing the number of channels in the ASMS than that presented in Section 6.1.1.

## **8.3 Outlook**

The discovery of the non-visual effect of light on humans is a relatively new and ongoing endeavor for researchers in the respective fields. In building science and lighting research, work is ongoing to implement discoveries that pertain to non-visual aspects of light in the evaluation of illumination in the form of recommendations, frameworks and spectral simulation tools for architects and light designers to implement in practice.

Following the need, this thesis presented a novel method for the annual spectral simulation of daylight in combination with electric light. The results showed the benefit of using the developed spectral simulation method by improving the accuracy of illuminance and annual lighting energy demand. The next step would be to expand the method to be functional with the three-phase approach for matrix-based simulation of dynamic fenestration systems that prevent glare risk. Regarding evaluation metrics, the color rendering index will also be a valuable addition to the proposed simulation method, especially in scenarios with non-neutral surfaces.

Furthermore, in a broader context, it will be necessary to include heating and cooling systems along with thermal comfort metrics to evaluate the impact of providing (visually and non-visually) appropriate light levels on the overall annual energy demand. It remains to be determined whether the heat gain from elevated lighting needs will contribute to

reducing heating or increasing cooling in the spaces. In the future, similar investigations should be conducted for living spaces to holistically fulfill the requirements for illumination and thermal comfort while considering the annual energy demand.

Future work should include the possibility of spectral sky generation for intermediate conditions by finding and validating the correlation between luminance and correlated color temperature. The applicability of spectral sky generation in climates with a different atmospheric composition should be explored. It is possible that other relationships between the sky luminance and spectral power distribution would need to be established for different climates. A validation-based study is highly recommended for all new correlations introduced to the spectral sky generation framework.

This thesis showed that a matrix-based annual spectral simulation method is achievable through a customized workflow in a conventional lighting simulation tool. Despite the possible future enhancements, the proposed ASMS method, in combination with the spectral simulation of electric light, can serve as one of the decision-making tools to ensure an adequate level of light for visual tasks and healthy physiological functions while improving the prediction of the lighting energy demand. Designing a user-friendly alpha version of the tool would encourage its use by architects and light designers.



# Abbreviations

<i>ALFA</i>	Adaptive Lighting for Alertness
<i>ASMS</i>	Annual Spectral Matrix Simulation
<i>CS</i>	Circadian Stimulus
<i>CSA</i>	Circadian Stimulus Autonomy
<i>CL<sub>A</sub></i>	Circadian-effective Light
<i>CS<sub>d</sub></i>	Circadian-effective Light Dose
<i>CBDM</i>	Climate Based Daylight Modelling
<i>CQAT</i>	Color Quality Assessment Tool
<i>CIE</i>	Commission Internationale de l'Eclairage
<i>CCT</i>	Correlated Color Temperature
<i>DF</i>	Dimming Factor
<i>FL</i>	Fluorescent
<i>LLMF</i>	Lamp Luminous Flux Maintenance Factor
<i>LSF</i>	Lamp Survival Factor
<i>LED</i>	Light-emitting Diode
<i>LMF</i>	Luminaire Maintenance Factor
<i>LCF</i>	Luminance Color Factor
<i>MF</i>	Maintainance Factor
<i>MAPE</i>	Mean Absolute Percentage Error
<i>MEDI</i>	Melanopic Equivalent Daylight Illuminance
<i>OWL</i>	Occupant Wellbeing through Lighting
<i>PI</i>	Photopic Illuminance
<i>libRadtran</i>	Radiative Transfer Library
<i>RGB</i>	Red, Green, Blue
<i>RSMF</i>	Room Surface Maintenance Factor
<i>SCPAT</i>	Spectral Color Property Assessment Tool
<i>SD</i>	Standard Deviation (y)

# Nomenclature

Symbol	Description	Unit
$a_{cv}$	circadian action factor	[-]
$\eta_c$	circadian ratio	[-]
$C(\lambda)$	circadian spectral sensitivity function	[-]
$D_{\theta\varphi}$	daylight coefficient	[-]
$EML$	equivalent melanopic lux	[EML]
$E_e$	irradiance	[W/m <sup>2</sup> ]
$LE$	lighting energy	[Wh]
$K_{mel,v}^{D65}$	melanopic daylight (D65) efficacy ratio	[mW/lm]
$E_{v,mel}^{D65}$	melanopic equivalent daylight (D65) illuminance	[lx]
$E_{mel}$	melanopic illuminance	[melanopic-lx]
$s_{mel}(\lambda)$	melanopic spectral sensitivity function	[-]
$E_v$	photopic illuminance	[lx]
$L_v$	photopic luminance	[cd/m <sup>2</sup> ]
$V(\lambda)$	photopic spectral sensitivity function	[-]
$S_{\theta\varphi}$	projected solid angle of the sky element at an altitude of $\theta$ and azimuth of $\Phi$	[sr]
$E_{e,\lambda}$	spectral irradiance	[W/m <sup>2</sup> /nm]
$L_{e,\lambda}$	spectral radiance	[W/m <sup>2</sup> /sr/nm]
$\Delta t$	time increment in the simulation	[h]

Greek Symbol	Description
$\lambda$	wavelength
$\theta$	altitude
$\Phi$	azimuth
$\Delta$	change in a variable
$\varepsilon$	sky clearness
$\gamma_s$	solar altitude

## References

- [1] T. M. Brown et al., "Recommendations for daytime, evening, and nighttime indoor light exposure to best support physiology, sleep, and wakefulness in healthy adults", *PLOS Biology*, vol. 20, 2022.
- [2] Circadian Lighting Design, International WELL Building Institute. [Online]. Available: <https://standard.wellcertified.com/light/circadian-lighting-design>
- [3] Deutsche Energie-Agentur. "„DENA-GEBÄUDEREPORT 2023. Zahlen, Daten, Fakten zum Klimaschutz im Gebäudebestand”."
- [4] C. Cajochen, J. M. Zeitzer, C. A. Czeisler, and D. J. Dijk, "Dose-response relationship for light intensity and ocular and electroencephalographic correlates of human alertness", *Behavioural brain research*, vol. 115, no. 1, pp. 75–83, 2000.
- [5] C. Cajochen, "Alerting effects of light", *Sleep medicine reviews*, vol. 11, pp. 453–464, 2007.
- [6] K. C. H. J. Smolders, Y. A. W. de Kort, and P. J. M. Cluitmans, "A higher illuminance induces alertness even during office hours: findings on subjective measures, task performance and heart rate measures", *Physiology & behavior*, vol. 107, pp. 7–16, 2012.
- [7] L. M. Huiberts, K. C. H. J. Smolders, and Y. A. W. de Kort, "Shining light on memory: Effects of bright light on working memory performance", *Behavioural brain research*, vol. 294, pp. 234–245, 2015.
- [8] P. Badia, B. Myers, M. Boecker, J. Culpepper, and J. R. Harsh, "Bright light effects on body temperature, alertness, EEG and behavior", *Physiology & behavior*, vol. 50, no. 3, pp. 583–588, 1991.
- [9] A. J. Lewy, T. A. Wehr, F. K. Goodwin, D. A. Newsome, and S. P. Markey, "Light suppresses melatonin secretion in humans", *Science (New York, N.Y.)*, vol. 210, no. 4475, pp. 1267–1269, 1980.
- [10] C. A. Czeisler et al., "Bright light resets the human circadian pacemaker independent of the timing of the sleep-wake cycle", *Science (New York, N.Y.)*, vol. 233, no. 4764, pp. 667–671, 1986.
- [11] D. M. Berson, F. A. Dunn, and M. Takao, "Phototransduction by retinal ganglion cells that set the circadian clock", *Science (New York, N.Y.)*, vol. 295, no. 5557, pp. 1070–1073, 2002.
- [12] D. M. Dacey et al., "Melanopsin-expressing ganglion cells in primate retina signal colour and irradiance and project to the LGN", *Nature*, vol. 433, no. 7027, pp. 749–754, 2005.
- [13] M. W. Hankins and R. J. Lucas, "The primary visual pathway in humans is regulated according to long-term light exposure through the action of a nonclassical photopigment", *Current biology : CB*, vol. 12, no. 3, pp. 191–198, 2002.
- [14] S. Hattar, H. W. Liao, M. Takao, D. M. Berson, and K. W. Yau, "Melanopsin-containing retinal ganglion cells: architecture, projections, and intrinsic photosensitivity", *Science (New York, N.Y.)*, vol. 295, no. 5557, pp. 1065–1070, 2002.

- [15] Y. Zhu et al., "Effects of Illuminance and Correlated Color Temperature on Daytime Cognitive Performance, Subjective Mood, and Alertness in Healthy Adults", *Environment and Behavior*, vol. 51, no. 2, pp. 199–230, 2019.
- [16] A. Alkozei, R. Smith, N. S. Dailey, S. Bajaj, and W. D. S. Killgore, "Acute exposure to blue wavelength light during memory consolidation improves verbal memory performance", *PLoS ONE*, vol. 12, 2017.
- [17] N. Goel, M. Basner, H. Rao, and D. F. Dinges, "Circadian rhythms, sleep deprivation, and human performance", *Progress in molecular biology and translational science*, vol. 119, pp. 155–190, 2013.
- [18] F. H. Zaidi et al., "Short-wavelength light sensitivity of circadian, pupillary, and visual awareness in humans lacking an outer retina", *Current biology : CB*, vol. 17, no. 24, pp. 2122–2128, 2007.
- [19] S. W. Lockley, "Circadian Rhythms: Influence of Light in Humans" in *Encyclopedia of neuroscience*, L. R. Squire, Ed., [Amsterdam]: Elsevier, 2009, pp. 971–988.
- [20] A. D. Güler et al., "Melanopsin cells are the principal conduits for rod-cone input to non-image-forming vision.", *Nature*, vol. 453, pp. 102–105, 2008.
- [21] R. J. Lucas, G. S. Lall, A. E. Allen, and T. M. Brown, "How rod, cone, and melanopsin photoreceptors come together to enlighten the mammalian circadian clock.", *Progress in brain research*, vol. 199, pp. 1–18, 2012.
- [22] A. E. Allen, T. M. Brown, and R. J. Lucas, "A distinct contribution of short-wavelength-sensitive cones to light-evoked activity in the mouse pretectal olivary nucleus", *The Journal of Neuroscience*, vol. 31, no. 46, pp. 16833–16843, 2011.
- [23] J. J. Gooley, S. M. W. Rajaratnam, G. C. Brainard, R. E. Kronauer, C. A. Czeisler, and S. W. Lockley, "Spectral responses of the human circadian system depend on the irradiance and duration of exposure to light", *Science translational medicine*, vol. 2, no. 31, 2010.
- [24] K. C. Smolders and Y. A. de Kort, "Investigating daytime effects of correlated colour temperature on experiences, performance, and arousal", *Journal of Environmental Psychology*, vol. 50, pp. 80–93, 2017.
- [25] K. C. Smolders and Y. A. de Kort, "Bright light and mental fatigue: Effects on alertness, vitality, performance and physiological arousal", *Journal of Environmental Psychology*, vol. 39, pp. 77–91, 2014.
- [26] M. Alwalidi and S. Hoffmann, "Alerting Effect of Light: A Review of Daytime Studies", *Journal of Daylighting*, vol. 9, no. 2, pp. 150–163, 2022.
- [27] R. Lok, T. Woelders, M. C. M. Gordijn, R. A. Hut, and D. G. M. Beersma, "White Light During Daytime Does Not Improve Alertness in Well-rested Individuals", *Journal of biological rhythms*, vol. 33, pp. 637–648, 2018.
- [28] S. T. Peeters, K. Smolders, I. Vogels, and Y. de Kort, "Less is more? Effects of more vs. less electric light on alertness, mood, sleep and appraisals of light in an operational office", *Journal of Environmental Psychology*, vol. 74, 2021.
- [29] K. C. H. J. Smolders, S. T. Peeters, I. M. L. C. Vogels, and Y. A. W. de Kort, "Investigation of Dose-Response Relationships for Effects of White Light Exposure on Correlates of Alertness and Executive Control during Regular Daytime Working Hours", *Journal of biological rhythms*, vol. 33, pp. 649–661, 2018.

- [30] M. E. Kompier, K. Smolders, R. P. Kramer, W. D. van Marken Lichtenbelt, and Y. de Kort, "Contrasting dynamic light scenarios in an operational office: Effects on visual experience, alertness, cognitive performance, and sleep", *Building and Environment*, vol. 212, 2022.
- [31] M. E. Kompier, K. C. H. J. Smolders, and Y. A. W. de Kort, "Abrupt light transitions in illuminance and correlated colour temperature result in different temporal dynamics and interindividual variability for sensation, comfort and alertness", *PloS one*, vol. 16, 2021.
- [32] X. Luo et al., "Temporal Dynamics of Subjective and Objective Alertness During Exposure to Bright Light in the Afternoon for 5 h", *Frontiers in physiology*, vol. 12, 2021.
- [33] B. Rodríguez-Morilla, J. A. Madrid, E. Molina, J. Pérez-Navarro, and Á. Correa, "Blue-Enriched Light Enhances Alertness but Impairs Accurate Performance in Evening Chronotypes Driving in the Morning", *Frontiers in psychology*, vol. 9, 2018.
- [34] R. Lok et al., "Bright Light Increases Alertness and Not Cortisol in Healthy Men: A Forced Desynchrony Study Under Dim and Bright Light (I)", *Journal of biological rhythms*, vol. 37, pp. 403–416, 2022.
- [35] T. Askaripoor, M. Motamedzade, R. Golmohammadi, M. Farhadian, M. Babamiri, and M. Samavati, "Effects of light intervention on alertness and mental performance during the post-lunch dip: a multi-measure study", *Industrial health*, vol. 57, pp. 511–524, 2019.
- [36] C. A. Chaveznava-Treviño, *Physiological Effects of Pulsed LED Light Added to a Task Lamp to Improve Alertness on Employees of Hospital or Shift Workers*, 2020.
- [37] M. E. Kompier, K. C. H. J. Smolders, W. D. van Marken Lichtenbelt, and Y. A. W. de Kort, "Effects of light transitions on measures of alertness, arousal and comfort", *Physiology & behavior*, vol. 223, 2020.
- [38] E. Rautkylä, M. Puolakka, E. Tetri, and L. Halonen, "Effects of Correlated Colour Temperature and Timing of Light Exposure on Daytime Alertness in Lecture Environments", *J. Light & Vis. Env.*, vol. 34, no. 2, pp. 59–68, 2010.
- [39] L. Sahin, B. M. Wood, B. Plitnick, and M. G. Figueiro, "Daytime light exposure: effects on biomarkers, measures of alertness, and performance", *Behavioural brain research*, vol. 274, pp. 176–185, 2014.
- [40] N. Santhi, J. A. Groeger, S. N. Archer, M. Gimenez, L. J. M. Schlangen, and D.-J. Dijk, "Morning sleep inertia in alertness and performance: effect of cognitive domain and white light conditions", *PloS one*, vol. 8, 2013.
- [41] A. Y. Segal, T. L. Sletten, E. E. Flynn-Evans, S. W. Lockley, and S. M. W. Rajaratnam, "Daytime Exposure to Short- and Medium-Wavelength Light Did Not Improve Alertness and Neurobehavioral Performance", *Journal of biological rhythms*, vol. 31, pp. 470–482, 2016.
- [42] K. Łaszewska, A. Goroncy, P. Weber, T. Pracki, and M. Tafil-Klawe, "Influence of the Spectral Quality of Light on Daytime Alertness Levels in Humans", *Advances in cognitive psychology*, vol. 14, pp. 192–208, 2018.
- [43] M. Šmotek, P. Vlček, E. Saifutdinova, and J. Kopřivová, "Objective and Subjective Characteristics of Vigilance under Different Narrow-Bandwidth Light Conditions: Do Shorter Wavelengths Have an Alertness-Enhancing Effect?", *Neuropsychobiology*, vol. 78, pp. 238–248, 2019.

- [44] D. Gall and V. Lapuente, "Beleuchtungsrelevante Aspekte bei der Auswahl eines förderlichen Lampenspektrums", *Licht*, vol. 54, pp. 860–871, 2002.
- [45] M. S. Rea, M. G. Figueiro, and J. D. Bullough, "Circadian photobiology: an emerging framework for lighting practice and research", *Lighting Research & Technology*, vol. 34, no. 3, pp. 177–187, 2002.
- [46] G. C. Brainard et al., "Action spectrum for melatonin regulation in humans: evidence for a novel circadian photoreceptor", *The Journal of Neuroscience*, vol. 21, no. 16, pp. 6405–6412, 2001.
- [47] K. Thapan, J. Arendt, and D. J. Skene, "An action spectrum for melatonin suppression: evidence for a novel non-rod, non-cone photoreceptor system in humans", *The Journal of physiology*, vol. 535, Pt 1, pp. 261–267, 2001.
- [48] L. Bellia and F. Bisegna, "From radiometry to circadian photometry: A theoretical approach", *Building and Environment*, vol. 62, pp. 63–68, 2013.
- [49] J. a. Enezi, V. Revell, T. Brown, J. Wynne, L. Schlangen, and R. Lucas, "A "melanopic" spectral efficiency function predicts the sensitivity of melanopsin photoreceptors to polychromatic lights", *Journal of biological rhythms*, vol. 26, no. 4, pp. 314–323, 2011.
- [50] R. J. Lucas et al., "Measuring and using light in the melanopsin age", *Trends in Neurosciences*, vol. 37, pp. 1–9, 2014.
- [51] CIE System for Metrology of Optical Radiation for ipRGC-Influenced Responses to Light, CIE S 026:2018, International Commission on Illumination, 2018.
- [52] Circadian Lighting Design (WELL v2), International WELL Building Institute. [Online]. Available: <https://v2.wellcertified.com/en/wellv2/light/feature/3>
- [53] M. S. Rea, R. Nagare, and M. G. Figueiro, "Modeling Circadian Phototransduction: Quantitative Predictions of Psychophysical Data", *Frontiers in neuroscience*, vol. 15, 2021.
- [54] M. S. Rea, R. Nagare, and M. G. Figueiro, "Modeling Circadian Phototransduction: Retinal Neurophysiology and Neuroanatomy", *Frontiers in neuroscience*, vol. 14, 2020.
- [55] Light and Health Research Center. "CS Calculator 2.0." Accessed on 17.0.2024. [Online]. Available: <https://cscalculator.light-health.org/>
- [56] Underwriters' Laboratories, Design Guideline for Promoting Circadian Entrainment with Light for Day-active People: UL 24480. Underwriters Laboratories Incorporated, 2019.
- [57] C. S. Pechacek, M. Andersen, and S. W. Lockley, "Preliminary Method for Prospective Analysis of the Circadian Efficacy of (Day)Light with Applications to Healthcare Architecture", *LEUKOS*, vol. 5, no. 1, pp. 1–26, 2008.
- [58] M. Andersen, S. J. Gochenour, and S. W. Lockley, "Modelling 'non-visual' effects of daylighting in a residential environment", *Building and Environment*, vol. 70, pp. 138–149, 2013.
- [59] M. Amundadottir, S. Lockley, and M. Andersen, "Simulation-based evaluation of non-visual responses to daylight: Proof-of-concept study of healthcare re-design" in *Building Simulation 2013. Online Proceedings*, Chambery, France, E. Wurtz, Ed., 2013.
- [60] Robert McNeel and Associates, DAYSIM. Accessed on 31.01.2024. [Online]. Available: <https://github.com/MITSustainableDesignLab/Daysim>

- [61] M. Andersen, "Unweaving the human response in daylighting design", *Building and Environment*, vol. 91, pp. 101–117, 2015.
- [62] G. Ward, RADIANCE. Accessed on 31.01.2024. [Online]. Available: <https://www.radiance-online.org/>
- [63] M. Andersen, A. GUILLEMIN, M. L. AMUNDADOTTIR, and S. ROCKCASTLE, "Beyond Illumination: An Interactive Simulation Framework For Non-visual And Perceptual Aspects Of Daylighting Performance" in *Proceedings of Building Simulation 2013: 13th Conference of IBPSA*, 2013.
- [64] J. Mardaljevic, M. Andersen, N. Roy, and J. Christoffersen, "A framework for predicting the non-visual effects of daylight – Part II: The simulation model", *Lighting Research & Technology*, vol. 46, no. 4, pp. 388–406, 2014.
- [65] A. Amirazar et al., "Assessing the Circadian Potential of an Office Building in the Southeastern US" in *Proceedings of the 2018 Symposium on Simulation for Architecture and Urban Design (SimAUD 2018)*, Delft, Netherlands, 2018.
- [66] Q. Dai, Y. Huang, L. Hao, Y. Lin, and K. Chen, "Spatial and spectral illumination design for energy-efficient circadian lighting", *Building and Environment*, vol. 146, pp. 216–225, 2018.
- [67] Q. Yao, W. Cai, M. Li, Z. Hu, P. Xue, and Q. Dai, "Efficient circadian daylighting: A proposed equation, experimental validation, and the consequent importance of room surface reflectance", *Energy and Buildings*, vol. 210, p. 109784, 2020.
- [68] A. Sánchez-Cano and J. Aporta, "Optimization of Lighting Projects Including Photopic and Circadian Criteria: A Simplified Action Protocol", *Applied Sciences*, vol. 10, no. 22, 2020.
- [69] I. Acosta, M. Á. Campano, R. Leslie, and L. Radetsky, "Daylighting design for healthy environments: Analysis of educational spaces for optimal circadian stimulus", *Solar Energy*, vol. 193, pp. 584–596, 2019.
- [70] L. Bellia, I. Acosta, M. Á. Campano, and F. Fragliasso, "Impact of daylight saving time on lighting energy consumption and on the biological clock for occupants in office buildings", *Solar Energy*, vol. 211, pp. 1347–1364, 2020.
- [71] M. Inanici, M. Brennan, and E. Clark, "Spectral Lighting Simulations: Computing Circadian Light" in *Proceedings of Building Simulation 2015: 14th Conference of IBPSA*, 2015.
- [72] D. Geisler-Moroder and A. Dür, "Estimating Melatonin Suppression and Photosynthesis Activity in Real-World Scenes from Computer Generated Images", *cgiv*, vol. 5, no. 1, pp. 346–352, 2010.
- [73] P. KHADEMAGHA, J. F. DIEPENS, M. B. ARIES, A. L. ROSEMANN, and E. J. van LOENEN, "Effect of different design parameters on the visual and non-visual assessment criteria in office spaces", 2015.
- [74] M. Danell, M. Ámundadóttir, and S. Rockcastle, "Evaluating Temporal and Spatial Light Exposure Profiles for Typical Building Occupants" in *Proceedings of the 2020 Symposium on Simulation for Architecture and Urban Design (SimAUD 2018)*, Virtual Conference, 2020.
- [75] D. Geisler-Moroder and A. Dür, "Estimating Melatonin Suppression and Photosynthesis Activity in Real-World Scenes from Computer Generated Images", *Conference on Colour in Graphics, Imaging, and Vision*, vol. 5, no. 1, pp. 346–352, 2010.

- [76] I. T. Kim, A. S. Choi, and M. K. Sung, "Development of a Colour Quality Assessment Tool for indoor luminous environments affecting the circadian rhythm of occupants", *Building and Environment*, vol. 126, pp. 252–265, 2017.
- [77] I. T. Kim, A. S. Choi, and M. K. Sung, "Accuracy evaluation of a calculation tool based on the spectral colour property of indoor luminous environments", *Building and Environment*, vol. 139, pp. 157–169, 2018.
- [78] A. I. Ruppertsberg and M. Bloj, "Creating physically accurate visual stimuli for free: spectral rendering with RADIANCE", *Behav Res*, vol. 40, no. 1, pp. 304–308, 2008.
- [79] J. N. Yang and L. T. Maloney, "Illuminant cues in surface color perception: tests of three candidate cues", *Vision Research*, vol. 41, no. 20, pp. 2581–2600, 2001.
- [80] A. I. Ruppertsberg and M. Bloj, "Rendering complex scenes for psychophysics using RADIANCE: how accurate can you get?", *Journal of the Optical Society of America. A, Optics, image science, and vision*, vol. 23, no. 4, pp. 759–768, 2006.
- [81] R. Hall, *Illumination and color in computer generated imagery (Monographs in Visual Communication)*. Springer, 2012.
- [82] P. H. Ewing, J. Haymaker, and E. A. Edelstein, "Simulating Circadian Light: Multi-Dimensional Illuminance Analysis" in *Building Simulation Conference Proceedings*, 2017.
- [83] M. Alwalidi, A. Ganji Kheybari, S. Subramaniam, and S. Hoffmann, "Development of a multichannel spectral simulation tool and experimental validation with different lighting scenarios", *Lighting Research & Technology*, 150–163, 2023.
- [84] Solemma, ALFA – Adaptive lighting for alertness. Accessed on 25.01.2023. [Online]. Available: <https://www.solemma.com/alfa>
- [85] Robert McNeel and Associates, Rhinoceros 3D. Accessed on 29.01.2024. [Online]. Available: <https://www.rhino3d.com/>
- [86] P. Balakrishnan and A. Jakubiec, "Spectral rendering with daylight: a comparison of two spectral daylight simulation platforms" in *Proceedings of the 16th IBPSA Conference, Rome, Italy, Sep. 2019 - Sep. 2019*.
- [87] B. Mayer and A. Kylling, "Technical note: The libRadtran software package for radiative transfer calculations - description and examples of use", *Atmos. Chem. Phys.*, vol. 5, no. 7, pp. 1855–1877, 2005.
- [88] Sepide Saiedlue, Armin Amirazar, Jianxin Hu, and Wayne Place, "Assessing Circadian Stimulus Potential of Lighting Systems in Office Buildings by Simulations", *ConRepos*, 2019.
- [89] S. Safranek, J. M. Collier, A. Wilkerson, and R. G. Davis, "Energy impact of human health and wellness lighting recommendations for office and classroom applications", *Energy and Buildings*, vol. 226, p. 110365, 2020.
- [90] N. Altenberg Vaz and M. Inanici, "Syncing with the Sky: Daylight-Driven Circadian Lighting Design", *LEUKOS*, vol. 17, no. 3, pp. 291–309, 2021.
- [91] N. Elsayed and T. Rakha, "A Framework to Simulate the Non-Visual Effects of Daylight on the Cognitive Health of Mild Cognitive Impairment (MCI) People", *2020 Building Performance Analysis Conference and SimBuild*, vol. 9, pp. 119–129, 2020.
- [92] J. Potočnik, M. Košir, and M. Dovjak, "Colour preference in relation to personal determinants and implications for indoor circadian luminous environment", *Indoor and Built Environment*, vol. 31, no. 1, pp. 121–138, 2022.



- [93] J. Potočnik and M. Košir, "Influence of commercial glazing and wall colours on the resulting non-visual daylight conditions of an office", *Building and Environment*, vol. 171, 2020.
- [94] C. Pierson, M. Gkaintatzi-Masouti, M. Aarts, and M. Andersen, "Validation of Spectral Simulation Tools for the Prediction of Indoor Electric Light Exposure", *Proceedings of the Conference CIE 2021*, pp. 52–62, 2021.
- [95] C. Pierson, M. Aarts, and M. Andersen, "Validation of spectral simulation tools for the prediction of indoor daylight exposure" in *Proceedings of Building Simulation 2021: 17th Conference of IBPSA*, 2021.
- [96] C. Pierson, M. P. J. Aarts, and M. Andersen, "Validation of spectral simulation tools in the context of ipRGC-influenced light responses of building occupants", *Journal of Building Performance Simulation*, vol. 16, no. 2, pp. 179–197, 2023.
- [97] Robert McNeel and Associates, Grasshopper. Accessed on 27.01.2024. [Online]. Available: <https://www.grasshopper3d.com/>
- [98] Inanici M ZGF Architects LLP, Lark Spectral Lighting. Accessed on 27.01.2024. [Online]. Available: [https://faculty.washington.edu/inanici/Lark/Lark\\_home\\_page.html](https://faculty.washington.edu/inanici/Lark/Lark_home_page.html)
- [99] Inanici M, Pierson C, Gkaintatzi-Masouti M, Balakrishnan P, Jakubiec A, ZGF Architects LLP, Lark spectral lighting 2.0. Accessed on 27.01.2024. [Online]. Available: <https://www.food4rhino.com/en/app/lark-spectral-lighting>
- [100] B. Jung, Z. Cheng, M. Brennan, and M. Inanici, "Multispectral Lighting Simulation Approaches for Predicting Opsin-driven Metrics and their Application in a Neonatal Intensive Care Unit" in *Proceedings of Building Simulation 2023: 18th Conference of IBPSA*, 2023.
- [101] K. Konis, "A circadian design assist tool to evaluate daylight access in buildings for human biological lighting needs", *Solar Energy*, vol. 191, pp. 449–458, 2019.
- [102] M. Brennan and A. Collins, "Outcome-Based Design for Circadian Lighting: An Integrated Approach to Simulation & Metrics" in *2018 Building Performance Analysis Conference and SimBuild*, 26.09.2018-28.09.2018.
- [103] A. K. Diakite-Kortlever and M. Knoop, "Forecast accuracy of existing luminance-related spectral sky models and their practical implications for the assessment of the non-image-forming effectiveness of daylight", *Lighting Research & Technology*, vol. 53, no. 7, pp. 657–676, 2021.
- [104] M. Maskarenj, B. Deroisy, and S. Altomonte, "A new tool and workflow for the simulation of the non-image forming effects of light", *Energy and Buildings*, vol. 262, 2022.
- [105] CIE 015:2018 Colorimetry, 4th Edition, CIE TC 1-85.
- [106] J. Mardaljevic, "Daylight simulation: validation, sky models and daylight coefficients", Institute of Energy and Sustainable Development, De Montfort University Leicester, Leicester, 1999.
- [107] J. Wienold, C. Reetz, T. Kuhn, and J. Christoffersen, "Evalglare: a new RADIANCE-based tool to evaluate glare in office spaces" in *3rd international RADIANCE workshop*, Fribourg, Switzerland, 2004.
- [108] R. Guglielmetti, D. Macumber, and N. Long, "OpenStudio: an open source integrated analysis platform", 2011.

- [109] G. Molina, "Groundhog, A Sketchup Plugin for Radiance Analysis" in 14th International Radiance Workshop, Philadelphia, PA, USA, 2015.
- [110] M. Roudsari and S. Subramaniam, "Automating radiance workflows using Python" in 15th International Radiance Workshop, Padua, Italy, 2016.
- [111] P. R. Tregenza and I. M. Waters, "Daylight coefficients", *Lighting Research & Technology*, vol. 15, no. 2, pp. 65–71, 1983.
- [112] J. A. Jakubiec and C. Reinhart, "DIVA 2.0: Integrating daylight and thermal simulations using Rhinoceros 3D, DAYSIM and EnergyPlus", *Building Simulation* 2011, vol. 12, pp. 2202–2209, 2011.
- [113] M. Roudsari, M. Pak, and A. Viola, "Ladybug: A Parametric Environmental Plugin For Grasshopper To Help Designers Create An Environmentally-conscious Design", *Building Simulation* 2013, vol. 13, pp. 3128–3135, 2013.
- [114] G. Van Rossum and F. L. Drake, *The Python language reference*, 3rd ed. (Python documentation manual / Guido van Rossum; Fred L. Drake [ed.] ; Pt. 2). [Hampton, NH], [Redwood City, Calif.]: Python Software Foundation; SoHo Books, 2010.
- [115] C. F. Reinhart, *Daylight availability and manual lighting control in office buildings - simulation studies and analysis of measurement*, 2001. [Online]. Available: <https://publikationen.bibliothek.kit.edu/4842001>
- [116] R. Perez, R. Seals, and J. Michalsky, "All-weather model for sky luminance distribution—Preliminary configuration and validation", *Solar Energy*, vol. 50, no. 3, pp. 235–245, 1993.
- [117] R. Perez, P. Ineichen, R. Seals, J. Michalsky, and R. Stewart, "Modeling daylight availability and irradiance components from direct and global irradiance", *Solar Energy*, vol. 44, no. 5, pp. 271–289, 1990.
- [118] G. W. Larson, R. Shakespeare, and C. Ehrlich, *Rendering with Radiance: The art and science of lighting visualization*. Davis, Calif.: Space and Light, 2005.
- [119] A. Diakite and M. Knoop, "Data-driven spectral sky models: A review", 2019.
- [120] C. Chain, D. Dumortier, and M. Fontoynt, "A comprehensive model of luminance, correlated colour temperature and spectral distribution of skylight: comparison with experimental data", *Solar Energy*, vol. 65, no. 5, pp. 285–295, 1999.
- [121] A. Rusnák, "Meranie a hodnotenie spektrálnych charakteristík slnečného žiarenia", PhD Thesis, 2014.
- [122] C. Chain, "Caractérisation spectrale et directionnelle de la lumière naturelle : application à l'éclairage des bâtiments", PhD Thesis, 2004.
- [123] J. Wienold and A. Diakite, "Making Simulations More Colorful: Extension of gendaylit to Create a Colored Sky" in 17th International Radiance Workshop, Loughborough, UK, radiance-online.org, Ed., 2018.
- [124] G. Wyszecki and W. S. Stiles, *Color science: Concepts and methods, quantitative data, and formulae* (Wiley classics library). New York: John Wiley & Sons, 2000.
- [125] C. Reinhart, A. Jakubiec, and D. Ibarra, "Definition Of A Reference Office For Standardized Evaluations Of Dynamic Facade And Lighting Technologies" in *Proceedings of Building Simulation 2013: 13th Conference of IBPSA*, 2013.
- [126] J. A. Jakubiec, "Data-Driven Selection of Typical Opaque Material Reflectances for Lighting Simulation", *LEUKOS*, vol. 19, no. 2, pp. 176–189, 2023.

- [127] J. A. Jakubiec, M. Inanici, K. Van Den Wymelenberg, and A. Mahic, "Improving the Accuracy of Measurements in Daylit Interior Scenes Using High Dynamic Range Photography" in PLEA 2016 Los Angeles - 36th International Conference on Passive and Low Energy Architecture.: Cities, Buildings, People: Towards Regenerative Environments, Los Angeles, California, USA, 2016.
- [128] Lawrence Berkeley National Laboratory, OPTICS 6.0. Accessed on 27.03.2024. [Online]. Available: <https://windows.lbl.gov/optics-downloads>
- [129] G. Betti, F. Tartarini, C. Nguyen, and S. Schiavon, "CBE Clima Tool: a free and open-source web application for climate analysis tailored to sustainable building design", 2022.
- [130] Licht und Beleuchtung - Beleuchtung von Arbeitsstätten - Teil 1: Arbeitsstätten in Innenräumen; Deutsche Fassung EN 12464-1:2021, Deutsches Institut für Normung.
- [131] "CIE 97:2005-Guide on the maintenance of indoor electric lighting systems", Color Research & Application, vol. 31, no. 3, p. 243, 2006.

# Appendix A

**Table A.1.** Wavelength bands and their respective coefficients in a three-channel simulation.

Channels	Lower boundary (nm)	Upper boundary (nm)	Coefficient
1	380.0	499.0	0.065
2	499.0	586.5	0.670
3	586.5	780.0	0.265

**Table A.2.** Wavelength bands and their respective coefficients in a nine-channel simulation.

Channels	Lower boundary (nm)	Upper boundary (nm)	Coefficient
1	380.0	419.6	$2.963 \times 10^{-4}$
2	419.6	459.3	$9.253 \times 10^{-3}$
3	459.3	499.0	$5.541 \times 10^{-2}$
4	499.0	528.1	$1.570 \times 10^{-1}$
5	528.1	557.3	$2.594 \times 10^{-1}$
6	557.3	586.5	$2.539 \times 10^{-1}$
7	586.5	651.0	$2.494 \times 10^{-1}$
8	651.0	715.5	$1.524 \times 10^{-2}$
9	715.5	780.0	$1.877 \times 10^{-4}$

**Table A.3.** Wavelength bands and their respective coefficients in a 27-channel simulation.

Channels	Lower boundary (nm)	Upper boundary (nm)	Coefficient
1	380.0	393.2	$1.070 \times 10^{-5}$
2	393.2	406.4	$4.960 \times 10^{-5}$
3	406.4	419.6	$2.360 \times 10^{-4}$
4	419.6	432.8	$1.053 \times 10^{-3}$
5	432.8	446.1	$2.798 \times 10^{-3}$
6	446.1	459.3	$5.402 \times 10^{-3}$
7	459.3	472.5	$9.600 \times 10^{-3}$
8	472.5	485.7	$1.652 \times 10^{-2}$
9	485.7	499.0	$2.928 \times 10^{-2}$
10	499.0	508.7	$3.483 \times 10^{-2}$
11	508.7	518.4	$5.224 \times 10^{-2}$
12	518.4	528.1	$6.994 \times 10^{-2}$
13	528.1	537.8	$8.015 \times 10^{-2}$
14	537.8	547.6	$8.963 \times 10^{-2}$
15	547.6	557.3	$8.958 \times 10^{-2}$
16	557.3	567.0	$9.058 \times 10^{-2}$
17	567.0	576.7	$8.515 \times 10^{-2}$
18	576.7	586.5	$7.817 \times 10^{-2}$
19	586.5	608.0	$1.339 \times 10^{-1}$
20	608.0	629.5	$7.982 \times 10^{-2}$
21	629.5	651.0	$3.565 \times 10^{-2}$
22	651.0	672.5	$1.166 \times 10^{-2}$
23	672.5	694.0	$2.927 \times 10^{-3}$

24	694.0	715.5	$6.523 \times 10^{-4}$
25	715.5	737.0	$1.492 \times 10^{-4}$
26	737.0	758.5	$3.150 \times 10^{-5}$
27	758.5	780.0	$7.000 \times 10^{-6}$

**Table A.4.** Wavelength bands and their respective coefficients in an 81-channel simulation.

Channels	Lower boundary (nm)	Upper boundary (nm)	Coefficient
1	380.0	384.4	$1.900 \times 10^{-6}$
2	384.4	388.8	$3.300 \times 10^{-6}$
3	388.8	393.2	$5.500 \times 10^{-6}$
4	393.2	397.6	$9.700 \times 10^{-6}$
5	397.6	402.0	$1.600 \times 10^{-5}$
6	402.0	406.4	$2.390 \times 10^{-5}$
7	406.4	410.8	$4.300 \times 10^{-5}$
8	410.8	415.2	$6.970 \times 10^{-5}$
9	415.2	419.6	$1.233 \times 10^{-4}$
10	419.6	424.0	$2.093 \times 10^{-4}$
11	424.0	428.4	$3.315 \times 10^{-4}$
12	428.4	432.8	$5.123 \times 10^{-4}$
13	432.8	437.2	$6.768 \times 10^{-4}$
14	437.2	441.7	$9.341 \times 10^{-4}$
15	441.7	446.1	$1.187 \times 10^{-3}$
16	446.1	450.5	$1.445 \times 10^{-3}$
17	450.5	454.9	$1.735 \times 10^{-3}$
18	454.9	459.3	$2.222 \times 10^{-3}$
19	459.3	463.7	$2.570 \times 10^{-3}$
20	463.7	468.1	$3.229 \times 10^{-3}$
21	468.1	472.5	$3.801 \times 10^{-3}$
22	472.5	476.9	$4.471 \times 10^{-3}$
23	476.9	481.3	$5.636 \times 10^{-3}$
24	481.3	485.7	$6.418 \times 10^{-3}$
25	485.7	490.1	$8.022 \times 10^{-3}$
26	490.1	494.5	$9.478 \times 10^{-3}$
27	494.5	499.0	$1.178 \times 10^{-2}$
28	499.0	502.2	$9.626 \times 10^{-3}$
29	502.2	505.4	$1.151 \times 10^{-2}$
30	505.4	508.7	$1.370 \times 10^{-2}$
31	508.7	511.9	$1.519 \times 10^{-2}$
32	511.9	515.2	$1.834 \times 10^{-2}$
33	515.2	518.4	$1.871 \times 10^{-2}$
34	518.4	521.6	$2.188 \times 10^{-2}$
35	521.6	524.9	$2.291 \times 10^{-2}$
36	524.9	528.1	$2.515 \times 10^{-2}$
37	528.1	531.4	$2.569 \times 10^{-2}$
38	531.4	534.6	$2.763 \times 10^{-2}$
39	534.6	537.8	$2.683 \times 10^{-2}$
40	537.8	541.1	$3.022 \times 10^{-2}$

41	541.1	544.3	$2.812 \times 10^{-2}$
42	544.3	547.6	$3.129 \times 10^{-2}$
43	547.6	550.8	$2.881 \times 10^{-2}$
44	550.8	554.0	$3.083 \times 10^{-2}$
45	554.0	557.3	$2.994 \times 10^{-2}$
46	557.3	560.5	$3.079 \times 10^{-2}$
47	560.5	563.8	$2.962 \times 10^{-2}$
48	563.8	567.0	$3.017 \times 10^{-2}$
49	567.0	570.2	$2.876 \times 10^{-2}$
50	570.2	573.5	$2.901 \times 10^{-2}$
51	573.5	576.7	$2.738 \times 10^{-2}$
52	576.7	580.0	$2.735 \times 10^{-2}$
53	580.0	583.2	$2.556 \times 10^{-2}$
54	583.2	586.5	$2.526 \times 10^{-2}$
55	586.5	593.6	$5.024 \times 10^{-2}$
56	593.6	600.8	$4.435 \times 10^{-2}$
57	600.8	608.0	$3.929 \times 10^{-2}$
58	608.0	615.1	$3.215 \times 10^{-2}$
59	615.1	622.3	$2.639 \times 10^{-2}$
60	622.3	629.5	$2.128 \times 10^{-2}$
61	629.5	636.6	$1.565 \times 10^{-2}$
62	636.6	643.8	$1.158 \times 10^{-2}$
63	643.8	651.0	$8.427 \times 10^{-3}$
64	651.0	658.1	$5.588 \times 10^{-3}$
65	658.1	665.3	$3.687 \times 10^{-3}$
66	665.3	672.5	$2.385 \times 10^{-3}$
67	672.5	679.6	$1.458 \times 10^{-3}$
68	679.6	686.8	$9.151 \times 10^{-4}$
69	686.8	694.0	$5.541 \times 10^{-4}$
70	694.0	701.1	$3.237 \times 10^{-4}$
71	701.1	708.3	$2.013 \times 10^{-4}$
72	708.3	715.5	$1.272 \times 10^{-4}$
73	715.5	722.6	$7.510 \times 10^{-5}$
74	722.6	729.8	$4.580 \times 10^{-5}$
75	729.8	737.0	$2.820 \times 10^{-5}$
76	737.0	744.1	$1.610 \times 10^{-5}$
77	744.1	751.3	$9.500 \times 10^{-6}$
78	751.3	758.5	$5.900 \times 10^{-6}$
79	758.5	765.6	$3.500 \times 10^{-6}$
80	765.6	772.8	$2.100 \times 10^{-6}$
81	772.8	780.0	$1.300 \times 10^{-6}$

## Appendix B

Figure A.1 (a) shows that the maximum standard deviation at the horizontal desk level is  $\pm 0.17 \text{ W/m}^2$  (at  $9.0 \text{ W/m}^2$ ) in the simulations with three channels,  $\pm 0.15 \text{ W/m}^2$  (at  $7.0 \text{ W/m}^2$ ) in the simulations with nine channels,  $\pm 0.09 \text{ W/m}^2$  (at  $7.0 \text{ W/m}^2$ ) in the simulations with 27 channels and  $\pm 0.05 \text{ W/m}^2$  (at  $8.7 \text{ W/m}^2$ ) in the simulations with 81 channels for position 3. The maximum standard deviation at the vertical eye level is shown in Figure A.2 (b). The maximum standard deviation is  $\pm 0.16 \text{ W/m}^2$  (at  $4.4 \text{ W/m}^2$ ) in the simulations with three channels,  $\pm 0.15 \text{ W/m}^2$  (at  $4.4 \text{ W/m}^2$ ) in the simulations with nine channels,  $\pm 0.06 \text{ W/m}^2$  (at  $3.5 \text{ W/m}^2$ ) in the simulations with 27 channels and  $\pm 0.06 \text{ W/m}^2$  (at  $4.3 \text{ W/m}^2$ ) in the simulations with 81 channels.

The maximum standard deviation at the horizontal desk level is  $\pm 0.15 \text{ W/m}^2$  (at  $7.4 \text{ W/m}^2$ ) in the simulations with three channels,  $\pm 0.11 \text{ W/m}^2$  (at  $7.8 \text{ W/m}^2$ ) in the simulations with nine channels,  $\pm 0.08 \text{ W/m}^2$  (at  $8.6 \text{ W/m}^2$ ) in the simulations with 27 channels and  $\pm 0.06 \text{ W/m}^2$  (at  $7.3 \text{ W/m}^2$ ) in the simulations with 81 channels for position 4 as shown in Figure A.2 (a). The maximum standard deviation at the vertical eye level is shown in Figure A.2 (b). The maximum standard deviation is  $\pm 0.15 \text{ W/m}^2$  (at  $3.8 \text{ W/m}^2$ ) in the simulations with three channels,  $\pm 0.15 \text{ W/m}^2$  (at  $3.6 \text{ W/m}^2$ ) in the simulations with nine channels,  $\pm 0.06 \text{ W/m}^2$  (at  $3.5 \text{ W/m}^2$ ) in the simulations with 27 channels and  $\pm 0.04 \text{ W/m}^2$  (at  $3.7 \text{ W/m}^2$ ) in the simulations with 81 channels.

The maximum standard deviation at the horizontal desk level is  $\pm 0.16 \text{ W/m}^2$  (at  $3.2 \text{ W/m}^2$ ) in the simulations with three channels,  $\pm 0.07 \text{ W/m}^2$  (at  $3.1 \text{ W/m}^2$ ) in the simulations with nine channels,  $\pm 0.07 \text{ W/m}^2$  (at  $3.0 \text{ W/m}^2$ ) in the simulations with 27 channels and  $\pm 0.02 \text{ W/m}^2$  (at  $3.0 \text{ W/m}^2$ ) in the simulations with 81 channels for position 5 as shown in Figure A.3 (a). The maximum standard deviation at the vertical eye level is shown in Figure A.3 (b). The maximum standard deviation is  $\pm 0.16 \text{ W/m}^2$  (at  $1.9 \text{ W/m}^2$ ) in the simulations with three channels,  $\pm 0.16 \text{ W/m}^2$  (at  $0.06 \text{ W/m}^2$ ) in the simulations with nine channels,  $\pm 0.06 \text{ W/m}^2$  (at  $1.9 \text{ W/m}^2$ ) in the simulations with 27 channels and  $\pm 0.03 \text{ W/m}^2$  (at  $1.9 \text{ W/m}^2$ ) in the simulations with 81 channels.

Figure A.4 (a) shows that the maximum standard deviation at the horizontal desk level is  $\pm 0.13 \text{ W/m}^2$  (at  $3.1 \text{ W/m}^2$ ) in the simulations with three channels,  $\pm 0.10 \text{ W/m}^2$  (at  $2.7 \text{ W/m}^2$ ) in the simulations with nine channels,  $\pm 0.05 \text{ W/m}^2$  (at  $3.0 \text{ W/m}^2$ ) in the simulations with 27 channels and  $\pm 0.03 \text{ W/m}^2$  (at  $3.0 \text{ W/m}^2$ ) in the simulations with 81

channels for position 6. The maximum standard deviation at the vertical eye level is shown in Figure A.4 (b). The maximum standard deviation is  $\pm 0.12 \text{ W/m}^2$  (at  $1.7 \text{ W/m}^2$ ) in the simulations with three channels,  $\pm 0.10 \text{ W/m}^2$  (at  $1.5 \text{ W/m}^2$ ) in the simulations with nine channels,  $\pm 0.05 \text{ W/m}^2$  (at  $1.5 \text{ W/m}^2$ ) in the simulations with 27 channels and  $\pm 0.04 \text{ W/m}^2$  (at  $1.5 \text{ W/m}^2$ ) in the simulations with 81 channels.



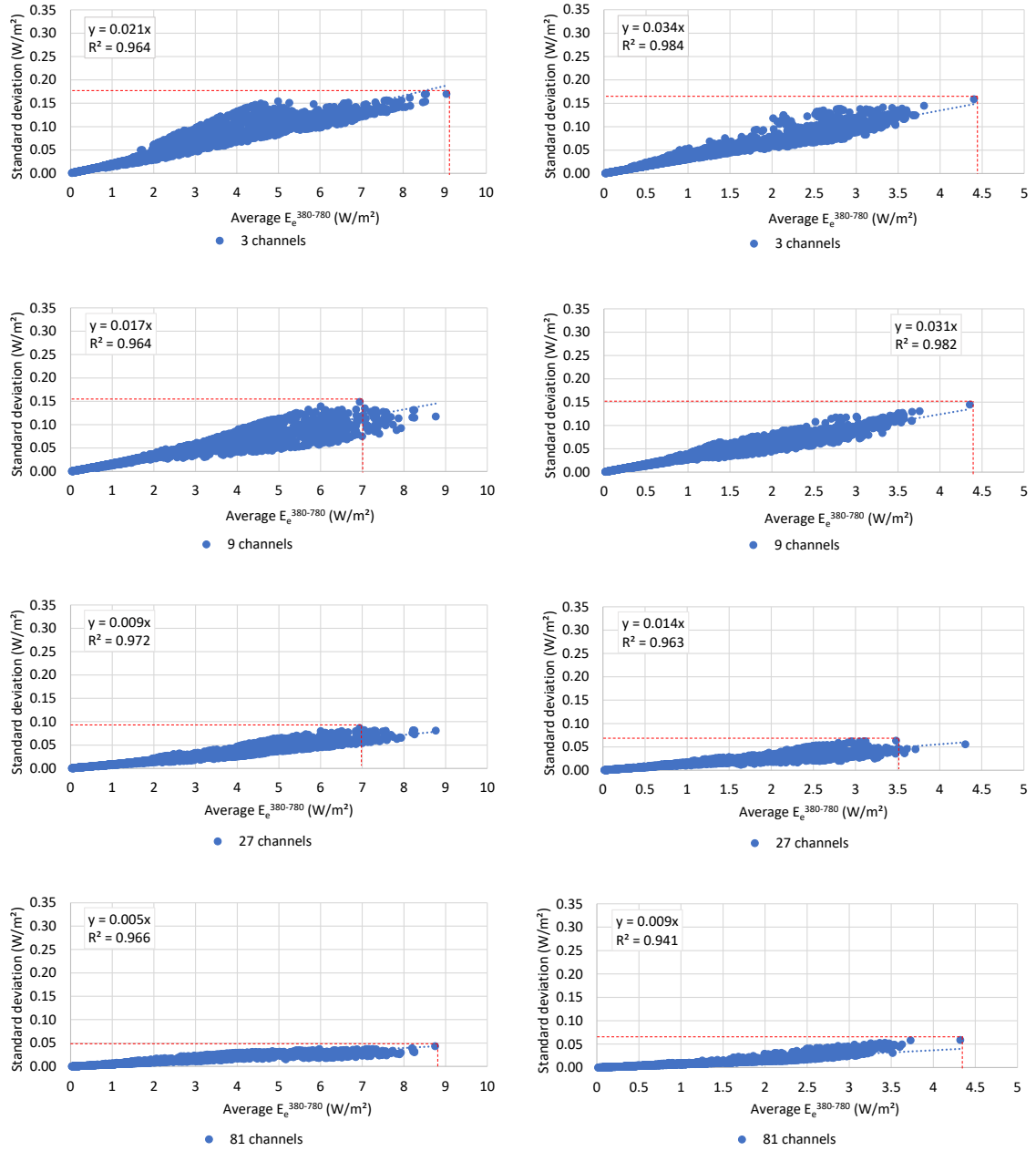


**Figure A.1.** Scatterplots show standard deviation (y-axis) plotted against the average  $E_e^{380-780}$  (x-axis) for positions 3. Row (a) presents the results at the horizontal desk level (0.80 m) and row (b) at the vertical eye level (1.20 m) for simulations with three, nine, 27 and 81 channels. Average  $E_e^{380-780}$  refers to ten simulation runs. The red dashed line represents the maximum standard deviation at the respective  $E_e^{380-780}$  in each scatter plot.

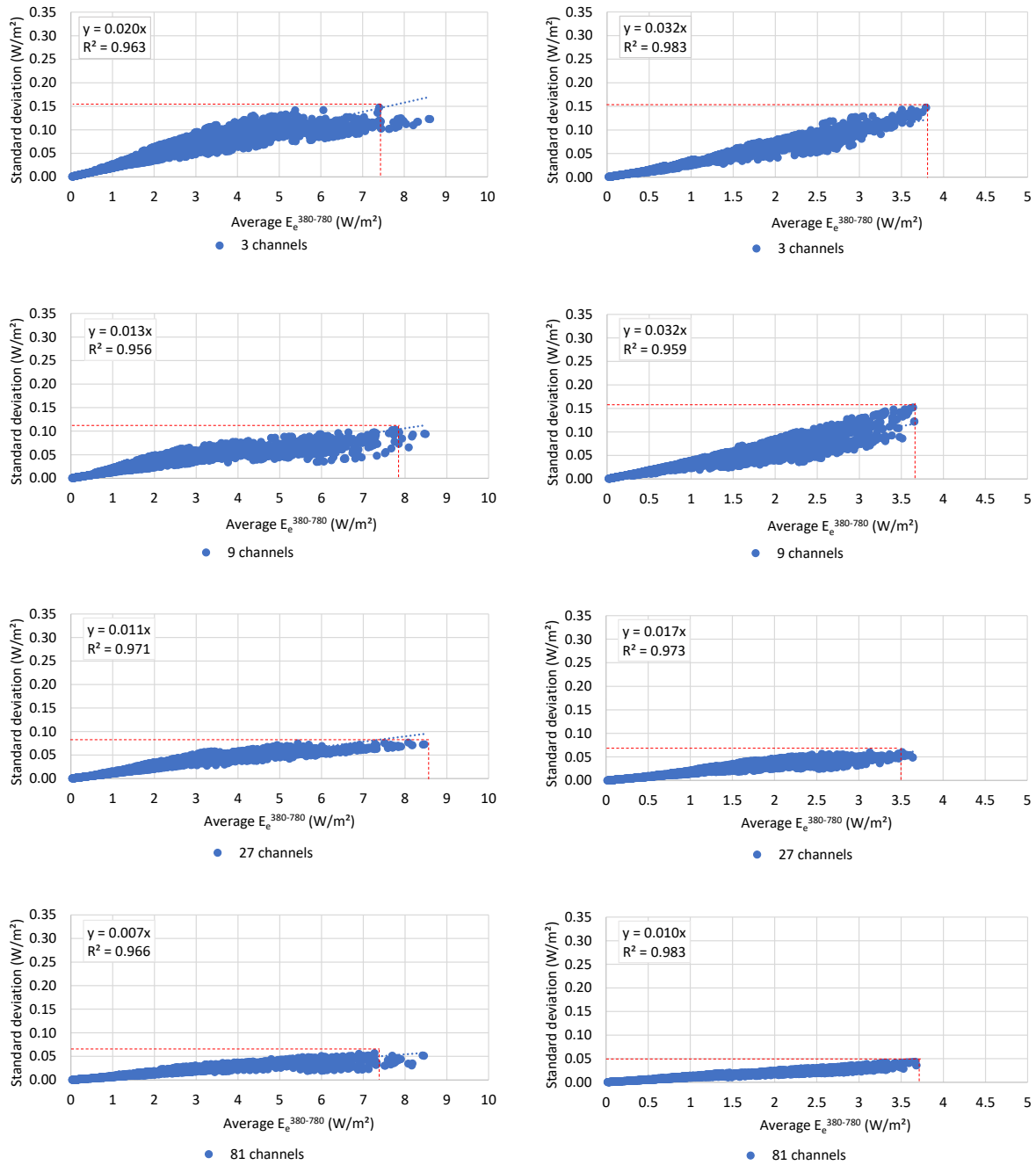


**Figure A.2.** Scatter plots show standard deviation (axis y) plotted against the average  $E_e^{380-780}$  (axis x) for position 4. Row (a) presents the results for the horizontal desk level (0.80 m) and row (b) at the vertical eye level (1.20 m) for simulations with three, nine, 27 and 81 channels. Average  $E_e^{380-780}$  refers to ten simulation runs. The red dashed line represents the maximum standard deviation at the respective  $E_e^{380-780}$  in each scatter plot.

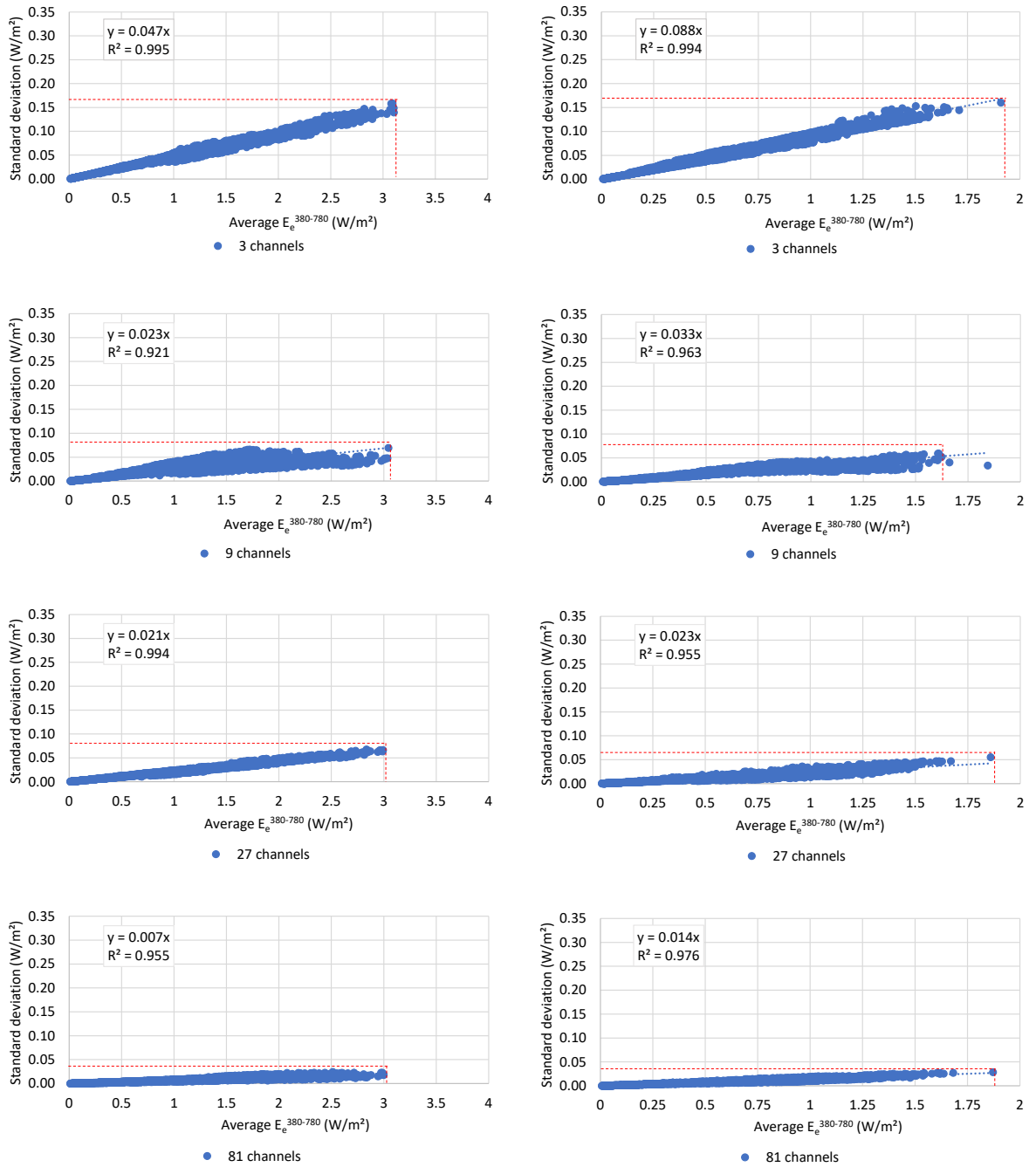


**Figure A.3.** Scatter plots show standard deviation (axis y) plotted against the average  $E_e^{380-780}$  (axis x) for position 5. Row (a) presents the results for the horizontal desk level (0.80 m) and row (b) at the vertical eye level (1.20 m) for simulations with three, nine, 27 and 81 channels. Average  $E_e^{380-780}$  refers to ten simulation runs. The red dashed line represents the maximum standard deviation at the respective  $E_e^{380-780}$  in each scatter plot.

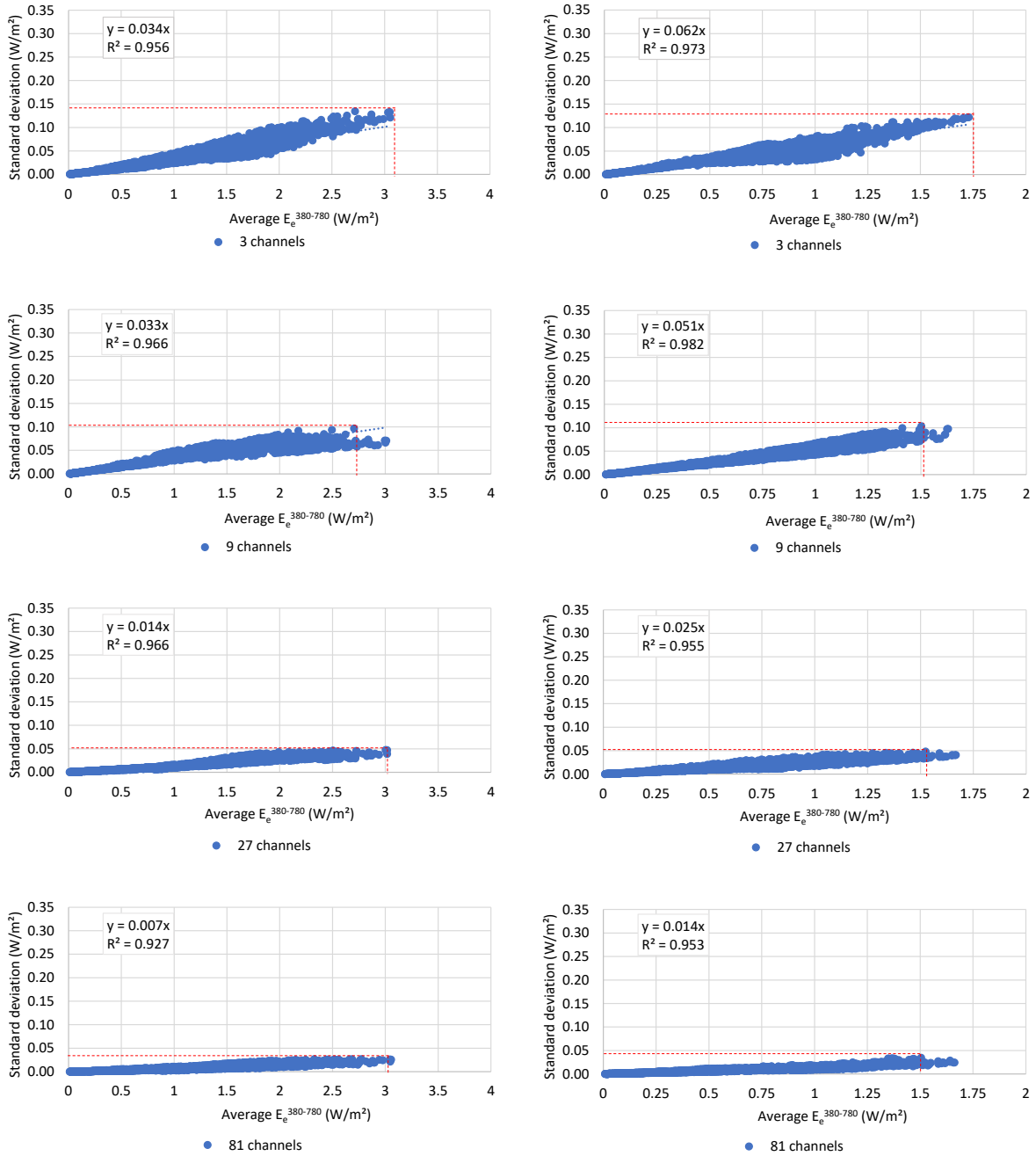


**Figure A.4.** Scatter plots show standard deviation (axis y) plotted against the average  $E_e^{380-780}$  (axis x) for position 6. Row (a) presents the results for the horizontal desk level (0.80 m) and row (b) at the vertical eye level (1.20 m) for simulations with three, nine, 27 and 81 channels. Average  $E_e^{380-780}$  refers to ten simulation runs. The red dashed line represents the maximum standard deviation at the respective  $E_e^{380-780}$  in each scatter plot.

# Appendix C

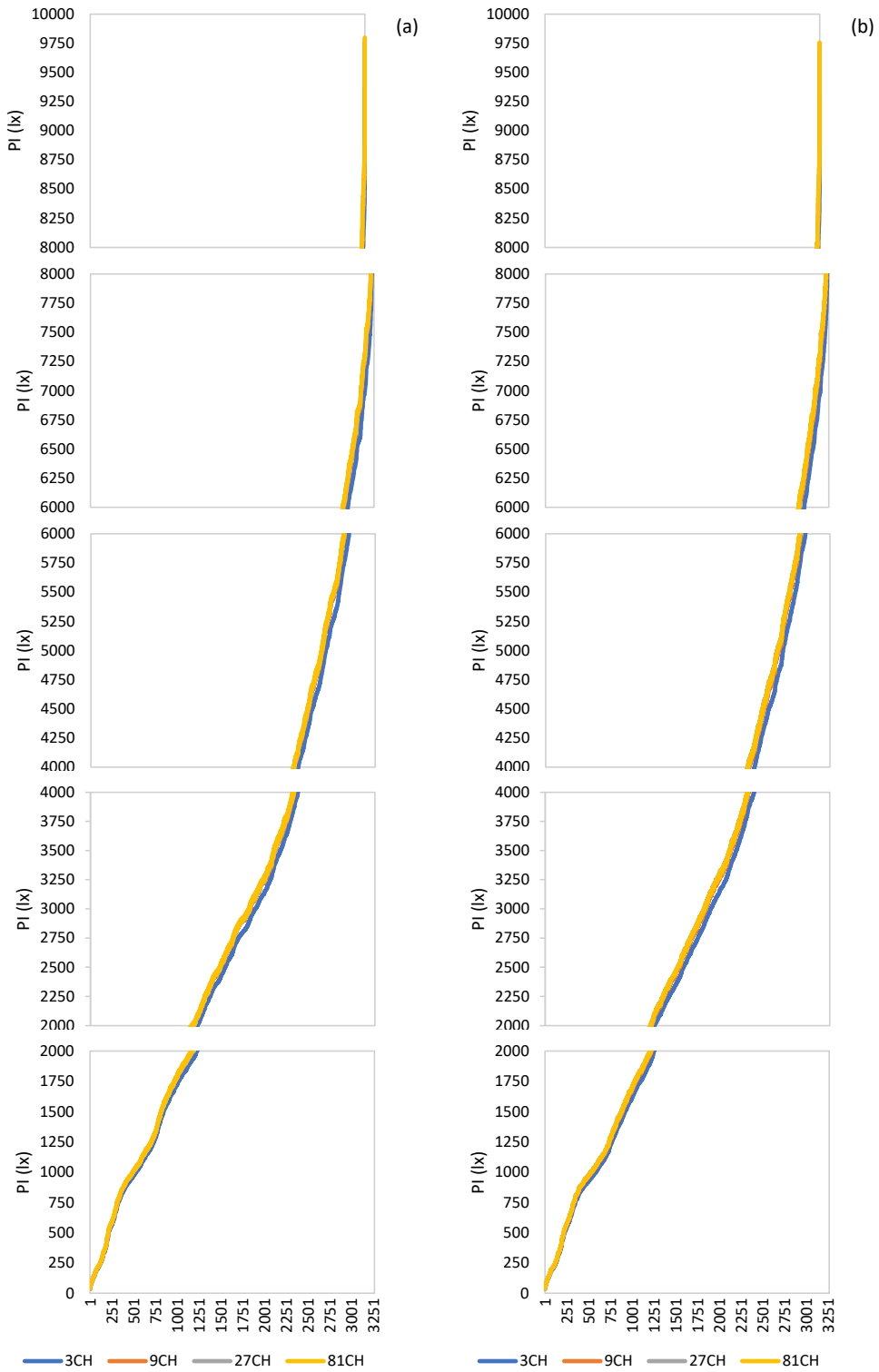


**Figure A.5.** Line chart of 3265 hours of photopic illuminance in a spectral simulation with three, nine, 27 and 81 channels recorded by horizontal desk-level sensors on position 1 (a) and position 2 (b).

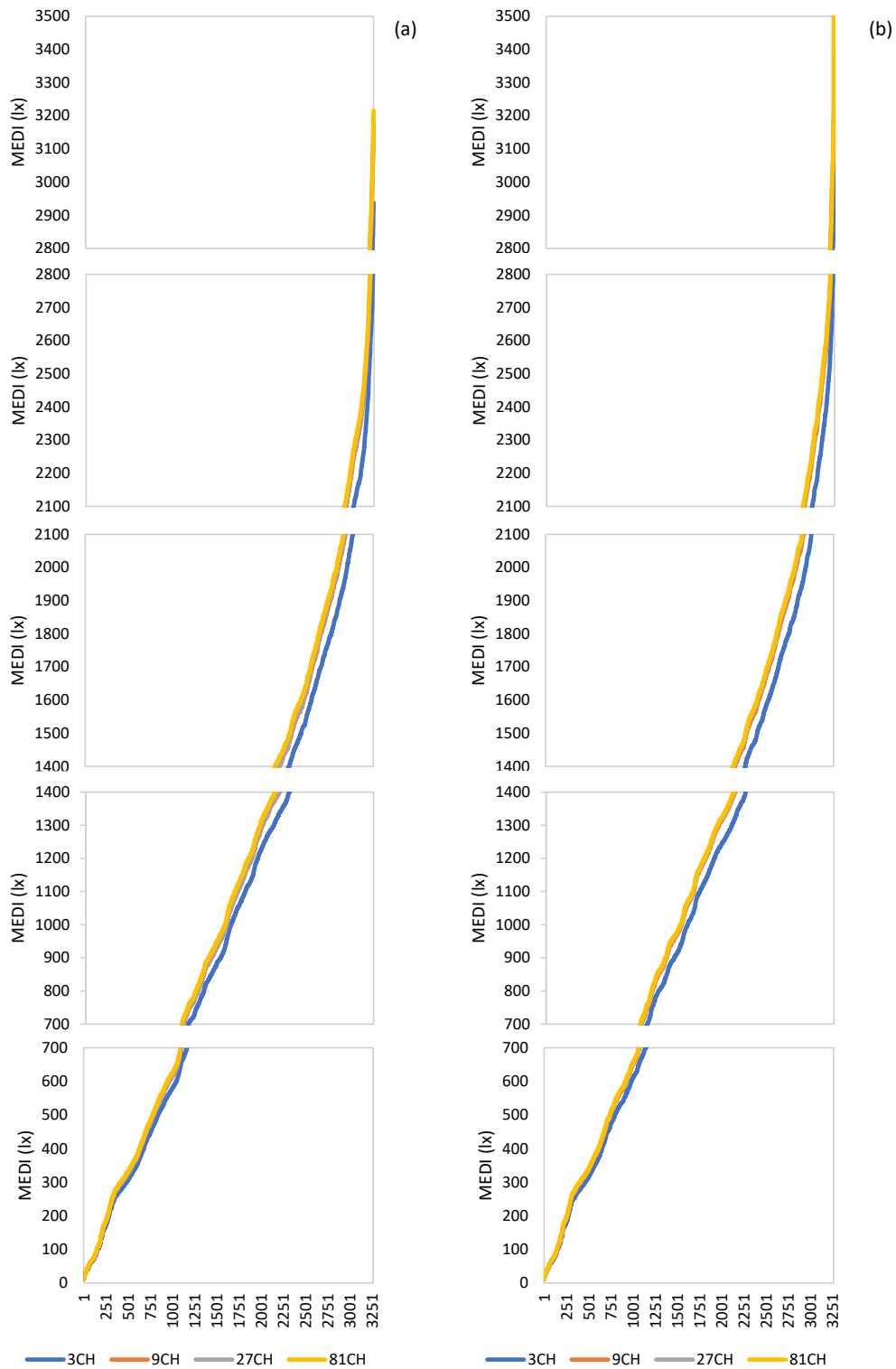


**Figure A.6.** Line chart of 3265 hours of melanopic equivalent daylight illuminance in a spectral simulation with three, nine 27 and 81 channels recorded by vertical eye-level sensors on position 1 (a) and position 2 (b).

The annual values of photopic and melanopic equivalent illuminance in the simulations with three, nine, 27 and 81 channels for positions 1 to 6 are presented here. The photopic illuminance on positions 1 to 6 that was computed via a simulation with three channels is lower in comparison to the simulations with the higher number of channels. The same trend is seen with melanopic equivalent daylight illuminance for positions 1 to 4. The deviation between baseline simulation with 81 channels and the rest of the multichannel simulation is minimal for melanopic equivalent illuminance on positions 5 and 6.

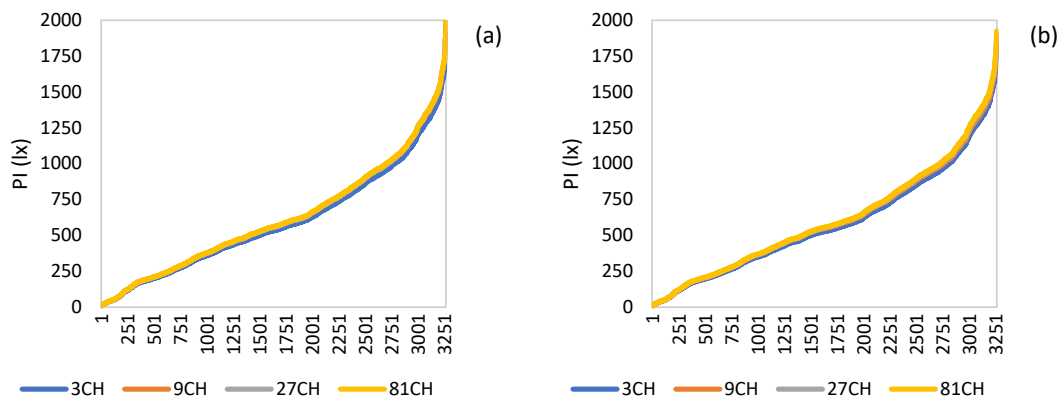


**Figure A.7.** Line chart of 3265 hours of photopic illuminance in a spectral simulation with three, nine 27 and 81 channels recorded by horizontal desk-level sensors on position 3 (a) and 4 (b).

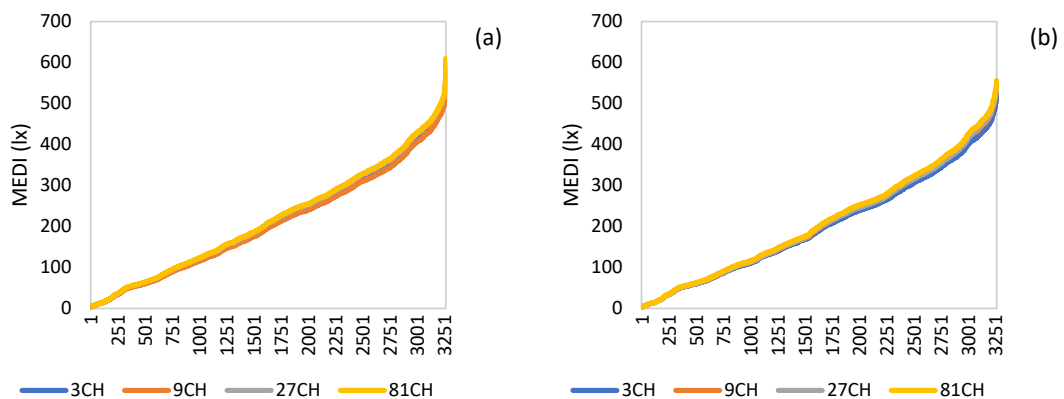


**Figure A.8.** Line chart of 3265 hours of melanopic equivalent daylight illuminance in a spectral simulation with three, nine 27 and 81 channels recorded by vertical eye-level sensors on position 3 (a) and position 4 (b).

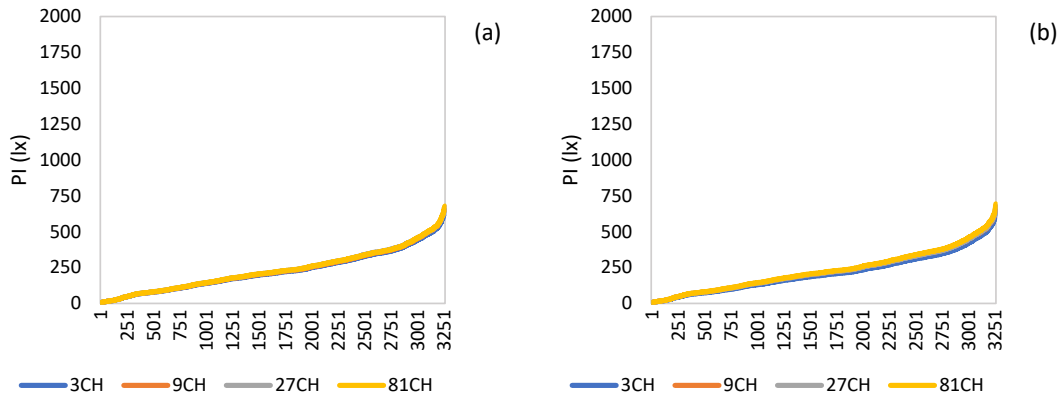


**Figure A.9.** Line chart of 3265 hours of photopic illuminance in a spectral simulation with three, nine 27 and 81channels recorded by horizontal desk-level sensors on position 5 (a) and position 6 (b).

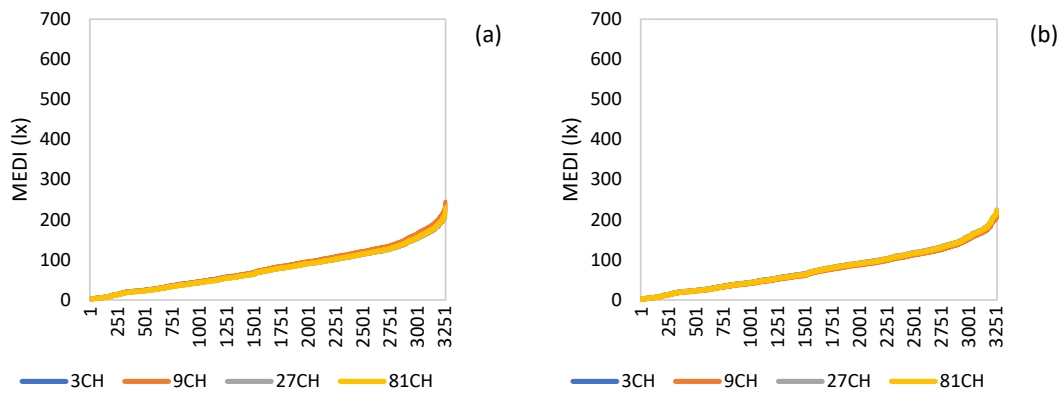


**Figure A.10.** Line chart of 3265 hours of melanopic equivalent daylight illuminance in a spectral simulation with three, nine 27 and 81channels recorded by vertical eye-level sensors on position 5 (a) and position 6 (b).



## Appendix D

### Photopic and melanopic equivalent illuminance produced by the luminaires

**Table A.5.** *Maximum photopic illuminance of the Philips LED luminaire (4000K) in a simulation with three, nine, 81 and 27 channel simulation on different positions.*

Channels	Position 1	Position 2	Position 3	Position 4	Position 5	Position 6
3	1120.8	1121.2	1121.3	1121.6	1129.4	1129.5
9	1126.7	1126.8	1126.7	1126.6	1135.1	1135.0
27	1127.8	1127.7	1127.1	1127.1	1136.2	1136.2
81	1128.1	1128.1	1127.7	1127.6	1136.6	1136.6

**Table A.6.** *Maximum melanopic equivalent daylight illuminance of the Philips LED luminaire (4000 K) in a simulation with three, nine, 81 and 27 channel simulation on different positions.*

Channels	Position 1	Position 2	Position 3	Position 4	Position 5	Position 6
3	411.5	411.6	406.4	406.4	408.8	408.8
9	400.5	400.5	396.6	396.6	398.2	398.2
27	391.1	391.1	387.4	387.4	388.9	388.9
81	388.9	389.0	385.3	385.3	386.8	386.8

**Table A.7.** *Maximum photopic illuminance of the Philips LED luminaire (6500K) in a simulation with three, nine, 81 and 27 channel simulation on different positions.*

Channels	Position 1	Position 2	Position 3	Position 4	Position 5	Position 6
3	1116.2	1115.9	1115.7	1115.8	1122.8	1122.4
9	1123.7	1123.8	1123.4	1123.4	1132.1	1132.0
27	1123.9	1124.0	1123.4	1123.5	1132.2	1132.1
81	1124.4	1124.4	1123.7	1123.8	1132.3	1132.2

**Table A.8.** *Maximum melanopic equivalent daylight illuminance of the Philips LED luminaire (6500 K) in a simulation with three, nine, 81 and 27 channel simulation on different positions.*

Channels	Position 1	Position 2	Position 3	Position 4	Position 5	Position 6
3	474.7	474.7	468.9	469.0	471.5	471.4
9	426.5	426.6	422.2	422.3	424.1	424.1
27	426.0	426.0	421.8	421.7	423.5	423.6
81	422.9	422.9	418.7	418.7	420.5	420.5

**Table A.9.** *Maximum photopic illuminance of the Sylvania fluorescent luminaire (3500 K) in a simulation with three, nine, 81 and 27 channel simulation on different positions.*

Channels	Position 1	Position 2	Position 3	Position 4	Position 5	Position 6
3	1135.2	1135.7	1137.5	1137.4	1150.2	1150.2
9	1142.4	1142.2	1144.2	1144.0	1158.9	1159.0
27	1147.5	1147.7	1148.9	1148.9	1163.7	1163.3
81	1153.2	1152.8	1155.2	1155.0	1170.2	1170.0

**Table A.10.** *Maximum melanopic equivalent daylight illuminance of the Sylvania fluorescent luminaire (3500 K) in a simulation with three, nine, 81 and 27 channel simulation on different positions.*

Channels	Position 1	Position 2	Position 3	Position 4	Position 5	Position 6
3	379.7	379.8	374.3	374.3	378.5	378.4
9	267.3	267.3	263.8	263.7	266.4	266.2
27	254.8	254.8	251.5	251.4	253.9	253.9
81	248.8	248.9	245.6	245.6	248.0	248.0

# Appendix E

Figure A.11 in the Appendix shows the dimming of the groups one to three when only photopic illuminance is evaluated for  $N$ - channel simulations. Figure A.12 presents the dimming behavior when only melanopic equivalent daylight illuminance is regarded. Figure A.13 shows photopic- and melanopic-based dimming.

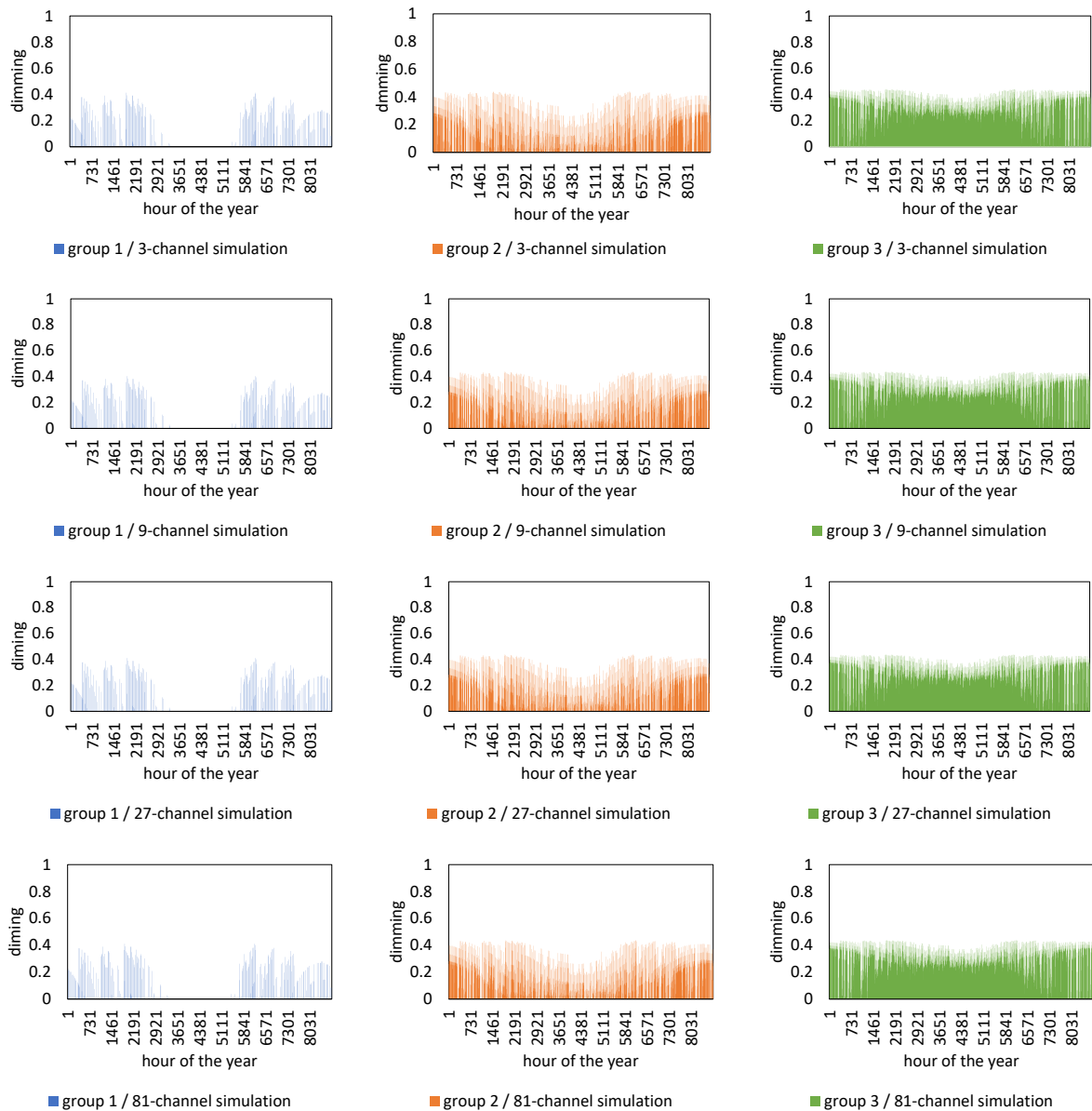


**Figure A.11.** Dimming behavior based on the dimming factor of the photopic illuminance. The dimming factor is presented for each of the three groups in the office room for the simulations with three, nine, 27 and 81 channels. Simulated luminaire = LED with 4000 K.

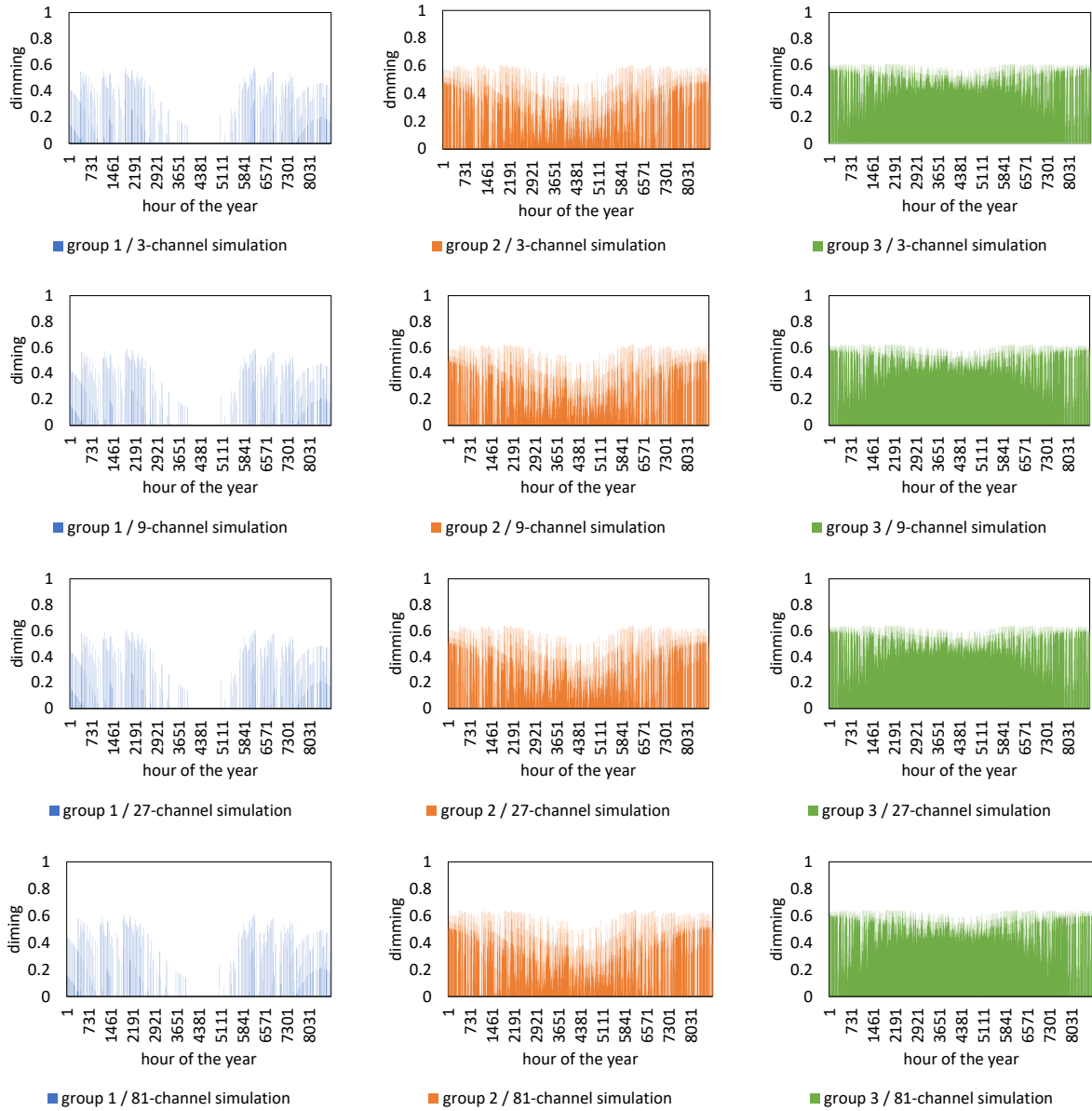


**Figure A.12.** Dimming behavior based on the dimming factor of the melanopic equivalent daylight illuminance. The dimming factor is presented for each of the three groups in the office room for the simulations with three, nine, 27 and 81 channels. Simulated luminaire = LED with 4000 K.

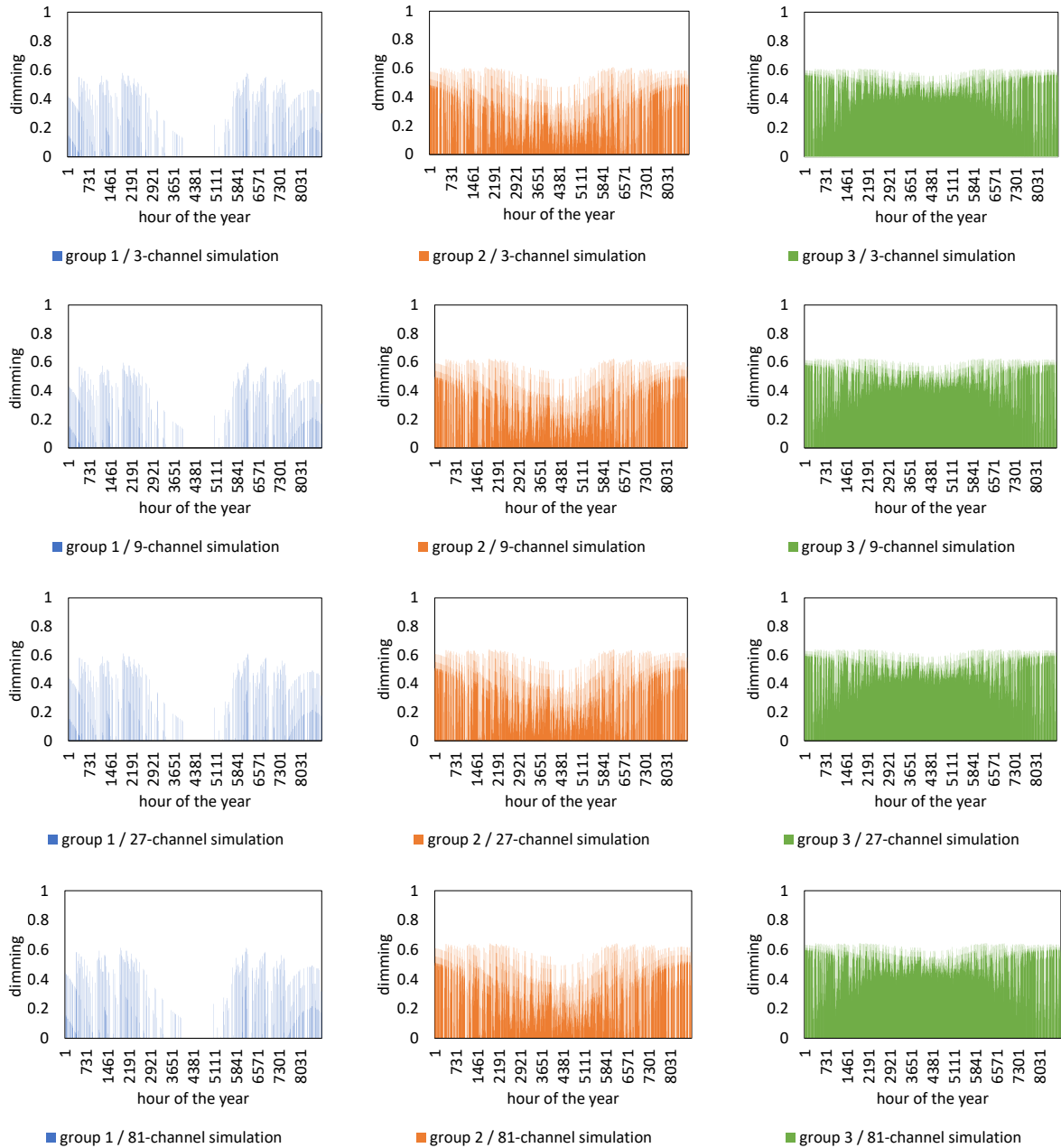


**Figure A.13.** Dimming behavior based on the higher dimming factor of the photopic and melanopic equivalent daylight illuminance. The dimming factor is presented for each of the three groups in the office room for the simulations with three, nine, 27 and 81 channels. Simulated luminaire = LED with 4000 K.

# List of Figures

Figure 1. Aspects that need to be considered in the development of the annual multichannel lighting simulation. ....2

Figure 2. Relative spectral sensitivity in the visible spectrum (from 380 nm to 780 nm) of the five photoreceptors and their photopigments: ipRGCs (melanopsin), rods (rhodopsin), S-cone (cyanopsin), M-cone (chloropsin) and L-cone (erythropsin). ....7

Figure 3. Summary of the selection process of the studies for the review that investigated the alerting effect of light during daytime. ....8

Figure 4. The main conclusions of the studies that investigated the alerting effect of illuminance during daytime. ....9

Figure 5. The main conclusions of the studies investigated the alerting effect of CCT during daytime. ....10

Figure 6. The main conclusions of the studies that investigated the alerting effect of monochromatic light during daytime. ....10

Figure 7. (a) Dimensions of the model with a removed wall positioned against a glazed façade. (b) Grid of the sensors points. Points 1-5 recorded horizontal illuminance on the floor of the model. Points 6-14 recorded vertical illuminance; the sensors were placed flat against the wall 0.20 m above the floor level. Points 15-17 were included additionally to measure vertical illuminance in the lighting scenario with electric light. ....22

Figure 8. Graphical representation of daylight coefficient shows luminance contribution from a discrete sky patch on arbitrary point in the room. Contributions from all patches make up the total photopic illuminance at any point in the room. Picture source: Christoph Reinhart, 2001 [115].....26

Figure 9. The output file of the gendaymtx program. The second line shows the sky color inputs (-c option) that are used to represent the default sky in Radiance. The triplets represent the RGB radiance values. The first 8760 RGB values show that the ground patch is not affected by the color option, as seen in the top screenshot for the first sixteen timesteps (i.e.,  $R = G = B$ ). The -c option affects the rest of the sky patches differently, as seen in the lower image, where  $R \neq G \neq B$ . ....27

Figure 10. Schematic framework of precomputation of the sky patch matrix and steps for the ASMS based on the daylight coefficient. ....28

Figure 11. The output file of the gendaymtx program when the color option is set to grey (-c 1 1 1). The triplets represent the RGB radiance values. Each patch shows that the radiance at any time of the year equals  $(R + G + B) / 3$ . ....29

Figure 12. Measured (black line) and discretized (colored lines) relative spectral radiance of the D65 illuminant with 6504 K.. ....33

Figure 13. Reference office room and the dimensions. The room is divided into three groups based on the proximity to the window. The room has six positions in total. Each group has two positions. ....37

Figure 14. a) Spectral reflectance of the white paint (ceiling), yellow paint (walls), wooden parquet (floor) and concrete (ground) from 380 nm to 780 nm. b) Spectral reflectance of the double pane low-E glazing from 380 nm to 780 nm. ....38

Figure 15. The x-axis represents 24 hours of the day. The y-axis shows the magnitude of direct normal radiation in Wh/m<sup>2</sup>. Orange points indicate hourly values of direct normal radiation for each month extracted from the weather data. The orange line is the trend line based on the hourly values. Source: CBE Clima Tool [129]. ....39

Figure 16. Hourly values of direct normal radiation represented as heatmap. The x-axis represents months. The y-axis shows hours of the day. The magnitude of direct normal radiation is color-coded and presented in Wh/m<sup>2</sup>. Source: CBE Clima Tool [129]. ....39

Figure 17. The x-axis represents 24 hours of the day. The y-axis shows the magnitude of diffuse horizontal radiation in Wh/m<sup>2</sup>. The orange points indicate hourly values of diffuse horizontal radiation for each month extracted from the weather data. The orange line is the trend line based on the hourly value. Source: CBE Clima Tool [129]. ....40

Figure 18. Hourly values of diffuse horizontal radiation represented as heatmap. The x-axis represents months. The y-axis shows hours of the day. The magnitude of diffuse horizontal radiation is color-coded and presented in Wh/m<sup>2</sup>. Source: CBE Clima Tool [129]. ....40

Figure 19. The annual profile of the diffuse horizontal and direct normal radiation in Mannheim as the output of epw2wea Radiance program and input for the ASMS. The x-axis represents hours. The y-axis shows magnitude of radiation in Wh/m<sup>2</sup>. ....40

Figure 20. Scatterplots show standard deviation (y-axis) plotted against the average  $E_e^{380-780}$  (x-axis) for positions 1. Row (a) presents the results at the horizontal desk level (0.80 m) and row (b) at the vertical eye level (1.20 m) for simulations with three, nine, 27 and 81 channels. Average  $E_e^{380-780}$  refers to ten simulation runs. The red dashed line represents the maximum standard deviation at the respective  $E_e^{380-780}$  in each scatter plot. ....42

Figure 21. Scatterplots show standard deviation (y-axis) plotted against the average  $E_e^{380-780}$  (x-axis) for positions 2. Row (a) presents the results at the horizontal desk level (0.80 m) and row (b) at the vertical eye level (1.20 m) for simulations with three, nine, 27 and 81 channels. Average  $E_e^{380-780}$  refers to ten simulation runs. The red dashed line represents the maximum standard deviation at the respective  $E_e^{380-780}$  in each scatter plot. ....44

Figure 22. The absolute difference in photopic illuminance for the simulations with three, nine and 27 channels in comparison to the baseline illuminance with 81 channels for positions 1 (a) to 6 (f). The x-axis represents the baseline illuminance in the simulation with 81 channels. The y-axis represents the absolute difference from the baseline simulation for the rest of the N-channel simulations in lx. ....46

Figure 23. The absolute difference in melanopic equivalent daylight illuminance for the simulations with three, nine and 27 channels in comparison to the baseline illuminance with 81 channels for positions 1 (a) to 6 (f). The x-axis represents the baseline illuminance in the simulation with 81 channels. The y-axis represents the absolute difference from the baseline simulation for the rest of the N-channel simulations in lx. ....48

Figure 24. Hours when the photopic illuminance is below the 500-lx threshold on the horizontal desk level for position 1 (a) and position 2 (b). The x-axis represents hours. The y-axis presents the illuminance range. The red dashed lines represent hours when photopic illuminance is between zero and 500 lx, corresponding to the threshold of photopic illuminance. PI = photopic illuminance in lx. ....49

Figure 25. Hours when the melanopic equivalent daylight illuminance is below the 250-lx threshold on the vertical eye level for position 1 (a) and position 2 (b). The x-axis represents hours. The y-axis presents the illuminance range. The red dashed lines represent hours when melanopic equivalent daylight illuminance is between zero and 250 lx, corresponding to the threshold of melanopic equivalent daylight illuminance. MEDI = melanopic equivalent daylight illuminance in lx. ....49

Figure 26. Photopic (a) and melanopic (b) sensitivity curves along with the spectral irradiance for the three-channel and 81-channel simulation for position 1 on the horizontal desk level (a) and vertical eye level (b) on 01.01 at 15:30. The x-axis represents the visible spectrum from 380 nm to 780 nm. The left y-axis shows the spectral irradiance in W/m<sup>2</sup>/nm. The right y-axis refers to the relative spectral sensitivity of photopic and melanopic curves... ....50

Figure 27. Polar luminous intensity graphs of LED with 4000 K (a), LED with 6500 K (b) and fluorescent luminaire with 3500 K (c). The distribution of luminous intensity is in candelas for frontal plane (C0/180) and the side plane (C90/270). ....52

Figure 28. Relative spectral power distribution of LED with 4000 K (a), LED with 6500 K (b) and fluorescent luminaire with 3500 K (c). The x-axis represents the visible spectrum from 380 nm to 780 nm. The y-axis shows the spectral power distribution normalized to one.....53



Figure 29. Three groups for independent lighting control in the office room. Group 1 represents the positions near the window that receive the most daylight, group 2 depicts the middle positions that receive less daylight and group 3 shows the positions that are located the farthest from the window and have the least amount of daylight. Photopic illuminance, shown by the green dot, is a theoretical sensor for illuminance at the desk level on the horizontal plane (0.80 m). The blue dots represent theoretical sensors that record melanopic equivalent daylight illuminance at eye level on a vertical plane (1.20 m). Pos. = position.....55

Figure 30. Relative spectral irradiance of LED with 4000 K (a), LED with 6500 K (b) and fluorescent luminaire with 3500 K (c) in a three, nine, 27, and 81-channel simulation at the eye level from position 1. CH = channels. ....56

Figure 31. Absolute spectral irradiance in a three, nine, 27 and 81-channel simulation with LED with 4000 K (1), LED with 6500 K (2) and fluorescent light with 3500 K on position 1 at the desk level alongside the photopic sensitivity curve (a) and at the eye level alongside the melanopic sensitivity curve (b). CH = channels. ....59

Figure 32. Dimming behavior based on photopic illuminance (a), melanopic equivalent daylight illuminance (b) and both (c). The dimming factor is presented for the three groups in the office room for the simulations 81 channels. Luminaire = LED with 4000 K. The lower x-axis represents the hours of the year; the upper x-axis shows the months of the year; the y-axis is the dimming magnitude.. ....65

Figure 33. Annual absolute dimming triggering based on the thresholds for photopic illuminance and melanopic equivalent daylight illuminance in Groups 1, 2 and 3 in the office room with LED with 4000 K (a). Pie chart of the photopic and melanopic dimming factor distribution among the three groups in the office room. The results are presented as percentages (b). Luminaire = LED with 4000 K. ....66

Figure 34. Annual lighting energy demand in the office room with LED luminaires with 4000 K with respect to number of channels in the simulations. The results are presented for the simulations with three, nine, 27 and 81 channels to one decimal place. ....67

Figure 35. Annual lighting energy demand in the office room with LED luminaires with 6500 K with respect to number of channels in the simulations. The results are presented for the simulations with three, nine, 27 and 81 channels to one decimal place. ....67

Figure 36. Annual lighting energy demand in the office room with fluorescent luminaires with 3500 K with respect to number of channels in the simulations. The results are presented for the simulations with three, nine, 27 and 81 channels to one decimal place...68

Figure 37. Variations in the annual lighting energy demand in the office room with LED luminaires with 4000 K that is controlled based on the threshold for photopic illuminance (500 lx at the horizontal desk level) with three, nine, 27 and 81-channel simulations of daylight and electric light The results are presented to one decimal place. ....73

Figure 38. Variations in the annual lighting energy demand in the office room with LED luminaires with 6500 K that is controlled based on the threshold for photopic illuminance (500 lx at the horizontal desk level) with three, nine, 27 and 81-channel simulations of daylight and electric light. The results are presented to one decimal place. ....74

Figure 39. Variations in the annual lighting energy demand in the office room with fluorescent luminaires with 3500 K that is controlled based on the threshold for photopic illuminance (500 lx at the horizontal desk level) with three, nine, 27 and 81-channel simulations of daylight and electric light. The results are presented to one decimal place..74

Figure 40. Hourly dimming behavior in Group 1, Group 2 and Group 3 in January and February. Pale blue color represents hours of the year for which spectral simulation is not possible due to limitation of spectral sky generation. White color represents no electric light. Shades of orange represent the use of luminaires, where pale color represents a low dimming factor (i.e., luminaire on but with a low intensity) and the saturated orange color represents luminaire on with full output. ....77

Figure 41. Hourly dimming behavior in Group 1, Group 2 and Group 3 in March and April. Pale blue color represents hours of the year for which spectral simulation is not possible due to limitation of spectral sky generation. White color represents no electric light. Shades of orange represent the use of luminaires, where pale color represents a low dimming factor (i.e., luminaire on but with a low intensity) and the saturated orange color represents luminaire on with full output. ....77

Figure 42. Hourly dimming behavior in Group 1, Group 2 and Group 3 in May and June. Pale blue color represents hours of the year for which spectral simulation is not possible due to limitation of spectral sky generation. White color represents no electric light. Shades of orange represent the use of luminaires, where pale color represents a low dimming factor (i.e., luminaire on but with a low intensity) and the saturated orange color represents luminaire on with full output. ....78

Figure 43. Hourly dimming behavior in Group 1, Group 2 and Group 3 in July and August. Pale blue color represents hours of the year for which spectral simulation is not possible due to limitation of spectral sky generation. White color represents no electric light. Shades of orange represent the use of luminaires, where pale color represents a low dimming factor (i.e., luminaire on but with a low intensity) and the saturated orange color represents luminaire on with full output. ....78

Figure 44. Hourly dimming behavior in Group 1, Group 2 and Group 3 in September and October. Pale blue color represents hours of the year for which spectral simulation is not possible due to limitation of spectral sky generation. White color represents no electric light. Shades of orange represent the use of luminaires, where pale color represents a low dimming factor (i.e., luminaire on but with a low intensity) and the saturated orange color represents luminaire on with full output. ....79

Figure 45. Hourly dimming behavior in group 1, group 2 and group 3 in November and December. Pale blue color represents hours of the year for which spectral simulation is not possible due to limitation of spectral sky generation. White color represents no electric light. Shades of orange represent the use of luminaires, where pale color represents a low dimming factor (i.e., luminaire on but with a low intensity) and the saturated orange color represents luminaire on with full output. ....79

Figure 46. Average hourly dimming factor from January to June for group 1, group 2 and group 3 based on the 81-channel simulation and LED luminaire with 6500 K. ....80

Figure 47. Average hourly dimming factor from July to December for group 1, group 2 and group 3 based on the 81-channel simulation and LED luminaire with 6500 K. ....81

Figure 48. Hourly photopic-based dimming in Group 1, Group 2 and Group 3 in January and February. Pale blue color represents hours of the year for which spectral simulation is not possible due to limitation of spectral sky generation. White color represents no electric light. Shades of orange represent the use of luminaires, where pale color represents a low dimming factor (i.e., luminaire on but with low intensity) and the saturated orange color represents luminaire on with a full output. ....83

Figure 49. Hourly photopic-based dimming in Group 1, Group 2 and Group 3 in March and April. Pale blue color represents hours of the year for which spectral simulation is not possible due to limitation of spectral sky generation. White color represents no electric light. Shades of orange represent the use of luminaires, where pale color represents a low dimming factor (i.e., luminaire on but with low intensity) and the saturated orange color represents luminaire on with a full output. ....83

Figure 50. Hourly photopic-based dimming in Group 1, Group 2 and Group 3 in May and June. Pale blue color represents hours of the year for which spectral simulation is not possible due to limitation of spectral sky generation. White color represents no electric light. Shades of orange represent the use of luminaires, where pale color represents a low dimming factor (i.e., luminaire on but with low intensity) and the saturated orange color represents luminaire on with a full output. ....84

Figure 51. Hourly photopic-based dimming in Group 1, Group 2 and Group 3 in July and August. Pale blue color represents hours of the year for which spectral simulation is not possible due to limitation of spectral sky generation. White color represents no electric light. Shades of orange represent the use of luminaires, where pale color represents a low dimming factor (i.e., luminaire on but with low intensity) and the saturated orange color represents luminaire on with a full output. ....84

Figure 52. Hourly photopic-based dimming in Group 1, Group 2 and Group 3 in September and October. Pale blue color represents hours of the year for which spectral simulation is not possible due to limitation of spectral sky generation. White color represents no electric light. Shades of orange represent the use of luminaires, where pale color represents a low dimming factor (i.e., luminaire on but with low intensity) and the saturated orange color represents luminaire on with a full output. ....85

Figure 53. Hourly photopic-based dimming in Group 1, Group 2 and Group 3 in November and December. Pale blue color represents hours of the year for which spectral simulation is not possible due to limitation of spectral sky generation. White color represents no electric light. Shades of orange represent the use of luminaires, where pale color represents a low dimming factor (i.e., luminaire on but with low intensity) and the saturated orange color represents luminaire on with a full output. ....85

Figure 54. Average hourly photopic-based dimming factor from January to June for group 1, group 2 and group 3 based on the 81-channel simulation and LED luminaire with 6500 K. ....86

Figure 55. Average hourly photopic-based dimming factor from July to December for group 1, group 2 and group 3 based on the 81-channel simulation and LED luminaire with 6500 K. ....87

Figure A.1. Scatter plots show standard deviation (axis y) plotted against the average  $E_e^{380-780}$  (axis x) for position 3. Row (a) presents the results for the horizontal desk level (0.80 m) and row (b) at the vertical eye level (1.20 m) for simulations with three, nine, 27 and 81 channels. Average  $E_e^{380-780}$  refers to ten simulation runs. The red dashed line represents the maximum standard deviation at the respective  $E_e^{380-780}$  in each scatter plot.....117

Figure A.2. Scatter plots show standard deviation (axis y) plotted against the average  $E_e^{380-780}$  (axis x) for position 4. Row (a) presents the results for the horizontal desk level (0.80 m) and row (b) at the vertical eye level (1.20 m) for simulations with three, nine, 27 and 81 channels. Average  $E_e^{380-780}$  refers to ten simulation runs. The red dashed line represents the maximum standard deviation at the respective  $E_e^{380-780}$  in each scatter plot.....118

Figure A.3. Scatter plots show standard deviation (axis y) plotted against the average  $E_e^{380-780}$  (axis x) for position 5. Row (a) presents the results for the horizontal desk level (0.80 m) and row (b) at the vertical eye level (1.20 m) for simulations with three, nine, 27 and 81 channels. Average  $E_e^{380-780}$  refers to ten simulation runs. The red dashed line represents the maximum standard deviation at the respective  $E_e^{380-780}$  in each scatter plot.....119

Figure A.4. Scatter plots show standard deviation (axis y) plotted against the average  $E_e^{380-780}$  (axis x) for position 6. Row (a) presents the results for the horizontal desk level (0.80 m) and row (b) at the vertical eye level (1.20 m) for simulations with three, nine, 27 and 81 channels. Average  $E_e^{380-780}$  refers to ten simulation runs. The red dashed line represents the maximum standard deviation at the respective  $E_e^{380-780}$  in each scatter plot.....120

Figure A.5. Line chart of 3265 hours of photopic illuminance in a spectral simulation with three, nine 27 and 81 channels recorded by horizontal desk-level sensors on position 1 (a) and position 2 (b).....121

Figure A.6. Line chart of 3265 hours of melanopic equivalent daylight illuminance in a spectral simulation with three, nine 27 and 81 channels recorded by vertical eye-level sensors on position 1 (a) and position 2 (b). .....122

Figure A.7. Line chart of 3265 hours of photopic illuminance in a spectral simulation with three, nine 27 and 81 channels recorded by horizontal desk-level sensors on position 3 (a) and 4 (b) .....123

Figure A.8. Line chart of 3265 hours of melanopic equivalent daylight illuminance in a spectral simulation with three, nine 27 and 81 channels recorded by vertical eye-level sensors on position 3 (a) and position 4 (b). .....123

Figure A.9. Line chart of 3265 hours of photopic illuminance in a spectral simulation with three, nine 27 and 81 channels recorded by horizontal desk-level sensors on position 5 (a) and position 6 (b). .....124

Figure A.10. Line chart of 3265 hours of melanopic equivalent daylight illuminance in a spectral simulation with three, nine 27 and 81 channels recorded by vertical eye-level sensors on position 5 (a) and position 6 (b). .....124

Figure A.11. Dimming behavior based on the dimming factor of the photopic illuminance. The dimming factor is presented for each of the three groups in the office room for the simulations with three, nine, 27 and 81 channels. Simulated luminaire = LED with 4000 K.....127

Figure A.12. Dimming behavior based on the dimming factor of the melanopic equivalent daylight illuminance. The dimming factor is presented for each of the three groups in the office room for the simulations with three, nine, 27 and 81 channels. Simulated luminaire = LED with 4000 K. ....128

Figure A.13. Dimming behavior based on the higher dimming factor of the photopic and melanopic equivalent daylight illuminance. The dimming factor is presented for each of the three groups in the office room for the simulations with three, nine, 27 and 81 channels. Simulated luminaire = LED with 4000 K.....129

# List of Tables

Table 1. Validated luminance-to-CCT correlations for clear and overcast sky types. Correlations for clear sky are to be based on the luminance range of each individual patch. CCT of overcast sky is constant. L = Luminance (cd/m<sup>2</sup>); LCF = Luminance Color Factor.....30

Table 2. Materials selected for the reference office room with the reflectance and transmittance values presented in percentages.....38

Table 3. Standard deviation that occurs on positions 1-3 on the vertical and horizontal planes for the simulation with three, nine, 27 and 81 channels. The regression model is based on ten Radiance simulation runs with three, nine, 27 and 81 channel discretization.....45

Table 4. Standard deviation that occurs on positions 4-6 on the vertical and horizontal planes for the simulation with three, nine, 27 and 81 channels. The regression model is based on ten Radiance simulation runs with three, nine, 27 and 81 channel discretization.....45

Table 5. The difference in photopic illuminance presented in percent for the simulations with three, nine, 27 and 81 channels in comparison to the maximum baseline illuminance for positions 1 to 6. ....47

Table 6. The difference in melanopic equivalent daylight illuminance presented in percent for the simulations with three, nine, 27 and 81 channels in comparison to the maximum baseline illuminance for positions 1 to 6. ....47

Table 7. Factors needed to calculate luminaire-specific maintenance factors according to Equation 21. The resulting maintenance factor is presented in bold font. FL = fluorescent.....54

Table 8. Standard deviation for irradiance at the desk level (horizontal plane at 0.80 m) for three-channel, nine-channel, 27-channel, and 81-channel discretization based on five simulation runs. The results are presented for each position in the office room with LED luminaire with 4000 K.....57

Table 9. Standard deviation for irradiance at the eye level (vertical plane at 1.20 m) for three-channel, nine-channel, 27-channel, and 81-channel discretization based on five simulation runs. The results are presented for each position in the office room with LED luminaire with 4000 K.....57

Table 10. Deviation of photopic and melanopic equivalent daylight illuminance from the baseline simulation with 81 channels for the three-, nine- and 27-channel discretization in percent for position 1. Negative values present overestimation. Lumin. = Luminaires; Chann. = Channels; 4000 K = LED with 4000 K; 6500 K = LED with 6500 K; 3500 K = Fluorescent with 3500 K.....58

Table 11. A hypothetical example of supplementary electric illuminance during hour X for Group 1 in a three-channel simulation. PI = photopic illuminance; MEDI = melanopic equivalent daylight illuminance.....61

Table 12. Maximum illuminance output of the LED luminaire with 4000 K for Group 1. The values are an average of illuminance on positions 1 and 2. PI = photopic illuminance; MEDI = melanopic equivalent daylight illuminance.....62

Table 13 Maximum dimming factor during hour X for Group 1 in a three-channel simulation. PI = photopic illuminance; MEDI = melanopic equivalent daylight illuminance.....62

Table 14. Difference in electric lighting demand of both LED and fluorescent luminaires in percent considering a baseline with 81 channels. Negative values represent overprediction. CH = channels.....69

Table 15. Difference in electric lighting demand of LED luminaires with 4000 K in percent considering the 81-channel simulation of electric light to be the baseline. Negative values represent overprediction. CH = channels.....70

Table 16. Difference in electric lighting demand of LED luminaires with 6500 K in percent considering the 81-channel simulation of electric light to be the baseline. Negative values represent overprediction. CH = channels.....70

Table 17. Difference in electric lighting demand of fluorescent luminaires with 3500 K in percent considering the 81-channel simulation of electric light to be the baseline. Negative values represent overprediction. CH = channel, FL = fluorescent.....70

Table 18. Difference in lighting energy demand in comparison to the baseline, which is a simulation with 81 channels for daylighting and electric lighting. In italic bold font: counterintuitive finding that shows lower deviation from the baseline in a three-channel simulation in comparison to a nine-channel simulation. Negative values show an overprediction of the electric lighting demand. Electric light = LED with 4000 K .....71

Table 19. Difference in lighting energy demand in comparison to the baseline, which is a simulation with 81 channels for daylighting and electric lighting. Negative values show overprediction of the electric lighting demand. Electric light = LED with 6500 K.....72

Table 20. Difference in lighting energy demand in comparison to the baseline, which is a simulation with 81 channels for daylighting and electric lighting. Negative values show overprediction of the electric lighting demand. Electric light = fluorescent with 3500 K.....72

Table 21. Difference in lighting energy demand in comparison to the baseline, which is a simulation with 81 channels for daylighting and electric lighting. In italic bold font: counterintuitive finding that shows lower deviation from the baseline in a three-channel simulation in comparison to a nine-channel simulation. Negative values show an overprediction of the electric lighting demand. Electric light = LED with 4000 K.....75

Table 22. Difference in lighting energy demand in comparison to the baseline, which is a simulation with 81 channels for daylighting and electric lighting. In italic bold font: counterintuitive finding that shows lower deviation from the baseline in a three-channel simulation in comparison to a nine-channel simulation. Negative values show an overprediction of the electric lighting demand. Electric light = LED with 6500 K.....75

Table 23. Difference in lighting energy demand in comparison to the baseline, which is a simulation with 81 channels for daylighting and electric lighting. In italic bold font: counterintuitive finding that shows lower deviation from the baseline in a three-channel simulation in comparison to a nine-channel simulation. Negative values show an overprediction of the electric lighting demand. Electric light = fluorescent light with 3500 K.....75

Table 24. Underestimation of lighting energy demand in percent when only photopic illuminance is maintained in comparison to the light energy demand when both photopic and melanopic equivalent daylight illuminance thresholds are maintained. Electric light = LED with 4000 K.....75

Table 25. Underestimation of lighting energy demand in percent when only photopic illuminance is maintained in comparison to the light energy demand when both photopic and melanopic equivalent daylight illuminance thresholds are maintained. Electric light = LED with 6500 K.....76

Table 26. Underestimation of lighting energy demand in percent when only photopic illuminance is maintained in comparison to the light energy demand when both photopic and melanopic equivalent daylight illuminance thresholds are maintained. Electric light = fluorescent (FL) with 3500 K.....76

Table A.1. Wavelength bands and their respective coefficients in a three-channel simulation.....112

Table A.2. Wavelength bands and their respective coefficients in a nine-channel simulation.....112

Table A.3. Wavelength bands and their respective coefficients in a 27-channel simulation.....112

Table A.4. Wavelength bands and their respective coefficients in a 81-channel simulation.....113

Table A.5. Maximum photopic illuminance of the LED luminaire (4000K) in a simulation with three, nine, 81 and 27 channel simulation on different positions.....125

Table A.6. Maximum melanopic equivalent daylight illuminance of the LED luminaire (4000 K) in a simulation with three, nine, 81 and 27 channel simulation on different positions.....125

Table A.7. Maximum photopic illuminance of the LED luminaire (6500K) in a simulation with three, nine, 81 and 27 channel simulation on different positions.....125



Table A.8. Maximum melanopic equivalent daylight illuminance of the LED luminaire (6500 K) in a simulation with three, nine, 81 and 27 channel simulation on different positions.....126

Table A.9. Maximum photopic illuminance of the fluorescent luminaire (3500 K) in a simulation with three, nine, 81 and 27 channel simulation on different positions.....126

Table A.10. Maximum melanopic equivalent daylight illuminance of the fluorescent luminaire (3500 K) in a simulation with three, nine, 81 and 27 channel simulation on different positions.....126

# Declaration

I hereby declare that I wrote the dissertation entitled "*Development of the Annual Spectral Matrix Simulation Method and Assessment of the Effect of Spectral Discretization on Annual Lighting Energy Demand*" independently. All the resources that were used in this work are clearly listed in the thesis. I confirm that I have not submitted the dissertation or parts thereof for a state or scientific examination. I have not previously submitted this or any other dissertation to any other department or university.

20.04.2024



.....  
Margarita Alwalidi

# Curriculum Vitae

Name: Margarita Alwalidi

Nationality: jordanian, russian

## Academic Education

### **RPTU, Kaiserslautern, Germany**

December 2019

- Accepted as a doctoral candidate at the Faculty of Civil Engineering in the field of Built Environment

### **Technical University Munich, Germany**

October 2017 – November 2019

- M.Sc. Energy-efficient and Sustainable Building

### **German Jordanian University, Amman, Jordan**

September 2012 – August 2017

- B.Sc. Architecture

## Experiences

### **RPTU, Kaiserslautern, Germany**

December 2019 - Present

- Research assistant at the Chair of Built Environment
- Student assistant at the Chair of Built Environment

### **Drees & Sommer, Munich, Germany**

November 2018 – August 2019

- Student assistant in the project management department

### **Forschungsstelle für Energiewirtschaft, Munich, Germany**

March 2018 – September 2018

- Student assistant at the Research Center for Energy Economics

### **Planerkollektiv Architekten Part Gmbb, Hamburg, Germany**

March 2016 – August 2016

- Architectural internship during Bachelor program